Experimental and Analytical Studies on Scrap Tire Rubber Pads for Application to Seismic Isolation of Structures

Huma Kanta MISHRA

2012

Experimental and Analytical Studies on Scrap Tire Rubber Pads for Application to Seismic Isolation of Structures

A dissertation submitted in partial fulfillment
of the requirements for the degree of
Doctor of Philosophy in Civil Engineering

Graduate School of Engineering
Kyoto University, Japan
2012

by

Huma Kanta Mishra

Examination Committee: Professor Akira Igarashi (Supervisor)
Professor Takeshi Koike (Chairman)
Professor Kunitomo Sugiura

In memory of my mother,

Abstract

Past earthquakes have caused tremendous damage to infrastructures and loss of lives especially when it occurs in developing countries. Majority of the loss of lives is due to the collapse of poorly constructed concrete and masonry buildings. If the seismic demand on these structures were reduced through a simple but reliable engineering solution such as base isolation, this would result in fewer buildings failure and less loss of lives. The problem with adopting base isolation system in developing countries is that the conventional seismic isolators are large, heavy and expensive.

This research work is particularly focused to check the viability of using scrap tire rubber pad (STRP) to develop seismic isolation device. A series of experimental tests and analytical studies are carried out to investigate the mechanical properties of the proposed base isolation system. Experimental tests are conducted on two types of STRP specimens; layer-unbonded STRP and layer-bonded STRP. To effectively simulate the STRP, Mooney-Rivlin material constants are determined by conducting uniaxial tension tests and the key components of the tire rubber is evaluated by conducting gas chromatography analysis.

In the first part of the study, experimental test and finite element analyses (FE analysis) is conducted on layer-unbonded STRP specimen. The vertical compression and shear loading tests are conducted for the case of unbonded application with support interfaces which allows roll-off behavior when subjected to shear deformation. The results show that these types of bearings can withstand axial pressure comparable to commercially available seismic isolator. This part of study suggests for bonding the STRP layers and to increase the aspect ratio in order to improve the performance in terms of shear deformation capacity and stability.

Similar studies on layer-bonded STRP specimens are carried to determine the mechanical properties in vertical compression and in cyclic shear loadings. The test results indicate that the bonding is sufficiently strong in transmitting the shear forces and consequently improves the shear deformation capacity.

In the next part of the study, STRP bearings are designed for a three-story reinforced concrete building as per the standard code provisions. Numerical modeling of STRP bearings including building under unidirectional seismic excitation is verified by conducting pseudodynamic tests. The reduction of floor absolute accelerations, floor drifts and base shear transmission to the superstructure indicates the seismic response performance of the purpose base isolation system.

In order to investigate the seismic response of base isolated building with STRP bearings under bidirectional seismic excitations, three dimensional nonlinear time history analysis is performed. This study concludes that the seismic responses are reduced to acceptable limits for all level of seismic excitations, the building including isolation system is stable and all the STRP bearings are participating in base isolation system.

In addition, stability analysis of individual STRP bearings is evaluated. This study suggests that the nominal axial stress plays a crucial role in shear deformation capacity of the STRP bearings and an eventual instability of the isolation unit.

The mechanical properties are further compared with the relevant code provisions to check the viability of such devices in seismic isolation purpose and are considered appropriate. Finally, it can be concluded that the use of STRP to develop seismic isolation device is feasible for application to seismic isolation of structures.

Acknowledgement

The research work on Experimental and Analytical Studies on Scrap Tire Rubber Pads for Application to Seismic Isolation of Structures in this thesis was carried out in the Structural Dynamics Laboratory, Department of Urban Management, Graduate School of Engineering at the Kyoto University, under the overall guidance of Prof. Akira Igarashi.

I would like to express my deepest appreciation to my supervisor, Prof. Akira Igarashi for his enduring patience, invaluable advice, kindly guidance and encouragement throughout this research effort. Prof. Igarashi's warm communications due to his enthusiasm and cheerful heart are greatly appreciated.

I would like to express my deepest gratitude to the Ministry of Education, Culture, Sports, Science and Technology (MEXT), Japan for granting me the financial support "Monbugakakusho Scholarship" during the study period in Japan.

My sincere appreciation is also extended to the dissertation committee Professor Takeshi Koike and Professor Kunitomo Sugiura for their valuable advice and contribution in reviewing my Ph.D. dissertation.

I gratefully acknowledge the contribution of Tokai Rubber Industries Ltd., Japan for the assistance in preparation of specimen samples and gas chromatography analysis.

I would like to express my sincere gratitude to Prof. Aiko Furukawa for her valuable suggestions and support in this research. Similarly, I would like to express my gratitude towards Dr. H. R. Parajuli of RGIRD, Ritsumeikan University for his valuable advice, support and suggestions. Also, I would like to express a great amount of gratitude to Dr. Dang Ji whose advice and assistance in experimental tests have been invaluable and greatly appreciated.

I would like to thank all of the technical staff working at the Experimental Laboratory for all their advice and assistance during the experimental phases of the research.

I would like to express my gratitude to the Government of Nepal for granting me the study leave during my Ph. D study period.

I would like to thank my friends and colleagues in the Structural Dynamics Laboratory for their cooperation, support, help and encouragement during my stay in Japan.

Finally, I would like to thank to my friends and family for their support, understanding and encouragement throughout the entire duration of Ph. D study.

Huma Kanta Mishra
August 30th 2012, Kyoto, Japan

Table of Contents

5. Experimental and analytical study of layer-bonded STRP bearings

6. Design of STRP bearings, numerical modeling and validation by pseudodynamic test

List of Figures

List of Tables

1

Introduction

The first chapter of this dissertation intends to introduce about the background of the research. In this chapter, brief description about the seismic isolation devices and brief history of base isolation system is also presented. The primary focus of the chapter is to provide objective of the study as well as scope and outline of the dissertation.

1.1 Background of the research

The past earthquakes around the world have caused tremendous damage to infrastructures and loss of lives. This effect is more pronounced when happens in developing countries due to collapse of poorly constructed concrete and masonry buildings. The damaging effect and loss of lives could be reduced, if the seismic demand on these buildings were reduced through a simple but reliable engineering solution [1]. Many aseismic design and construction technologies have been developed over the years to mitigate the damaging effects of earthquake on building structures. Attenuating the effects of severe ground motions on the buildings is always one of the most popular topics in the field of structural engineering research and attracts the attention of many researches around the world.

In order to mitigate the severe effects of earthquake on building structures, the possible techniques are a) increase the earthquake-resistant capacity of the structure b) use of bracing system c) use of added damping devices and d) reduce the seismic demand on the structure by incorporating the base isolation system. Increasing the earthquake-resistant capacity of the structure is based on the principle of increasing the size of structural members and requires good quality materials to achieve the target strength. Due to this reason, it increases the overall cost of the structure. Bracing system increases the stiffness of the structure but doesn’t decrease the

seismic forces on the structure. If the level of seismic demand cannot be decreased, it is difficult to economically justify the use of bracing system for ordinary residential buildings. Use of damping devices could be an appropriate solution to reduce the seismic forces but it increases the overall cost which cannot be adopted for common buildings. More recently, the attraction is towards the reduction of seismic demand instead of increasing the seismic resistant capacity of the structures. The reason is that the expectation of better performance of base isolated building structures were satisfied during the 1994 Northridge earthquake in California and 1995 Kobe earthquake in Japan [2]. During the 1995 Kobe earthquake the observed damage to buildings also produced a sense of doubt regarding the reliability of traditional construction approaches [3]. The basic concept of adopting different methods and their effect on seismic forces is shown in Fig. 1.1.

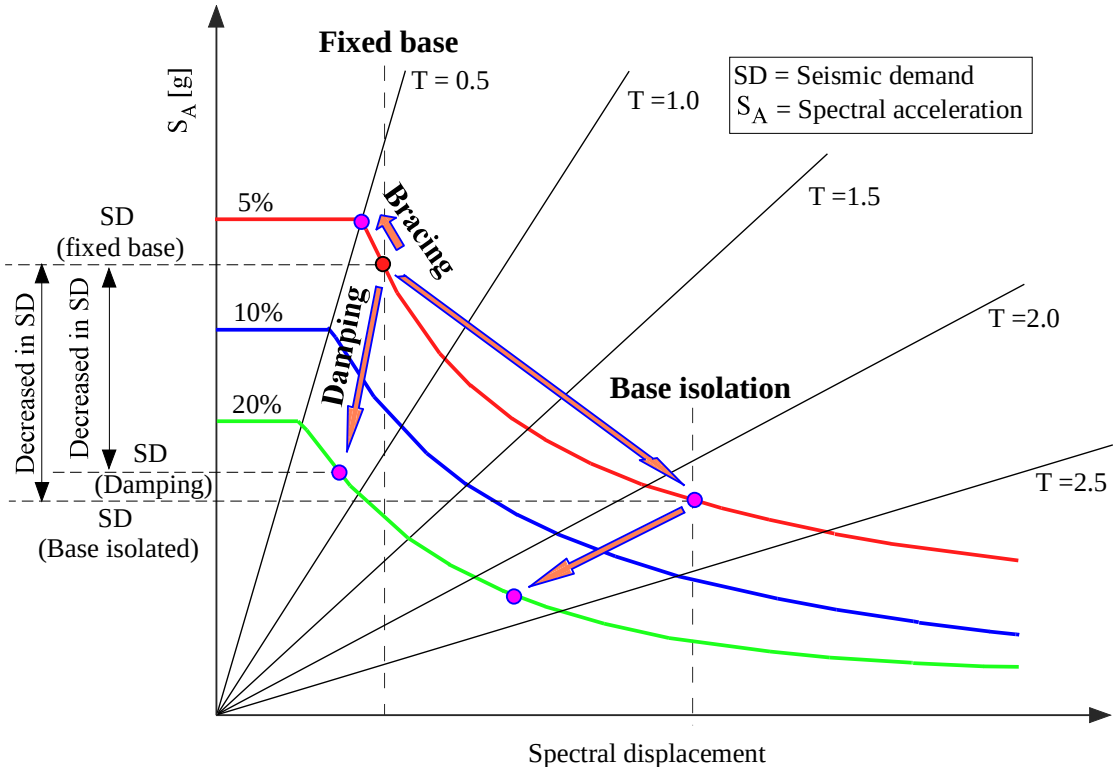

Figure 1.1 Response spectra showing different approaches and their effect on seismic demand

The reduction of seismic demand on structures can be achieved by providing certain degree of flexibility in the structure by installing the devices having low horizontal stiffness. There are many kinds of seismic isolation devices to serve this purpose. Among these, elastomeric bearings, sliding bearings and hybrid systems are the most widely used seismic isolation devices.

The elastomeric bearing is an attractive device for base isolation as the elastomeric material provides a restoring force and leaves no residual displacements of the isolated structure after an earthquake. The elastomeric bearings are available in different forms to serve the desired purposes such as steel laminated rubber bearings, lead rubber bearings and high damping rubber bearings. Nowadays, this technology is becoming attractive alternative to the conventional seismic resistant design methods and is gaining widespread acceptance in the global engineering community.

The application of the base isolation system is limited to the important and valuable structures. The reason behind this is the weight and incurred cost of the seismic isolation system [4]. However, it will be very useful when base isolation technique can be scaled down and adapted for use in more common building structures such as housing, schools and other public buildings, especially in high seismicity regions of the developing countries. Therefore, it seems necessary to develop a base isolation system which shall be effective in reducing the seismic demand on structures with due consideration of purchasing capacity of the common public of the developing countries. Therefore, a research work called experimental and analytical studies on scrap tire rubber pads for application to seismic isolation of is carried out. The objective of the research is to develop an effective but relatively low-cost base isolation system as an alternative to the earthquake-resistant design techniques in developing countries.

1.2 Base isolation

Base isolation is the technique to reduce the seismic demand on structures instead of increasing the seismic-resistant capacity of the structures. This technique serves to uncouple the structure from the ground and thereby protecting it from the damaging effects of earthquake motions. This uncoupling is achieved by supporting the structure on an isolation system with considerably horizontal flexibility so that during an earthquake, when the ground vibrates strongly under the structure, only moderate motions are transmitted to the superstructure itself. The support system lowers the natural frequency of the structure so that it falls below the predominant frequency content of the earthquake. When frequency is low, the accelerations induced in the structure are decreased and the damaging effects of the ground motion on the structure are reduced. Meanwhile, the increased period of the isolation system, results in large displacements across the isolation interface which shall be within an acceptable limit.

Elastomeric bearings, sliding and hybrid systems are the most widely used seismic isolation devices. The most commonly used device to achieve a horizontal flexibility is the elastomeric bearing system. The elastomeric bearings consist of multiple layers of elastomer and steel shims, which carry the gravity load of the superstructure and simultaneously provide the horizontal flexibility to reduce the level of seismic forces transmitted to the superstructure. As already mentioned the reason behind the popularity of the elastomeric bearings is the restoring force provided by the elastomeric material. Sliding isolation systems work by placing a low friction material beneath the superstructure, thus by allowing the entire structure to move at the base level as a rigid body under a seismic loading. A hybrid system simply uses both elastomeric and sliding bearings to achieve the desired performance. Other isolation systems that are being used include elastomeric bearings coupled with devices to provide additional energy dissipation.

The isolation system needs four basic principal features to be effective. Firstly, the system needs to have sufficient lateral flexibility to lengthen the period of the structure to adequately reduce the seismic demand on the structure. Secondly, the lateral displacement of the system needs to be within a acceptable limit, which is achieved by energy dissipation in the isolator itself or by using supplemental damping system. The third feature is the high initial horizontal stiffness to assure the superstructure is not adversely affected by service loads such as wind and vibrations caused by minor earthquakes. The fourth and the last requirement is the vertical stiffness of the isolation system which should be sufficiently high to protect the rocking motion of the superstructure.

1.3 Base isolation systems

Elastomeric, sliding and hybrid systems are the most widely used seismic isolation devices. Elastomeric bearings system works by deforming in shear and dissipate energy either through the rubber alone or in conjunction with a lead core. The elastomeric bearings system is an attractive device for seismic isolation as the elastomeric material provides a restoring force. Sliding isolation systems works by placing a low friction material beneath the superstructure, thus allowing the entire structure to move at the base level as a rigid body under seismic loading. In the past, this had been achieved simply by placing materials such as sand or talc beneath the structure. A hybrid system simply uses both elastomeric and sliding bearings system to achieve the desire performance.

1.3.1 Elastomeric bearing system

Elastomeric bearings have been used for several decades are the most common type of devices used for base isolation. Elastomeric isolation bearings are introduced between the superstructure and the substructure to provide lateral flexibility and energy dissipation. The lateral flexibility leads to a fundamental period of the base isolated structure that is much longer than both its fixed base period and the predominant periods of the ground motion. These types of rubber bearings consist of rubber and steel plates bonded together in multiple layers as shown in Fig. 1.2. The steel shims serve to provide the required vertical stiffness as well as preventing the elastomeric bearing from bulging under pressure induced by the weight of the structure. There are two main types of steel reinforced elastomeric bearings. The first is layered elastomer and steel, while the second is a lead rubber bearing which was invented in New Zealand in 1975, Fig 1.3. The purpose of added lead plug is to provide an initial stiffness to satisfy the serviceability loads, such as wind and of small amount of ground vibration caused by minor earthquakes.

Generally, elastomeric bearings have low damping value, approximately 2-3% of critical damping [5]. Therefore, it was necessary to increase the damping properties of the elastomer to keep the lateral displacement within an acceptable limit which resulted in high damping rubber bearings.

Figure 1.2 Steel laminated elastomeric bearings

Figure 1.3 Lead rubber bearing

1.3.2 Sliding system

The principle behind the sliding system consists of cutting off the load transmission path of the structure. The sliding interfaces provide a discontinuity between the ground motion and the superstructure and limit the transfer of shear forces to the superstructure. Two types of sliding systems are available; namely, the sliding isolation system and friction pendulum system as shown in Fig 1.4. Both types of isolators have been used in several projects around the world for new and existing construction, but remain less popular compare to elastomeric bearings. To overcome the lack of restoring capability of sliding system, friction pendulum system was developed. The friction pendulum system provides strength and stability that exceed those of rubber bearings. Its properties are not affected by aging and temperature.

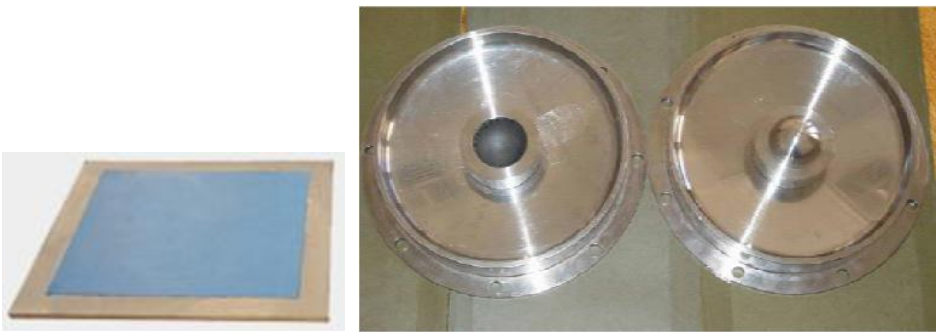

Figure 1.4 Sliding bearing and friction pendulum systems

1.4 History and application of base isolation

The idea of protecting building structures from damaging effect of earthquakes through base isolation system has a long history. The first documented innovative design seems to belong to Johannes Avetican Calantarients (1909), an English medical doctor, proposing construction of building on a layer of fine sand, mica and talc, that would allow the building to slide in case of strong earthquake [5].

The isolation system was first considered as a seismic-resistant design strategy by the Italian government after the great Messimo-Reggio earthquake of 1908, which killed about 160000 people in unreinforced masonry buildings. Almost all of the buildings of this type were collapsed [2]. The commission formed by Italian government at that period suggested two alternative earthquake-resistant design methods; namely, isolate the building from ground by either interposing a sand layer in its foundation or using roller under the column to allow the building to move horizontally, the second approach involved a fixed base design with height limitations and a lateral force design requirements. The latter approach was recommended for implementation.

In the severe Indian earthquake of Dhubai (1930) and Nepal-Bihar (1934), it was observed that the small masonry buildings which had freedom of rigid body displacement survived the earthquake while other similar but fixed at base were destroyed [6]. Based on these observations and because small masonry buildings cannot be isolated cost-effectively using elastomeric bearings, a sliding system was proposed by Arya [6]. Considerable analysis was done on this approach, and an experimental program using a shock-type shake table was carried out and demonstrated the effectiveness of the approach [5].

The first case of a building structure being isolated using elastomeric bearings was the Pestalozzi elementary school completed in 1969 in Skopje in the former Yugoslavia [2] which is shown in Fig. 1.5. The bearings were solid unreinforced natural rubber block. The lack of reinforcement resulted in equal order of horizontal and vertical stiffness, making the structure susceptible to rocking type of response. About the same time, Yokohama Rubber Co., Japan developed and used the steel rubber laminated bearings shown in Fig. 1.6 [8]. The unreinforced rubber bearings of Pestalozzi elementary school were replaced with high damping rubber bearing in 2010 [7]. The present elastomeric bearings are produced by using the reinforcement

plates placed between the layers of the elastomer, in order to increase the vertical stiffness which ultimately protects the rocking motion of the superstructure. It is almost three decades that base isolation has become feasible and practical solution for seismic mitigation of building structures through the use of isolation devices. Base isolation is now an accepted seismic design solution in many seismically active areas of the world [5].

Figure 1.5 The first isolated building using rubber bearings: Pestalozzi elementary school, Skopje

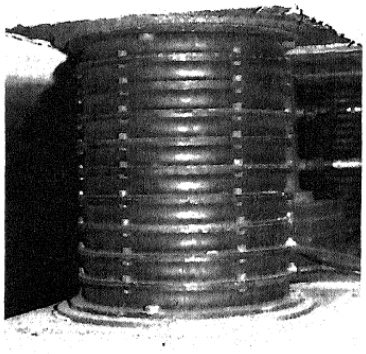

Figure 1.6 Steel rubber laminated bearing by Yokohama Rubber Co., 1969

Currently, most widespread use of seismic isolation is in Japan. At present, there are more than 2000 buildings constructed using this approach [9]. The majority of the buildings use natural

rubber bearings. One of the largest base isolated buildings in the world is the six-story West Japan Postal Savings Computer Center which is located in Sanda, Kobe Prefecture [2]. This buildings experienced severe ground motion during the 1995 Kobe earthquake. The peak ground acceleration under the isolators was 0.41g and was reduced by the isolation system to 0.13g at the sixth floor [2]. There was no damage to the isolated building; however, a fixed-base building adjacent to the computer center experienced some damage. The building is shown in Fig. 1.7. The recent 2011 Tohoku earthquake in Japan, confirmed once again the effectiveness of base isolation system. A 29-story reinforced concrete base isolated building shown in Fig. 1.8 remains structurally undamaged during the strongest 2011, Tohoku earthquake, Japan [10].

Figure 1.7 West Japan Postal Savings Computer Centre in Sanda, Kobe, Japan

Base isolation has been extensively used in United States and New Zealand. Some of the examples in United States are the Foothill Communities Law and Justice Center, University of Southern California teaching hospital, San Francisco City Hall, U.S. Court of Appeals, Oakland City Hall and similarly, in New Zealand, William Clayton building in Wellington, New Zealand Parliament House etc. In the recent years, Armenia is also becoming one of the countries adopting base isolation systems. Armenia is the only developing country where seismic isolation is highly developed for apartment buildings, schools and hospitals. There are about 33 buildings have already been installed seismic isolation devices [11].

Figure 1.8 29-story base isolated reinforced concrete building survived during 2011 Tohoku earthquake, Japan without structural damage

Figure 1.9 43-story high rise condominium base isolated building, Japan [12]

One of the examples of base isolated residential building is the Rapolla house shown in Fig. 1.10. The base isolation of low-rise residential building was completed in southern Italy at Rapolla [13]. This building is a three-story reinforced concrete frame structure with brick infill masonry walls. The building and used elastomeric bearing is shown in Fig. 1.10. The isolation

bearings are the high damping rubber bearings and a mixed type with sliding bearings. This building contains the lateral load testing facility itself. The purpose of that project was to demonstrate the effectiveness of base isolation system in case of low axial pressures on elastomeric bearings. The author mentioned that the building successfully withstands the design displacement during the field tests. This research shows that the base isolation system is effective for low-rise residential buildings.

In this chapter, it is also tried to show that the use of base isolation technique is widespread in the context of type of buildings. The base isolation technique can be adopted for high-rise apartments to low-rise residential buildings as illustrated in Figs. 1.8, 1.9 and 1.10. These buildings are the examples of feasibility and attractiveness of earthquake-resistant design techniques using base isolation.

Figure 1.10 Three-story base isolated building with special mixed bearings (HDRB + Slider), Rapolla, Italy

1.5 Objective of the research

There is an increasing interest in applying seismic isolation technology to public housings, schools and hospitals in the developing countries where the replacement of cost due to earthquake damage could be significant [14]. In recent years, several practical techniques for achieving base isolation and a variety of energy dissipating devices have been developed and implemented around the world. Due to the size, weight and incurred cost of the available

seismic isolation devices, it is almost out of reach in the developing countries. This research work proposes an alternative seismic isolation system particularly suitable for developing countries, making use of used tire rubber. The primary objective of the research is to develop a base isolation system which shall be effective in reducing the seismic demand on structures, easily available materials at an affordable cost. Another issue is the domestic production of the elastomeric bearings so that application encouragement to the public is possible. This type of base isolation system is intended to be used in low-rise residential buildings, school buildings and public buildings of the developing countries.

The isolation system needs to be demonstrated through a series of experimental tests as well as analytical studies. The first objective of the research is to investigate the material properties of the purposed base isolation system. The second objective of the research is to carryout experimental and analytical investigations on specimen isolation bearings in order to identify the behavior of the proposed seismic isolation with vertical compressive and cyclic shear loadings. These results have to be compared with the relevant code provisions to check the viability of the purposed seismic isolation system. The third objective of the research is to evaluate the dynamic response characteristic of the purpose base isolation system. This part of study has to conduct by means of pseudodynamic tests and nonlinear time history analysis. In nonlinear time history analysis, pairs of horizontal components of earthquakes have to be used to study the effect of bidirectional seismic excitations. The other important objective of the research is to identify the stability condition of the individual bearings as well as whole isolation system including building structure. This part of study is mainly focused to identify the axial load and corresponding shear deformation capacity of the layer-bonded STRP bearings.

1.6 Scope and outline of the dissertation

This research seeks to develop low-cost base isolation system using STRP by means of experimental tests and analytical studies. The following outline describes the scope and structure of the dissertation.

To evaluate the currently available base isolation devices in terms of availability, seismic performance and incurred cost, a review of currently available seismic isolation devices are presented in Chapter 2. In chapter 3, fabrication process of STRP as well as layer-unbonded STRP bearings is presented. In addition, complex material properties of rubber are investigated.

A feasible and efficient procedure for determining the hyperelastic material properties of rubber is described in this chapter. A brief discussion about the gas chromatography analysis is also presented.

Chapter 4 contains the experimental test and finite element analysis (FE analysis) of layer-unbonded STRP specimen bearings. This chapter describes in detail about the vertical compression and shear loading tests to compute the mechanical properties of the layer-unbonded STRP specimen bearing including effective stiffness and damping ratios. The FE analysis results are compared with the experimental test results to validate the finite element model. In chapter 5, the experimental tests and FE analysis of layer-bonded STRP specimen bearings is presented. The methodology used in this chapter is similar to that of the chapter 4 and only the difference is the type of specimen bearings used.

Chapter 6 presents the basic concept of design of individual STRP bearings, numerical modeling of STRP bearings including superstructure. In addition, the chapter describes about the pseudodynamic tests of base isolated building using STRP bearings subjected to El Centro earthquake excitation which is commonly considered as a standard input excitation. The main purpose of the chapter is to validate the analytical results by conducting pseudodynamic tests. Comparisons are also made for base isolated and fixed base buildings to evaluate the seismic performance of the purpose seismic isolation system. Chapter 7 presents a brief description about seismic isolation system design and dynamic analysis of the base isolated structure. In this chapter, a basic concept of seismic performance analysis of base isolated buildings subjected to bidirectional seismic excitations is presented. This chapter describes in detail about the seismicity of the site, scaling of ground motion records, design of isolation system and nonlinear direct integration time history analysis. The stability of the individual bearing as well as whole isolation system is discussed in Chapter 8.

Finally, some conclusions and recommendations for the further research on STRP bearings are presented in Chapter 9.

References

[1] Hamid Toopchi-Nezhad, Michael J. Tait, Robert G. Drysdale. Testing and modeling of square carbon fiber-reinforced elastomeric seismic isolators. *Structural Control and*

Health Monitoring, 2008, Vol. 15(6), pp: 876-900.

[2] James M. Kelly, Dimitrios A. Konstantinidis. Mechanics of rubber bearings for seismic and vibration isolation. John Willey and sons, Ltd. 2011.

[3] Peng Pan, Dan Zamfirescu, Masayoshi Nakashima, Nariaki Nakayasu, Hisatoshi Kashiwa. Base-isolation design practice in Japan: Introduction to the post Kobe approach. *Journal of Earthquake Engineering*, 2005, Vol. 9(1), pp: 147-171.

[4] James M. Kelly, Dimitrios Konstantinidis. Low-cost seismic isolators for housing in highly-seismic developing countries. *10th World Conference on Seismic Isolation, Energy Dissipation and Active Vibrations Control of Structures*, Istanbul, Turkey, 2007,May 28-31

[5] Farzad Naeim, James M. Kelly. Design of seismic isolated structures from theory to practice. John Willey and sons, Inc. 1999.

[6] A. S. Arya. Sliding concept for mitigation of earthquake disaster to masonry buildings. Proc. of 8th World Conference on Earthquake Engineering, San Francisco, CA, 1984, Vol. 1984.

[7] Mihail Garevski. Development, production and implementation of low cost rubber bearings. Earthquake Engineering in Europe, Geotechnical, *Geological and Earthquake Engineering*, 2010, Vol. 17(5), pp:411-437

[8] Masanori Izumi. Base isolation and passive seismic response control. *Proc. of Ninth World Conference on Earthquake Engineering*, August 2-9, Tokyo-Kyoto, Japan, 1988, Vol. 8, pp: 385-396.

[9] Nagahide Kani. Current state of seismic isolation design. *Journal of Disaster Research*, 2009, Vol. 4(3), pp: 175-176.

[10] Reiji Tanaka. Quick reconnaissance report of east Japan earthquake disaster. Tohoku Institute of Technology, March, 2011.

[11] Mikayel Melkumyan. Armenia is the one of the world leaders in development and application of base isolation technologies. American University of Armenia (AUA), Engineering Research Center (ERC), Yerevan, Armenia, 2006.

[12] http://www.okumuragumi.co.jp/en/technology/building.html

[13] Franco Braga, Michelangelo Laterza. Field testing of low-rise base isolated building. *Engineering Structures*, 2004, Vol. 26(11), pp: 1599-1610.

[14] Hing-Ho Tsang. Seismic isolation by rubber-soil mixtures for developing countries. *Earthquake Engineering and Structural Dynamics*, 2007, Vol. 37 (2), pp: 283-303.

2

Literature review

This chapter presents a summary of the previous studies that try to address the application aspects of building isolation with particular focus on the cost-effective seismic isolation devices applicable to structures in developing countries. Experimental and analytical studies conducted on design, manufacturing and response characteristics of different types of elastomeric bearings are elaborated. Finally, brief discussion about the STRP and its issues related to the production and application aspects is also presented.

2.1 General

The introduction of seismic isolation system as a practical tool has provided a rich source of experimental and analytical work both in the dynamics of the isolated structural systems and in the mechanics of the bearings themselves. Many studies have discussed and considered seismic isolation devices particularly focusing on laminated rubber bearings. These studies include various kinds of isolation systems and experimental studies on their performances, performance of building structures with their isolation system in earthquake excitation, shaking table tests of scaled model structures mounted on isolation devices and numerical studies of response of simulated structures with isolation systems. Seismic isolation reduces the response accelerations at the expense of relatively large base displacements when compared to the conventional fixed base building. To accommodate the lateral displacement, sufficient moat (gap) between the isolated and adjacent buildings is necessary.

The concept of introducing base isolation systems to mitigate the seismic effects is a well-known technique and development of many practical base isolation devices has already been done. Majority of the isolation devices are developed using rubber and steel shims which

includes natural rubber bearings, lead rubber bearings, high damping rubber bearings and sometime mix of these [1]. Although the base isolation showed its effectiveness, the technology is still perceived as expensive and difficult to implement in common buildings of the developing countries. In order to apply seismic isolation system for common buildings and public housing, cost and weight of the isolators must be reduced [2]. In addition, the availability of the isolation devices plays an important role in their application. Thus, in the recent years a new approach emerges in the research field and this approach consists in developing a low-cost base isolation system in order to extend the use of this earthquake-resistant design technology in developing countries. In the following, only the research works promising towards the development of cost-effective isolation systems are reviewed.

2.2 Review of some recent research works

James M. Kelly, Dimitrios Konstantinidis (2007) [3] conducted a research on standard bridge bearings to produce low-cost seismic isolators for application in developing countries. In this research work, the authors mentioned that the problem with adopting seismic isolation system in developing countries is that the conventional isolators are large, heavy and expensive. Each isolator can weight one ton or more and cost as much as $10,000. To extend this valuable earthquake-resistant strategy to housing and commercial building, it is necessary to reduce the weight and cost of the isolators. That research work was carried out to study the feasibility of using standard thermal expansion bridge bearings as light weight low-cost elastomeric isolators for application to housing, schools and other public building in highly seismic areas of the world. In that research work, the authors tried to reduce the weight and cost of the isolators by using thinner steel plates. Another interesting factor of the research was to exclude the thick steel end-plates which could further reduce the cost of isolators. The application of seismic isolators between the superstructure and substructure was without any connection system. By conducting the experimental as well as FE analysis, the authors concluded that these types of isolators can be used as low-cost seismic isolation devices. The steel laminated elastomeric isolators used in that study is shown in Fig. 2.1.

Kelly et al. (2007) conclude that the weight and the cost of isolators is reduced by using thinner steel reinforcing plates, no end-plates and no bonding to the support interfaces, thereby offering a low-cost light weight seismic isolation system for housing and public buildings in developing countries. The availability of these types of seismic isolators in developing countries was not

considered in that study. Kelly et al. (2007) mentioned that the cost of proposed elastomeric isolators is in the hundreds of dollars as compared to the cost of conventional isolators in the thousands of dollars. In addition, the cost of steel laminated elastomeric isolators is mainly due to the process of preparing steel plates and bonding them to rubber layers which is labor intensive. It seems necessary to reduce the materials and labor cost to produce the low-cost seismic isolators for application in common buildings of the developing countries.

Figure 2.1 Steel laminated elastomeric bearing without fastening system

James M. Kelly, Shakhzod M. Takhirov (2002) [4] conducted research on fiber-reinforced elastomeric bearings to replace the steel plates by fiber reinforcement so that cost of elastomeric bearings could be reduced. The authors put their particular attention in reducing the weight and cost of the isolators. The authors mentioned that the primary weight in an isolator is due to the reinforcing steel plates, which are used to provide the vertical stiffness of the rubber steel composite element. A typical rubber isolator has two large steel end-plates (around 1 inch thick) and 20 thin reinforcing steel plates (1/8 inch thick). The high cost of producing the seismic isolator results from the labor involved in preparing the steel plates and laying-up of the rubber sheets and steel plates for vulcanizing bonding in a mold. The purpose of that research was to suggest that both the weight and cost of isolators can be reduced by eliminating the steel reinforcing plates and replacing them with fiber reinforcement. The weight reduction is possible as fiber materials are available with an elastic stiffness that is of the same order as steel. Thus the reinforcement needed to provide the vertical stiffness may be obtained by using a similar volume of very much lighter material. The cost savings may be possible if the use of fiber allows a simpler, less labor-intensive manufacturing process. The elastomeric isolator used in that research work is shown in Fig. 2.2.

In the context of the developing countries, the availability of fiber reinforcement and incurred cost plays an important role in their applications. The authors did not mention about the cost of fiber reinforcement but these isolators are still expensive in the context of poor families of the developing countries.

Figure 2.2 Deformed state of fiber reinforced elastomeric isolator at 100% shear strain

W. Taniwangsa, J. M. Kelly (1996) [5] conducted research to produce cost-effective elastomeric bearings and implemented through demonstration buildings. The objective of that research was to develop and promote an effective but relatively low-cost seismic isolation system as an alternative to the traditional earthquake-resistant construction techniques in developing countries. The study was carried out by constructing a four-story reinforced concrete building, supported on high damping natural rubber bearings, in Java, Indonesia. Taniwangsa et al (1996) mentioned that, for any innovative system to be widely adopted in developing regions, it must be cost-effective and technically efficient. In that research, high damping natural rubber bearings were used with recessed connection system between the superstructure and substructure. The deformed state and connection system of the bearing is shown in Fig. 2.3. This technique reduces the fastening cost of isolators but still needed thinner end-plates. The bearings were tested in cyclic shear loadings and three dimensional time history analysis was also carried out. Taniwangsa et al (1996) conclude that the well designed, fabricated, installed and maintained high damping rubber isolation system can be an excellent choice in providing protection from strong earthquake for public buildings, such as schools and hospitals.

In that research work, the cost reduction is achieved only by avoiding the fastening system with contact supports. These types of seismic isolators consist of steel laminated with high damping rubber. Cost of individual high damping rubber bearing at that period was about $600. As

mentioned above, the cost of labor involved in vulcanization process and cost of steel plates used to make recess connection system still adds noticeable cost to the seismic isolator. Further improvement to reduce the cost of seismic isolation bearings is essential.

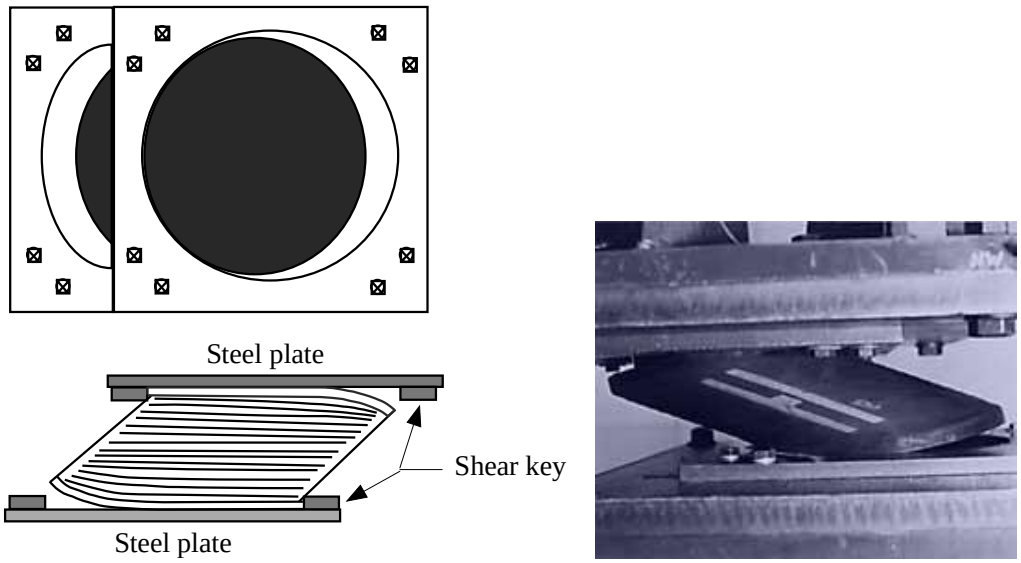

Figure 2.3 Deformation pattern and deformed state of high damping rubber bearing with recess connection system

Hamid Toopchi-Nezhad et al. (2008) [6] manufactured and tested fiber reinforced elastomeric bearings applicable to low-rise residential buildings. That research also intends to develop cost-effective seismic isolators applicable to ordinary housing and commercial building. That research work was carried out using fiber reinforced elastomeric isolators, which utilize fibers as the reinforcing materials instead of steel plates. Hamid Toopchi-Nezhad et al. (2008) mentioned that the steel reinforced elastomeric bearings are typically large, heavy and expensive. Due to these reasons, their application as a superior earthquake-resistant strategy is primarily justified for large and expensive buildings. The potential cost savings exist if the steel plates are replaced with other material having approximately the same order of elastic stiffness as steel, so that the construction process of bearings becomes easier and less labor intensive. Fiber reinforced elastomeric bearings have several advantages over traditional steel laminated elastomeric bearings including superior damping properties, lower manufacturing cost, light weight and the possibility of being produced in long rectangular strips. In order to reduce the cost of isolators, authors carried out experimental test without having the fastening system with contact supports as shown in Fig. 2.4. The tested isolators were loaded only up to 1.6MPa axial

pressure. It appears that the design axial load capacity of the isolator is low as compared to the anticipated weight of a low-rise building structure.

Figure 2.4 Deformed state of fiber reinforced elastomeric isolator at 200% shear strain

Mihail Garevski (2010) [7] conducted research on high damping rubber bearing by reducing the size and weight of the bearings. That research was particularly focused to replace the existing unreinforced rubber bearings of the Pestalozzi elementary school building which was the first building isolated with rubber bearings. The author describes that the base isolation technique has rarely been used in developing countries due to non-existence of domestic production of bearing and high cost of the bearings produced in the developed countries. In some of the countries as Indonesia, Iran and Algeria, there have been some attempts to popularize this technique through development of low-cost bearings and their installation in demonstration structures, but still no attempts for domestic production has been made and hence there hasn't been any mass application of such bearings. In that research, the author used 2mm thick steel shims and 10mm thick steel end-plates and the vulcanization process was similar to steel laminated rubber bearing production. The cost reduction was achieved only by reducing the size of the bearings which were 450mm in diameter and 228mm in overall thickness and focused was to promote domestic production which further reduces the transportation cost. The final conclusion is the production of rubber bearings is not complex and that it is possible to be carried out in developing countries of none or little experience in production of rubber bearings. Even though the research work contributed a lot towards the domestic production but still cost reduction is needed to promote this technology in developing countries.

Figure 2.5 New rubber bearings used in Pestalozzi elementary school, Skopje

Byung-Young Moon et al. (2002) [8] compared the performance of a cylindrical carbon fiber reinforced elastomeric isolator with that of same size steel laminated elastomeric isolator. The difference between the steel plate and the fiber thickness was adjusted by using more layers of fiber and rubber in the fiber reinforced elastomeric isolator. Accordingly, bulging of the fiber reinforced elastomeric isolator was smaller than that of steel laminated rubber bearings due to the thinner layers of rubber used. Unlike other studies, where the bearings were produced without end-plates and were not bonded to the test machine during the tests, both types of bearings were bonded to thick end-plates. Byung-Young Moon et al. (2002) concluded that the performance of fiber reinforced elastomeric isolator was superior to that of steel laminated rubber bearings.

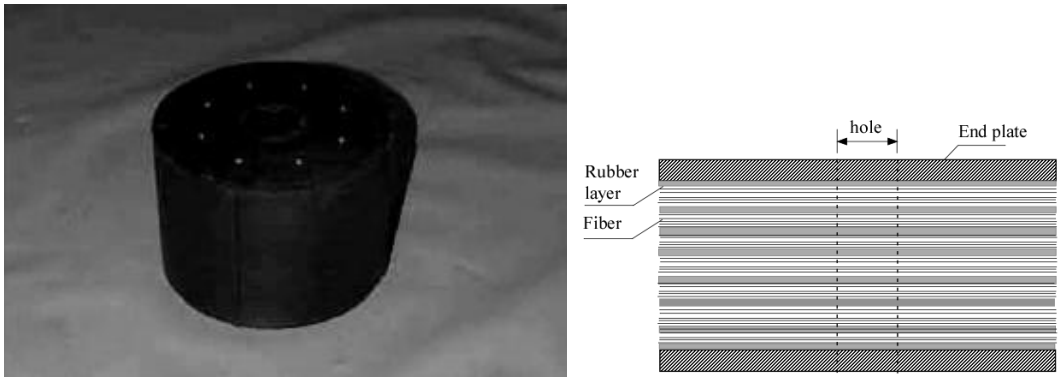

Figure 2.6 Circular fiber reinforced elastomeric isolator showing its cross section

However, additional comparative studies between fiber reinforced elastomeric isolator and steel laminated elastomeric isolator in unbonded application still needs to be carried out. Due to the

presence of thick steel end-plates, the research works seems to be more focused on performance comparison rather than reducing the cost. The cross-section and photograph of circular fiber reinforced elastomeric isolator used in that research is shown in Fig. 2.6.

Andrea Mordini, Alfred Strauss (2008) [9] proposed a new innovative isolation system for structures in earthquake regions. This contribution focuses on bearings strengthen with fibers instead of classical steel plates. The isolators were manufactured without having steel end-plates in order to reduce the cost and steel shims were replaced with glass fiber fabric. The experimental test as well as FE analysis was carried out to investigate the static and dynamic properties of the fiber reinforced isolators. That research work is almost similar to other research works conducted on fiber reinforced elastomeric bearings. These types of bearings consist of high damping rubber to achieve the required damping in the isolators. The cost reduction was tried to achieve by replacing the steel plates with fiber glass fabric and excluding the costly fastening system with contact supports which is shown in Fig. 2.7.

Figure 2.7 Deformed state of glass fiber reinforced elastomeric bearing

Ghasem Dehghani Ashkezari et al. (2008) [10] designed and manufactured fiber reinforced elastomeric seismic isolators by using woven carbon fibers and elastomer. In that research, the performance of elastomeric bearings were compared with steel laminated rubber bearings in terms of shear deformations, dynamic and mechanical characteristics including vertical stiffness, horizontal stiffness and damping ratios. The authors reported that the performance of fiber reinforced elastomeric bearings is similar to steel laminated elastomeric bearings. The main intension of the research was to produce lighter seismic isolator and simpler manufacturing process compared to the steel laminated elastomeric bearings. For that purpose, Ghasem

Dehghani Ashkezari et al. (2008) replaced the steel plates by woven carbon fibers but still needs thick end-plates in order to facilitate the bolted connection system. That research also revealed that the vertical stiffness of the fiber reinforced elastomeric bearings can be increased by increasing the shape factor of the elastomeric isolator. In addition, the researchers concluded that the cost of elastomeric bearings is reduced by avoiding the bonding process of steel plates with rubber, lighter material and simpler manufacturing process. In conclusion, it can be said that these types of elastomeric bearings are still heavy due to the presence of steel end-plates and costly fastening system with support interfaces.

Figure 2.8 1/4 scale fiber reinforced elastomeric isolator

Ahmet Turer, Bayezid Özden (2008) [11] introduced a new type of seismic isolation system using scrap tire pads (STP) as easily available material at low or negligible cost, in which, the authors produced specimen samples using car tires and tested in vertical compression and in cyclic shear loadings. The experimental tests were conducted only stacking the samples one on top of another without applying adhesive. The car tire usually contains synthetic fiber as reinforcing cords. Due to this reason, Turer et al. have mentioned that the scrap tire pad sample begins failure in compression at about 8.5MPa axial stress.

This research can be considered as innovative approach in order to produce the low-cost base isolation system but the result appears to show that the examined STP bearings were insufficient for the practical use of scrap tire rubber pad in building isolation. Fig. 2.9 contains the test setup with scrap tire pads.

Figure 2.9 Test setup with scrap tire pads

Huantian Xia et al. (2004) [12] proposed a new sliding type isolation system. In that research works, sliding materials were sand, lighting ridge pebble, polypropylene and PVC sheet and polythene membrane and the study was carried out by means of analysis and experimental test. The purpose of the research was also to achieve low-cost seismic isolation system using the domestically available materials. As mentioned in the introduction chapter, one of the key problems of sliding system is re-centering. This type of seismic isolation system adversely affects the management of utility system after an earthquake. This type of isolation system requires two levels slab on grade; one for sliding material rest and other is for the occupants of the building which again increase the cost of construction. When earthquake occurs, there is always possibility of breaking the sliding materials and the replacement of such material is not an easy work for the proposed construction shown in Fig. 2.10.

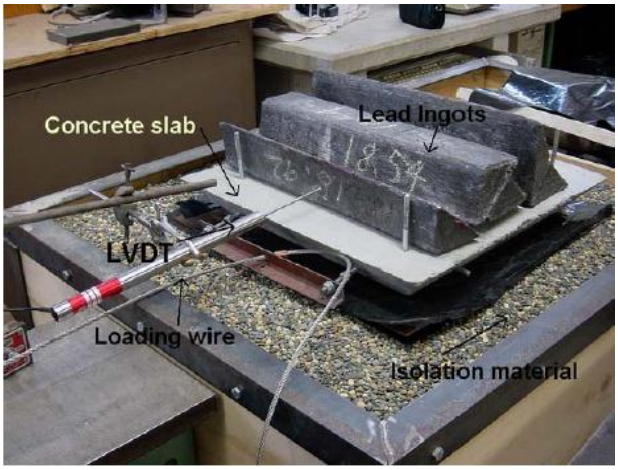

Figure 2.10 Dynamic test setup of sliding isolation system

Hing-Ho Tsang (2007) [13] proposes a seismic isolation method for developing countries using scrap tires. The proposed base isolation system has to be constructed by replacing the existing soil layer below the foundation with a designated proportion of rubber soil mixture (RSM) of thickness in the order of 10m for 10-story building as shown in Fig 2.11. The authors mentioned that, the low-cost of the proposed seismic protection scheme can greatly benefit those developing countries where resources and technology are not adequate for earthquake mitigation with well-developed, yet expensive techniques. However, researcher himself mentioned about the potential problems associated with this type of isolation system. One of the potential problems is that the structure has to be detached from the ground which is particularly not favorable in particular for small residential houses. While we concern about the cost, excavation of such a deep foundation and replacing with RSM may not be justifiable. Due to the low vertical stiffness of the mixed, there is always possibility of rocking motion of the building.

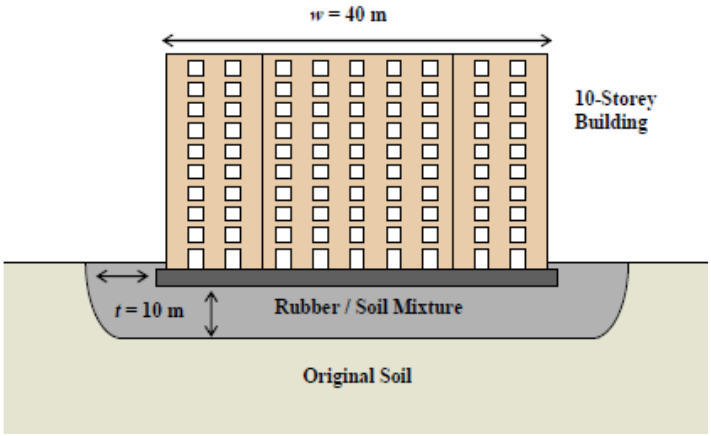

Figure 2.11 Schematic drawing of rubber soil mixture base isolation system

2.3 STRP in general

The preliminary idea of using the scrap tire for base isolation purpose is discussed by Turer et al. (2008) [11]. This research finds out the insufficiency of vertical load carrying capacity of the STPs produced by car tires. For the better performance and safety record, radial tires has been the industry standard for the last few decades. The radial tires are manufactured by using rubber and steel reinforcing cords to improve the durability and rigidity of the tread. In addition, these cords are responsible to carry the anticipated load of the truck/bus. These steel cords are

imbedded into the rubber material in the form of layers oriented in a specified angle with reference to the radial direction [14] of tire and are coated with chemical additives [15] to prevent the slip on large tensile deformation of the steel cords. The tread part of the tire is usually flat and its width varies between 162 to 240mm (truck/bus). On removing the uneven treads and carcass part of the tire, a flat piece of tire can be obtained which is termed as scrap tire rubber pad (STRP). The detail about the fabrication process of STRP specimen samples is discussed in chapter 3.

2.3.1 Application to seismic isolation

The idea of using STRP to produce seismic isolation devices is mainly come from the fact that the tires are manufactured from rubber and steel reinforcing cords. These steel reinforcing cords are expected to function similar to the steel plates used in conventional steel laminated rubber bearings. These cords shall be responsible to prevent the lateral bulging of the rubber when loaded by the weight of the structure. In addition, these reinforcing cords are responsible to provide adequate vertical stiffness of the proposed base isolation system. The required size of the bearings can be obtained by stacking the STRP in vertical layers. These layers have to be bonded together so that they can deform as a single unit during the vertical compressive and cyclic shear loadings.

It is expected that the bearings produced by using STRP can meet the principal requirements of the elastomeric bearings. The first requirement is to provide enough vertical stiffness so that the amplification of motion in the vertical direction is avoided as well as the rocking motion of the superstructure is minimized. The second requirement is to provide the required horizontal stiffness in order to achieve the desired horizontal frequency of vibration. The third requirement is to control the maximum shear strain under the designed earthquake excitation without failure. The fourth requirement is to provide sufficient damping to keep the displacements within the acceptable limits. In this regards, the study is focused to investigate the mechanical properties of the STRP and hence to check the viability of the aforementioned issues.

2.3.2 Issues related to STRP bearings

The important issues relating to the production and use of STRP for application to seismic

isolation of structures are discussed briefly.

Availability: Scrap tire are available everywhere in the world that uses transportation facilities and availability of STRP shall not be a problem.

Mechanized manufacturing process: STRP bearings have to be produced by mechanized process so that mass production can be achieved. This process can be aligned with companies specialized in tire re-processing for re-treading which is usually available everywhere even in the developing countries.

Bonding of layers: The individual layers of STRP should be bonded so that the resulted STRP bearing can function as a single unit during the vertical compressive and lateral shear loadings.

Functionality: The layer-bonded STRP bearing should withstand anticipated vertical compressive loads, designed horizontal shear loads as well as rotations around all axes.

Expected shear deformation: The shear deformation capacity of layer-bonded STRP bearings is expected to be more than 150% shear strain (based on the thickness of rubber).

Expected vertical compressive load carrying capacity: The average axial load on each of the columns of a three-story reinforced concrete building is estimated to be 330kN. The expected average axial pressure on layer-bonded STRP bearings is about 3.3-7.5MPa in order to achieve the target shear strain of 150%.

Standardization with code provisions: The mechanical properties of the proposed base isolation system have to be evaluated and compared with the relevant code provisions to check the viability of such devices in seismic isolation of structures.

Weathering effects: On the contrary of the elastomeric bearings, in which the steel shims are entirely enclosed by elastomer and is offering total protection against corrosion which is completely maintenance free, the outer part of the STRP which is cut from tread part of the tire is exposed to weathering effects, which may be affected by corrosion attack. To safeguard against corrosion, weathering proof paints can be applied on the exposed surfaces of the STRP.

Durability: Durability depends on the exposure condition. Aging and durability examination may be necessary before their practical application for seismic isolation of structures.

Incurred cost: Major part of cost of STRP bearings is due to the labor involved in cutting and layers bonding process. The materials of STRPs are available at negligible cost and hence the overall cost of STRP bearings shall be relatively lower than the commercially available seismic isolation devices. The most important features of these types of bearings are the domestic production, they do not have steel end-plates and no extra cost is required for connection system with support interfaces.

2.4 Conclusion

The aforementioned research works are striving and focused towards the development of low-cost seismic isolation system applicable to structures in developing countries. Some of the research works are encouraging to promote the seismic isolation technology by promoting the domestic production. But, we should always concentrate on the availability and affordability of earthquake-resistant design techniques to the common public of the developing countries.

The use of different fiber reinforcing materials to replace the steel plates have been investigated by [4], [6], [8], [9] and [10] and were found to be a suitable replacement, with carbon or glass fiber showing the most promising. Additional researches on the topic have shown that fiber reinforced elastomeric bearings can have performance comparable with steel reinforced elastomeric bearings. These types of seismic isolation bearings are still economically unacceptable considering the purchasing capacity of poor families in the developing countries. Thereby, it is necessary to develop base isolation devices which can be effective in reducing the seismic demand on structures and is made of easily available materials at an affordable cost. Furthermore, the use of base isolation system can be encouraged by promoting the domestic manufacturing process making use of locally available materials. For this purpose, investigation of mechanical properties and applicability aspects of the STRP bearings have been proposed.

References

[1] Peng Pan, Dan Zamfirescu, Masayoshi Nakashima, Nariaki Nakayasu, Hisatoshi Kashiwa. Base-isolation design practice in Japan: Introduction to the post Kobe approach. *Journal of Earthquake Engineering*, 2005, Vol. 9(1), pp: 147-171

[2] James M. Kelly. Seismic isolation systems for developing countries. *Earthquake*

Spectra, 2002, Vol. 18(3), pp: 385-406.

[3] James M. Kelly, Dimitrios Konstantinidis. Low-cost seismic isolators for housing in highly-seismic developing countries. *10th World Conference on Seismic Isolation, Energy Dissipation and Active Vibrations Control of Structures*, Istanbul, Turkey, 2007,May 28-31

[4] James M. Kelly, Shakhzod M. Takhirov. Analytical and experimental study of fiber reinforced strip isolators. Department of Civil and Environmental Engineering, University of California, Berkeley, PEER report 2002/11.

[5] W. Taniwangsa, J. M. Kelly. Studies on seismic isolation for housing in developing regions. *Eleventh World Conference on Earthquake Engineering*, 1996, Paper No. 261, ISBN: 008 042822 3.

[6] Hamid Toopchi-Nezhad, Michael J. Tait, Robert G. Drysdale. Testing and modeling of square carbon fiber-reinforced elastomeric seismic isolators. *Structural Control and Health Monitoring*, 2008, Vol. 15(6), pp: 876-900.

[7] Mihail Garevski. Development, production and implementation of low cost rubber bearings. *Earthquake Engineering in Europe, Geotechnical, Geological and Earthquake Engineering*, 2010, Vol. 17(5), pp:411-437

[8] Byung-Young Moon, Gyung-Ju Kang, Beom-Soo Kang, James M. Kelly. Design and manufacturing of fiber reinforced elastomeric isolator for seismic isolation. *Journal of Materials Processing Technology*, 2002, Vol. 130/131, pp: 145-150.

[9] Andrea Mordini, Alfred Strauss. An innovative earthquake isolation system using fiber reinforced rubber bearings. *Engineering Structures*, 2008, Vol. 30(10), pp: 2739-2751.

[10] Ghasem Dehghani Ashkezari, Ali Akbar Aghakouchak, Mehrdad Kokabi. Design, manufacturing and evaluation of the performance of steel like fiber reinforced elastomeric seismic isolators. *Journal of Material Processing Technology*, 2008, Vol. 197(1-3), pp: 140-150.

[11] Ahmet Turer, Bayezid Özden. Seismic base isolation using low-cost scrap tire pads (STP). *Materials and Structures*, 2008, Vol. 41 (5), pp: 891-908.

[12] Huantian Xia, J. W. Butterworth, Tam Larkin. Low-technology techniques for seismic isolation. *New Zealand Society of Earthquake Engineering Conference*, 2004, paper No. 36

[13] Hing-Ho Tsang. Seismic isolation by rubber-soil mixtures for developing countries. *Earthquake Engineering and Structural Dynamics*, 2007, Vol. 37 (2), pp: 283-303.

[14] J. Y. Wong. Theory of ground vehicle. 3rd edition, John Wiley and Sons, Inc., 2001.

[15] D. C. Prevorsek, R. K. Sharma. Role of adhesion in viscoelastic properties of rubber-tire cord composites. *Rubber Chemistry and Technology*, 1981, Vol. 54(1), pp: 72-90.

3

STRP specimen and material properties

This chapter describes in details about the fabrication process of individual STRP as well as layer-unbonded STRP specimen bearings. The main objective of the chapter is to discuss about the material properties of the STRP and their tests methods. In addition, a detail description about the hyperelastic material constants determination process is described. Finally, it also describes about the gas chromatography analysis of rubber samples in order to determine the key constituents.

3.1 Introduction

The aim of the research is to develop low-cost base isolation device for application to seismic isolation of structures in developing countries. To address this issue, the materials of the base isolation system should be easily available at an affordable cost. The rubber and the steel reinforcing cords used in manufacturing the tire are the alternative materials of the proposed base isolation system. Usually, the radial tire contains steel reinforcing cords in the form of layers oriented in specified directions [1] with respect to the radial direction of tire. The layout of cords in a single layer of STRP can be seen in Fig. 3.1 (photograph). The steel reinforcing cords are supposed to represent the steel plates used in conventional steel laminated elastomeric bearings. These steel reinforcing cords shall prevent the lateral bulging of the rubber bearings. In addition, these reinforcing cords are responsible to provide adequate vertical stiffness of the proposed base isolation system.

The objective of the study is to check the feasibility of using the STRP to develop seismic isolation devices. The feasibility study outlines the important parameters to be improved for the practical use of STRP as base isolation system. In this study, the scrap tires of bus/truck were

used to produce the specimen bearings. Only the rubber from the tread part of the scrap tire was used. The schematic representation for the production of STRP is shown in Fig. 3.2. The specimen bearings were produced by stacking the STRP layers one on top of another without applying the adhesive chemical, called as layer-unbonded STRP bearings. The detail specimen preparation procedure is described in the following chapter.

Figure 3.1 Photograph of single layer STRP showing layout of steel reinforcing cords

3.2 STRP and layer-unbonded STRP specimen

Several samples of STRP and layer-unbonded STRP bearings as shown in Fig.3.4 were fabricated for the purpose of vertical compressive and shear loading tests. Following steps describe the preparation procedure of individual layers of STRP as well as layer-unbonded STRP specimen samples:

1. The specimen samples were prepared by using recently scrap bus/truck tires
2. The STRP specimens were prepared by the companies specialized in tire re-processing for re-treading. This process is mechanized in Japan for the re-processing of tires.

Similar methodology can be adopted in developing countries to produce the STRP bearings. First of all, uneven part of the tread section was removed to make plain and smooth surface.

3. Both the side walls of the tire were cut and removed and long rectangular strip type specimen was prepared. Only the rubber along the tread part was used for the production of STRP specimen.

4. This rectangular strip type belt was cut to require size as per the designed size of rubber bearings. The maximum width of a bus/truck tire was found to be 162mm to 240mm, from which small to sufficiently large size rubber bearing production is possible.

5. Stacking of these small strips in different orientations for alternative layers can produce even larger size rubber bearings as per the requirements. The required thickness of rubber bearings were obtained by stacking one on top of another in vertical layers.

6. Original designed size of the STRP bearings were different than those used in the experimental test due to the capacity of the testing equipment available. Two STRP specimen samples of geometrical properties given in Table 3.1 were produced and tested in vertical compressive and in cyclic shear loadings.

Each layer of STRP bearing comprises the five layers of steel reinforcing cords interleaved and bonded between the layers of rubber as shown in Fig. 3.3. These steel reinforcing cords comprise a number of strands in a twisted form. The photograph including dimensions of the layer-unbonded STRP-6 bearing is shown in Fig. 3.4 (b) and the geometrical and material properties are given in Table 3.1.

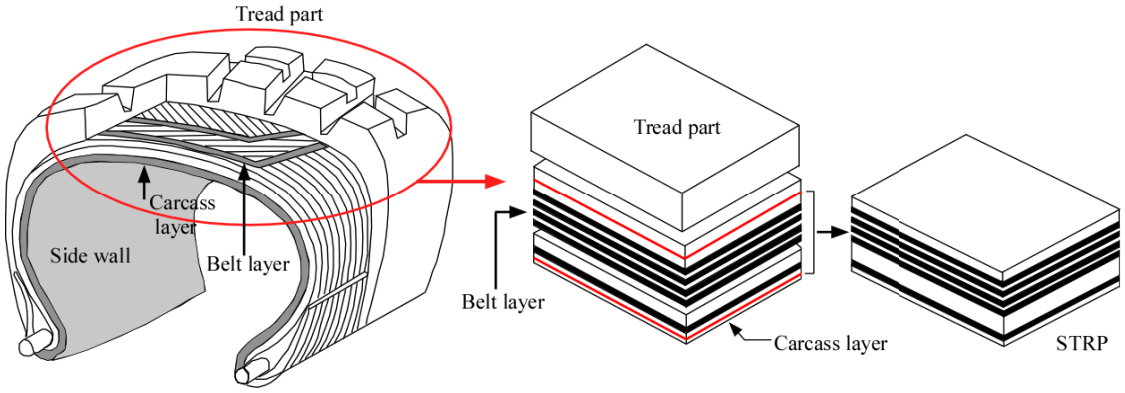

Figure 3.2 Schematics representation of STRP specimen preparation using tread part of tire

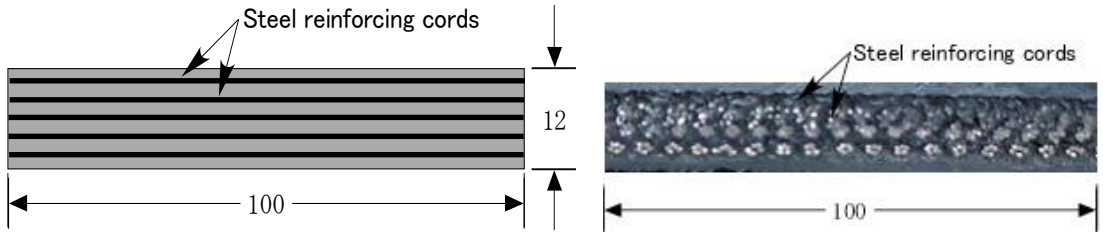

Figure 3.3 Cross section of a single layer STRP sketch and photograph

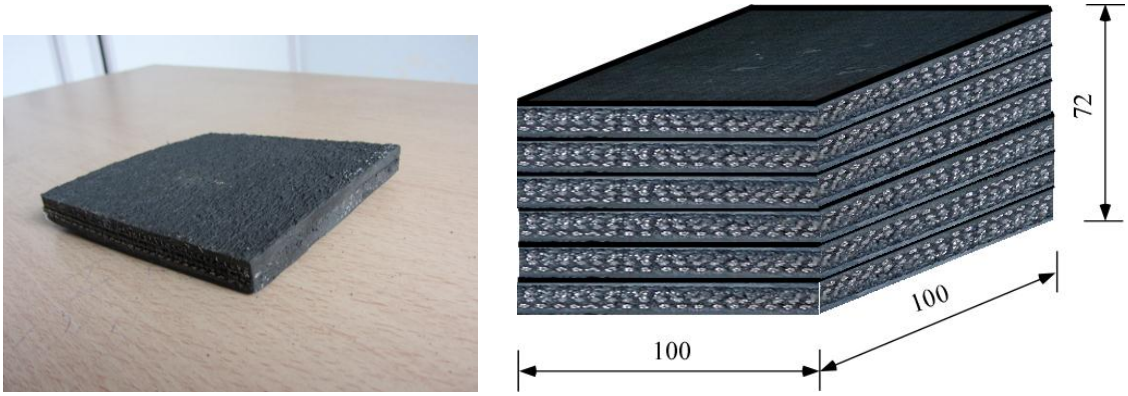

a) Single layer STRP b) Six layers STRP bearing

Figure 3.4 Photographs of STRP specimens (dimensions are in mm)

Table 3.1 Material and geometrical properties of STRP

Material properties	
Shear modulus of tire rubber G	= 0.89MPa
Poisson's ratio of steel reinforcing cords υ	= 0.30
Young's modulus of steel reinforcing cords E	= 200GPa
Geometrical properties	
Width of the STRP	= 100mm
Thickness of a single layer STRP	= 12mm
Thickness of steel reinforcing cords	= 0.4mm
Total thickness of six layer (STRP-6)	= 72mm
Total thickness of rubber	= 60mm

3.3 Material properties

3.3.1 Theoretical basis for constitutive modeling of rubber

Rubber consists of many interwoven, long chain polymers that initially are randomly oriented; therefore, rubber can be assumed to be isotropic. Also, rubber exhibits a nonlinearly elastic response up to a large strain. The loaded specimen will return nearly to its unloaded state after being stretched or compressed a great amount. Consequently, a hyperelastic model is used to characterize the rubber behavior in finite element modeling.

A hyperelastic model associates a state of strain to a unique state of stress. The strain energy potential can be defined at each point in the material based on this stress-strain relationship, and stresses can be found directly by taking appropriate derivatives of the strain energy density function. Since the material is assumed as isotropic, the strain energy potential can be written as a function of strain invariants. Among the available strain energy density functions, Mooney-Rivlin material law is well suited for most practical applications involving cord-rubber composite [2]. The strain energy polynomial is expressed as

$$W = \sum_{i,j=0}^{N} C_{ij} (I_1 - 3)^i (I_2 - 3)^j + \sum_{i=1}^{N} \frac{1}{D_i} (J_{el} - 1)^{2i} \tag{3.1}$$

where C_{ij} and D_i are the material parameters that are found from the test data, J_{el} is the elastic volume ratio, I_1 and I_2 are the first and second invariants of the green deformation tensor given in terms of principle stretch ratios and N represents the order of polynomial. In Eq. (3.1), the first summation is the contribution due to deviatoric effects and the second summation is the contribution due to volumetric effect. The earliest phenomenological theory of nonlinear elasticity was proposed by Mooney-Rivlin as (deviatoric contribution) [3]:

$$W = C_{10}(I_1 - 3) + C_{01}(I_2 - 3) \tag{3.2}$$

Although, it shows a good agreement with tensile test data up to 100% strains, it has been found inadequate in describing the compression mode of deformation. Moreover, the Mooney-Rivlin

material model expressed by Eq. (3.2) fails to account for the hardening of the material at large strains [4]. The retention of the third term in the Mooney-Rivlin strain energy density function leads to better agreement with tests data and stress-strain behavior can be described with excellent accuracy up to breaking stage of the specimen [5].

Three-term Mooney-Rivlin strain energy density function can be expressed as:

$$W = C_{10}(I_1 - 3) + C_{01}(I_2 - 3) + C_{11}(I_1 - 3)(I_2 - 3) \tag{3.3}$$

where C_{10}, C_{01} and C_{11} are the material constants known as Mooney-Rivlin material constants. These material constants have to be determined by conducting uniaxial tension tests as discussed in the following sections.

3.3.2 Uniaxial tension test

The uniaxial tension tests were carried out to engineering tensile strains up to 4.36. The uniaxial tension test is usually conducted until its failure in tension, in order to ensure that the strain energy function would adequately represent the severe engineering stresses and strains expected in the FE analysis. The main purpose of the uniaxial tension test was to validate the material model utilized in the FE analysis. In Eq. (3.2), the strain invariants are given by:

$$I_1 = \lambda_1^{\,2} + \lambda_2^{\,2} + \lambda_3^{\,2} \tag{3.4}$$

$$I_2 = \lambda_1^{\,2}\lambda_2^{\,2} + \lambda_2^{\,2}\lambda_3^{\,2} + \lambda_3^{\,2}\lambda_1^{\,2} \tag{3.5}$$

where λ_1, λ_2 and λ_3 are the principle stretch ratios in the respective directions. The stretch ratios are expressed in terms of uniaxial stretch [6].

$$\lambda_1 = \lambda \tag{3.6}$$

$$\lambda_2 = \lambda_3 = \frac{1}{\sqrt{\lambda}} \tag{3.7}$$

Equation (3.3) defines the stress-strain relationship for elastomer. The material constants C_{10}, C_{01} and C_{11} can easily be determined for linear relationship either using uniaxial tension test or compression test but for the nonlinear relationship, the determination of material constants is complicated. The model expressed by Eq. (3.2) contains only two material constants, due to this reason, the model is simple [7]. The material constants are usually determined using the uniaxial tension test, equi-biaxial tension test and planar shear test. These tests require sophisticated testing facility and data acquisition system. In case of STRP, the feasible one is the uniaxial tension test. The purpose of the uniaxial test is to validate the material constants which were used in the FE analysis of STRP specimen. The problem associated with uniaxial tension test is to prepare the specimen sample as per the ASTM or JIS standard using the used tire rubber which is quite difficult and time consuming. Vossoughi, 1995 [7] mentioned that these material constants can be evaluated from a simple test such as uniaxial tension test with minimum numbers of measurements; namely, axial stress and axial strain using first order polynomial of Eq. (3.1).

3.3.2.1 Dumbbell Specimen

Three types of rubber specimen samples are the mostly used in uniaxial tension test, namely dumbbell, parallel sided strip and ring type specimen. The dumbbell types of specimen samples are the most popular type used in uniaxial tension test of rubber like material [6]. The specimen samples were prepared by using recently scrap bus/truck tires. The uneven part of tread section was removed to make plain and smooth surface. The rubber between the tread and the steel reinforcing cords was cut using a shape knife. These flat samples were sanded to make an even surface with required uniform thickness. For this purpose, disc attached with sand paper was fitted in bench drilling machine and rotated at low speed in order to maintain the uniform sanding. Using this method, the samples of uniform thickness of 2.0 mm were prepared. These rubber specimen samples were used to prepare the dumbbell specimen samples as per the Japanese Industrial Standards (JIS No.3). The shape and dimensions of the JIS standard dumbbell shape specimen is shown in Fig.3.5. In order to prepare the dumbbell specimen as per exact shape and size, a template of the dumbbell shape and size was prepared and the rubber was cut with a sharp knife using the standard template. The photograph of dumbbell specimen is

shown in Fig. 3.6.

Uniaxial tension test has to perform on dumbbell shaped specimen. This arrangement provides for a uniform stress and strain distribution in the central gauge section, where these values are at a maximum. Thus, the specimen extends and fails under well-defined conditions. These specimens are usually prepared by direct molding of rubber compound.

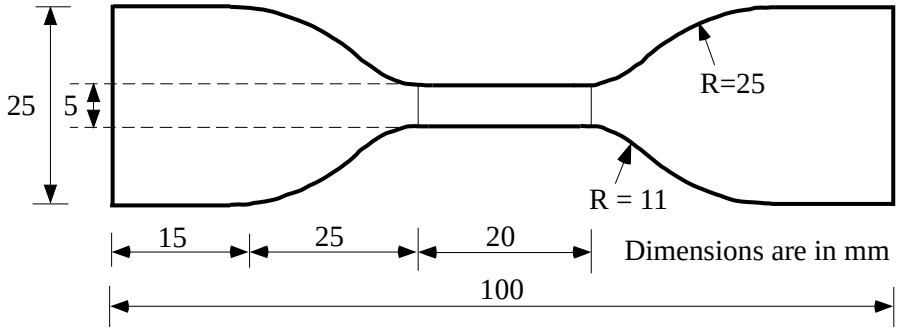

Figure 3.5 Dumbbell shape specimen with standard dimensions

Figure 3.6 Photograph of dumbbell specimen

3.3.2.2 Experimental setup and tests

All the specimens prepared for uniaxial tension test were measured before testing. The difference between the maximum and minimum thickness was less than 0.10mm for each specimen. The equipment used in the experiment was universal tensile test machine named Servo Pulser Shimadzu which is shown in the Fig.3.7 (a). This machine was controlled by Servo Controller 4830 which is shown in Fig. 3.7 (b). In all the tests, the constant rate of extension at

1mm/sec was maintained. Three samples were tested in monotonic uniaxial tension and one sample was tested in cyclic uniaxial tension with single reversed cycle at four maximum extension amplitudes of 25mm, 50mm, 75mm, and 100mm. The loads versus extension data were recorded. All the specimen samples were tested until their failure stage.

a) 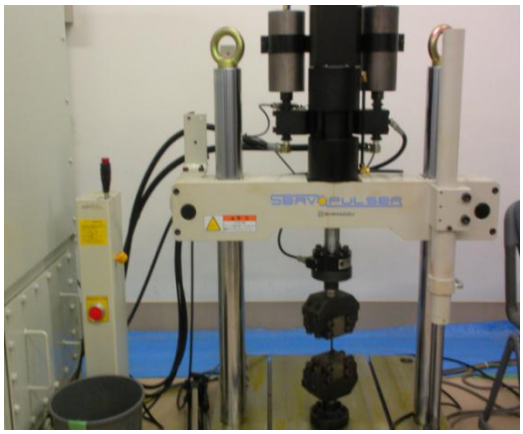 b) 

Figure 3.7 Photograph of a) tensile test equipment and b) Servo Controller 4830

a) 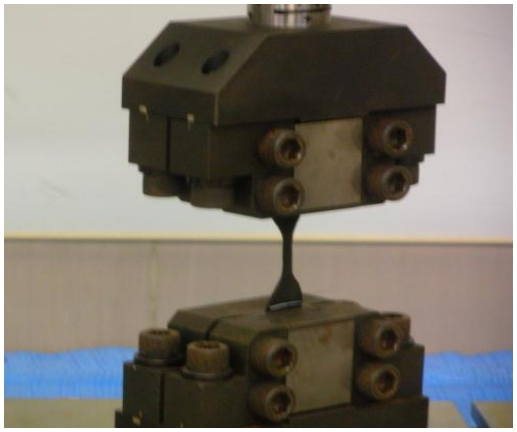 b) 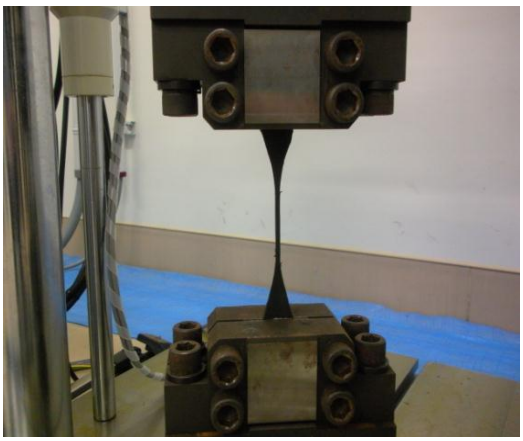

Figure 3.8 Photograph of specimen a) fitted in tensile test machine b) at breaking stage

The experimental data were recorded in excel format. The recorded data contents the uniaxial tension displacement versus tension load. These data were converted into engineering stress and strain data and were used to determine the Mooney-Rivlin material constants. Due to the nonuniform elongation near the grip, the total length between grips cannot be used to calculate the stretch ratio and engineering strain [6]. The relatively uniform stress and strain distribution occur in its central parallel portion which is 20mm. The nominal or engineering strains in the

direction of test are calculated as

$$\varepsilon = \frac{L - L_o}{L_o} \tag{3.8}$$

where ε is the strain at time t, L_o is the original length of the specimen at $t = 0$ and L is the final length at time $t = t$. The stretch ratio is expressed as $\lambda = 1 + \varepsilon$.

Similarly, the nominal or engineering stresses were calculated using the load values obtained during the uniaxial tension test and gross cross-section area of the specimen.

$$\sigma = \frac{P}{w_o t_o} \tag{3.9}$$

where σ is the axial stress, w_o is the original width of the specimen and t_o is the original thickness of the specimen.

These stress-strain data were used to determine the material constants of the rubber using least square fitting technique. The curve fitting was carried out by using MSC Marc [8], a commercially available finite element software package.

Initially, all the experimental test data were adjusted so that the curve passes through the origin. Secondly, the data were fitted using least square fit procedure which minimizes the sum of squared error between experimental and calculated stress values. Mathematically, the relative least squared error can be expressed by:

$$error = \sum_{i=1}^{N} \left(1 - \frac{\sigma_i^{cal}}{\sigma_i^{\exp}} \right)^2 \tag{3.10}$$

where N is the total number of data points, σ_i^{cal} and $\sigma_i^{\exp}$ is the calculated and experimental stresses, respectively. To minimize the residual of least squared error, higher order

Mooney-Rivlin strain energy polynomial was utilized. In this case, three terms Mooney-Rivlin material model was found to show close agreement with the experimental data fitting, then the constants were taken for modeling the STRP isolator. Results are presented in Figs.3.9 and the derived material constants are presented in Table 3.2.

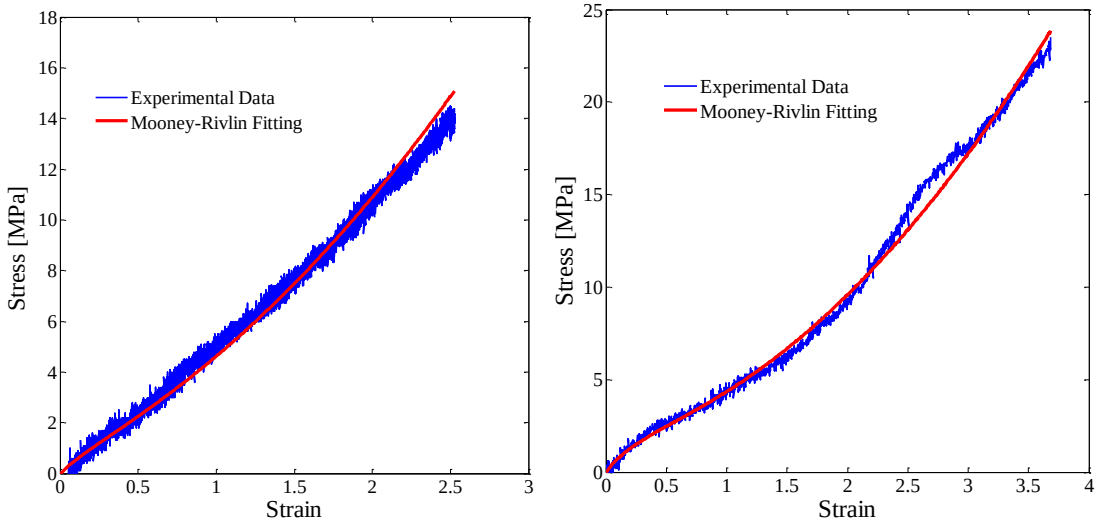

a) Monotonic tension test up to 50mm b) Monotonic tension test up to 73.65mm

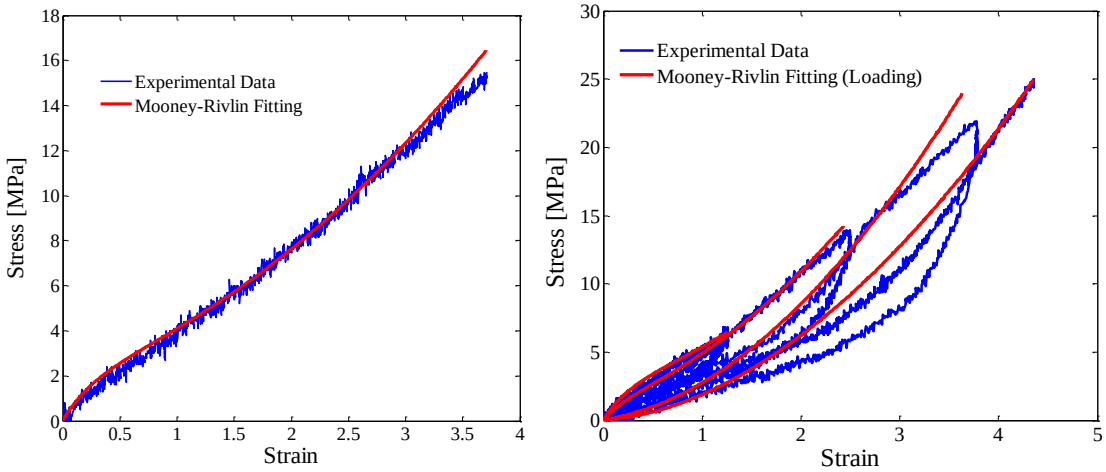

c) Monotonic tension test up to 74.2mm d) cyclic tension test up to 87.2mm

Figure 3.9 Experimental test data and Mooney-Rivlin curve fitting (a)-(c) monotonic uniaxial tension test and d) cyclic uniaxial tension test fitted only for loading history

3.3.3 Finite element analysis of dumbbell specimen

The purpose of the FE analysis is to derive the stress-strain relationship for different extension level of the dumbbell specimen. These types of data are usually required to be compared with that of the data obtained from the uniaxial experimental test. The FE analysis of the dumbbell shape rubber specimen was carried out in order to assess the uniaxial stress-strain relationship.

3.3.3.1 Modeling and analysis

The rubber was modeled using eight-node three-dimensional solid elements coded for incompressible applications with Herrmann formulation, since this element is preferred over higher-order element when used in simulating large deformation. The grip of the loading system was represented by two rigid surfaces on both ends of the specimen. In order to avoid the convergence problem and effectively simulate the specimen, adaptive stepping was used. The finite element model of dumbbell specimen is shown in Fig. 3.10. The results of FE analysis are presented in Figs.3.11 to Fig.3.13 for different levels of uniaxial stretches.

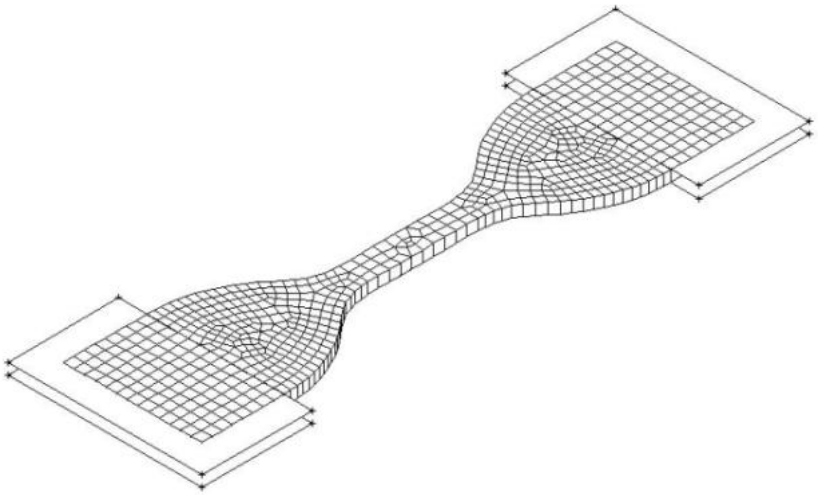

Figure 3.10 Finite element model of dumbbell specimen

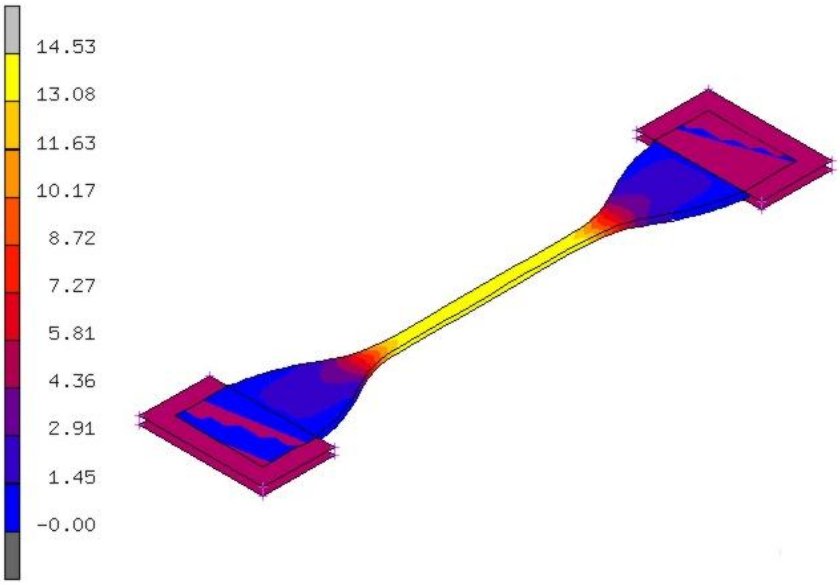

Figure 3.11 Stress (MPa) states at 50mm stretch

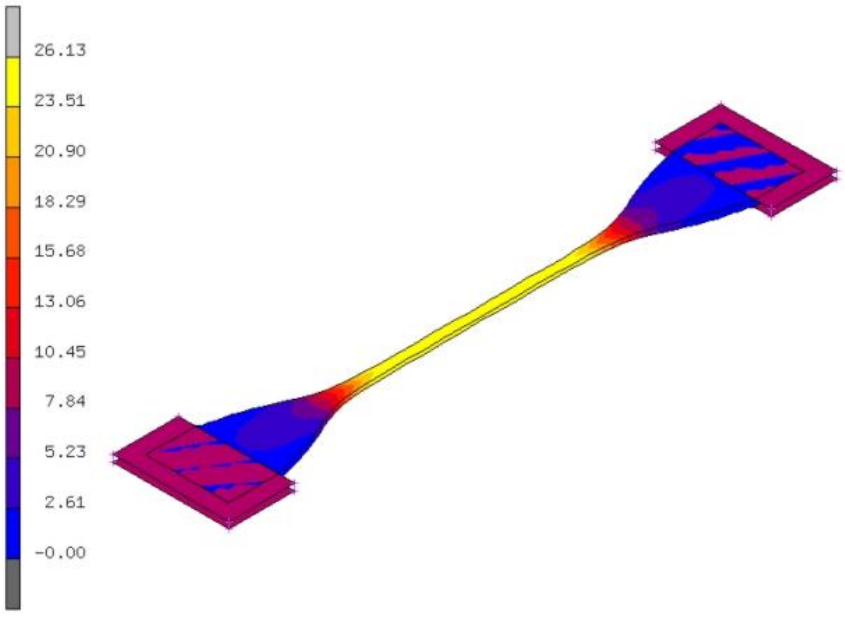

Figure 3.12 Stress (MPa) states at 73.65mm stretch

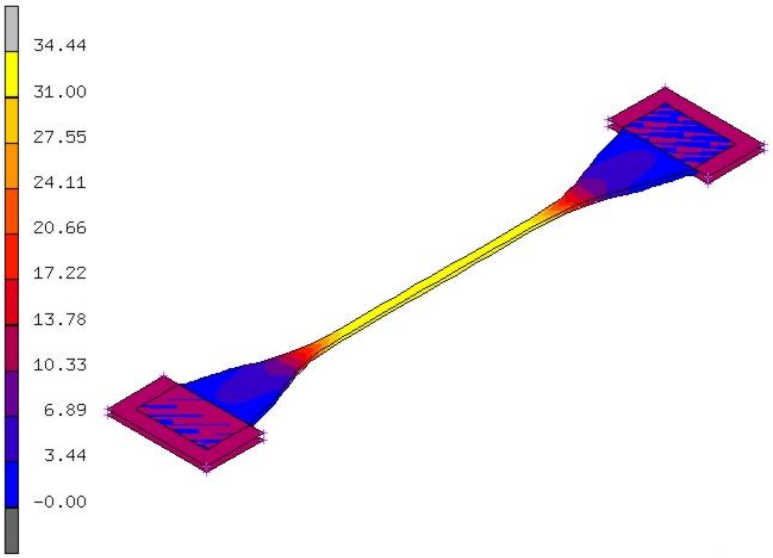

Figure 3.13 Stress (MPa) states at 87.2mm stretch

Table 3.2 Mooney-Rivlin material constants

Material constants (MPa)		
C_{10}	=	0.40
C_{01}	=	1.22315
C_{11}	=	0.18759

3.3.4 Results and discussion

Initially, individual Mooney-Rivlin constants were determined for each data set. The result of uniaxial tension tests and FE analysis of dumbbell shape specimen were compared in terms of stress-strain curve. The schematic representation shown in Fig. 3.14 shall be the useful way of comparing the results. During the comparison, small discrepancies were found between the uniaxial tension tests and FE analysis results obtained by using the two-term Mooney-Rivlin material model. Then, three-term Mooney-Rivlin material model was utilized to determine the hyperelastic material constants. With this material model, experimental data fit was carried out and compared with the test results and found close agreement. The average values of the entire specimen samples were calculated to represents the overall Mooney-Rivlin material constants. These material constants were then used in FE analysis of STRP specimen.

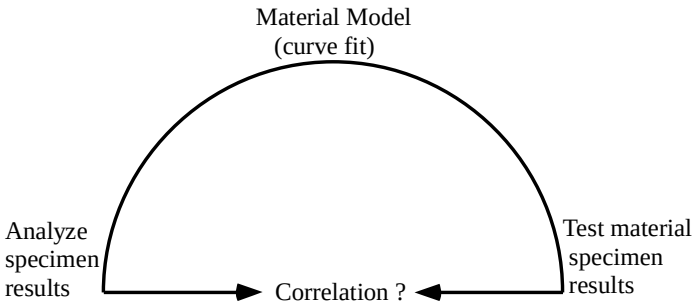

Figure 3.14 Schematic representation of experimental test and finite element analysis results comparison

These material constants are assumed to be the real representative of the STRP specimen as the dumbbell samples were prepared by using the same STRP sample that we had used in the shear loading test, even though the hyperelastic material constants are usually derived using three different deformational modes.

3.4 Gas chromatography analysis

The objective of this experiment was to separate the ingredients of tire rubber by gas chromatographic technique in order to determine the major constituents of the rubber. This technique is only applicable to volatile compounds.

Gas chromatography is a chromatographic technique that can be used to separate volatile organic compounds [9]. The sample solution is injected into a heated injection port where it rapidly volatilized. The volatilized sample is then swept via the carrier gas into the heated column where volatile compounds separate and are eluted separately. The eluted compounds are then detected in a heated detector to give an electrical signal which is amplified and recorded. The output is the plot of detector response and detention time called a chromatograph. The output (peak) is then compared with the standard calibrated curves to identify the compounds.

a)  b) 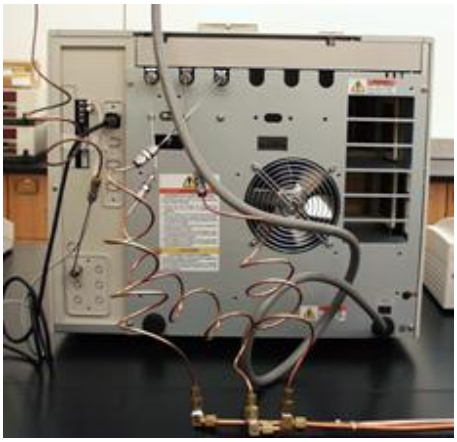

Figure 3.15 Gas chromatographic analysis equipment a) front view b) back view

The STRP specimen bearings were produced by using two different tire brands. Thus, it was necessary to identify the major constituents of both the tire brands. Two rubber samples were cut to represent each of the tire brands and gas chromatography analysis was carried out. The results obtained by gas chromatography analysis are shown in Figs. 3.16 and 3.17. The results of both the samples closely match with the natural rubber. The retention time of natural rubber is 2.564 minutes which is shown in Fig. 3.18.

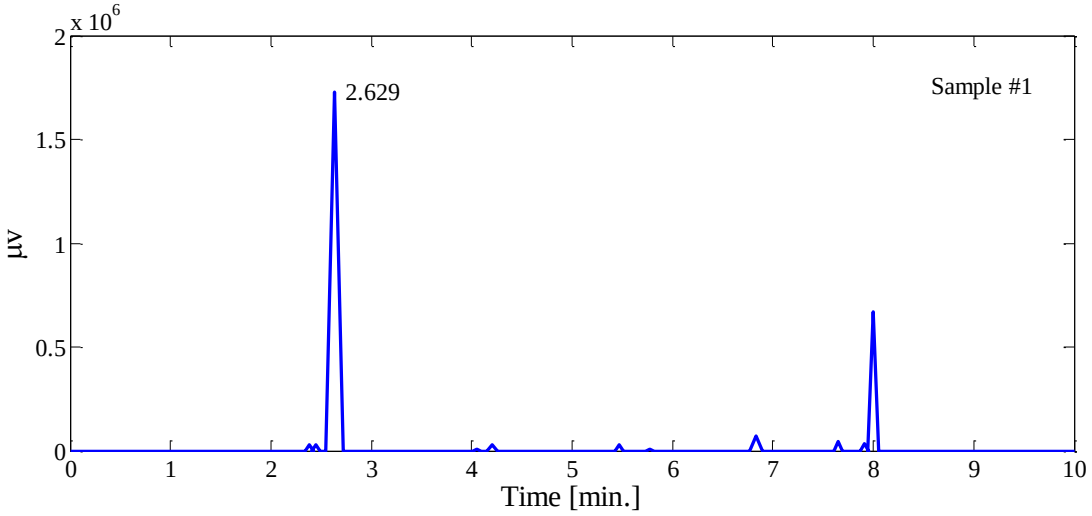

Figure 3.16 Chromatograph of rubber sample 1

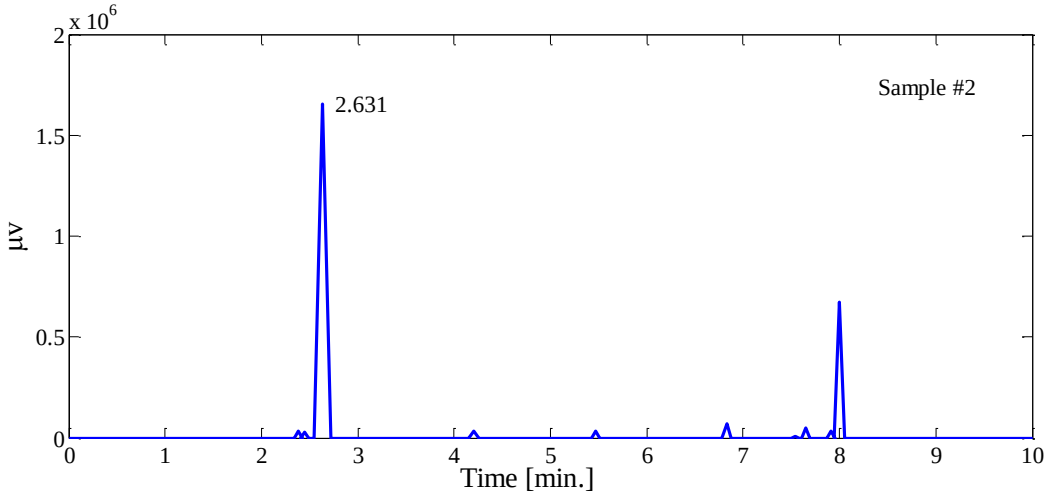

Figure 3.17 Chromatograph of rubber sample 2

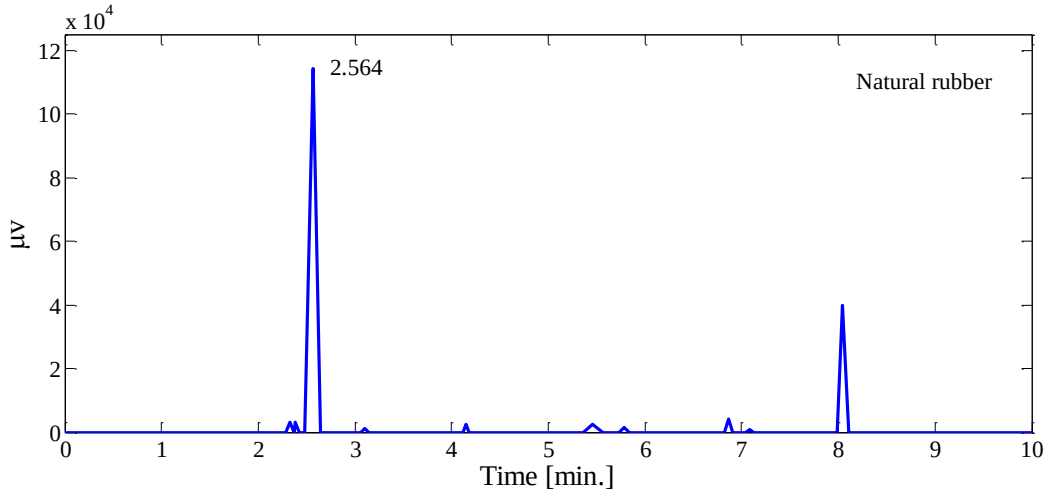

Figure 3.18 Chromatograph of natural rubber

3.5 Conclusion

The fabrication process of STRP specimen and production of layer-unbonded STRP bearings is discussed in detail. By conducting the uniaxial tension tests on dumbbell shape specimens, substantial amount of data were obtained in order to determine the hyperelastic material constants and are presented within this chapter. The average values of material constants were

computed and are presented in Table 3.2. These material constants are assumed to represent the properties of tire rubber so that accurate FE modeling of STRP bearings is possible. Similarly, valuable information about the key constituents of tire rubber was obtained by gas chromatography analysis.

References

[1] J. Y. Wong. Theory of ground vehicle. 3rd edition, John Wiley and Sons, Inc., 2001.

[2] P. Helnwein, C. H. Liu, G. Meschke and H. A. Mang. A new 3-D finite element model for cord-reinforced rubber composites-Application to analysis of automobile tires. *Finite Elements in Analysis and Design*, 1993, Vol. 14(1), pp: 1-16.

[3] MSC.Marc. Theory and user information, Vol. A Santa Ana, CA, MSC software Corporation; 2010

[4] MSC Software (2000) Nonlinear Finite Element Analysis of Elastomers, Whitepaper Santa Ana, California.

[5] Nicholas W. Tschoegl. Constitutive equations for elastomers. *Journal of Polymer Science Part-A: Polymer Chemistry*, 1971, Vol. 9(7), pp: 1959-1970.

[6] V. Vahapoglu, S. Karadeniz, and I. Yazici. Uniaxial tensile testing of rubber-like materials. *Experimental Techniques*, 2011, Vol. 35(1), pp: 17-23.

[7] J. Vossoughi. Determination of Mooney material constants for highly nonlinear isotropic incompressible materials under large elastic deformations. *Experimental Techniques*, 1995, Vol. 19(2), pp: 24-27.

[8] MSC Software (2008r1), MSC Marc 2010 and MSC Marc Mentat 2010, Santa Ana, California

[9] Ian A. Fowlis. Gas chromatography. 2nd edition London, John Wiley & Sons Ltd., 1995.

4

Experimental and analytical study of layer-unbonded STRP bearings

This chapter describes in detail about the experimental test of layer-unbonded STRP bearing and computation of mechanical properties in compression and cyclic shear loadings. In addition, a detailed description about the finite element modeling and analysis of layer-unbonded STRP is presented. The FE analysis results are compared with the experimental test results to validate the finite element model. The role of aspect ratio in shear deformation capacity is also studied by means of FE analysis.

4.1 Introduction

In this part of study, layer-unbonded STRP specimen bearings as described in chapter 3 are used. The experimental test on layer-unbonded STRP specimen is carried out for the case of unbonded application with the contact interfaces. At extreme lateral deformations, this connection system puts much lower demands on the internal bonding between the layers of STRP [1]. On the other hand, it also helps in reducing the overall cost of the seismic isolation system. This type of connection system was in practice in the early period of the rubber bearings [2]. The unbonded application of STRP bearings with support surfaces allows roll-off the contact supports during the shear deformation which creates, rollout instability and decrease in effective horizontal stiffness. The former type of phenomena is associated with the stability of the isolation system and maximum shear deformation capacity while the latter type of phenomena elongates the period of the isolation system which increases the efficiency of the isolation system provided that the stability is achieved [3].

In this study, the results of experimental test and FE analysis conducted on layer-unbonded square STRP-6 bearings are presented to investigate the performance of layer-unbonded STRP bearings. The hyperelastic material constants used in FE analysis were determined by conducting uniaxial tension tests, which is presented in chapter 3. The experimental test results were used to compute the mechanical properties of the STRP bearings including effective stiffness and effective damping ratios. The experimental test results were compared with FE analysis results in order to validate the finite element model. The results of FE analysis also provide the information about stress-strain state within the STRP bearings. These results were further compared with the relevant code provisions [4], [5] and [6] to check the viability of the layer-unbonded STRP bearings for practical use of base isolation device.

4.2 Experimental setup and tests

Figure 4.1 contains a sketch of the test setup to perform both the static vertical compression and horizontal shear loading tests. The layer-unbonded STRP-6 specimen bearing was placed between the upper and lower steel plate surfaces of the load test setup as shown in Fig. 4.1 and Fig.4.2. The vertical compressive load was applied to the specimen by the vertical hydraulic actuator through a stiff frame mounted on the floor and the reaction wall. The vertical hydraulic actuator had a maximum loading capacity of ±400kN and maximum displacement capacity of ±50mm in the vertical direction. The horizontal load was applied to the same frame by the horizontal actuator.

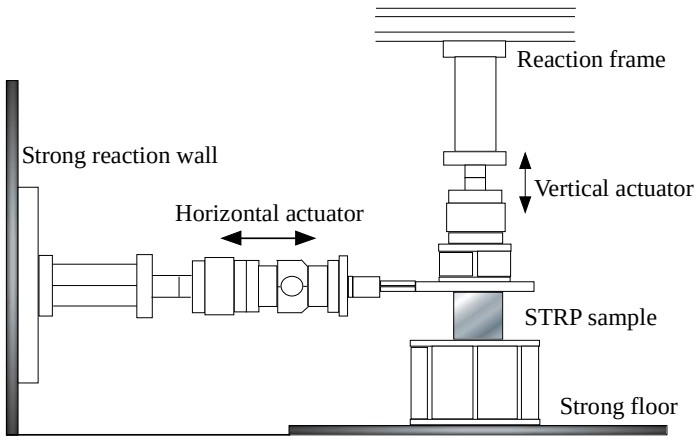

Figure 4.1 Schematic view of the test setup

The test machine had a maximum displacement capacity of ±125mm and a maximum loading capacity of ±400kN in the horizontal direction. The capacity of the testing equipment is also presented in Table 4.1. Two sets of tests on layer-unbonded STRP-6 specimens were conducted.

Table 4.1 Capacity of testing equipment

Actuator	Max. Displacement	Max. Load	Direction
No. 1	±125mm	±400KN	Horizontal
No. 2	±50mm	±400KN	Vertical

Figure 4.2 Photograph of test setup and instrumentation arrangement

4.2.1 Compression test

The compression modulus as well as the maximum vertical deflection of the specimen was evaluated through vertical compression tests. The layer-unbonded STRP-6 specimen bearings were tested under vertical displacement control. The first specimen was monotonically loaded to 12mm vertical displacement which results the equivalent vertical force of 91.9KN and is equivalent to 9.19MPa axial pressure on layer-unbonded STRP-6 bearing. In the final stage of the compression test, the specimen was monotonically unloaded. The displacement was increased by 1mm within 10sec interval. A similar test at an equivalent of 11.66MPa axial pressure was performed using the second sample to study the vertical stiffness at a higher value of vertical load. The results of compression test are presented in Figs. 4.3 and Fig.4.4.

The vertical stiffness of the bearings was computed using the vertical load-deflection

relationships shown in Figs. 4.3 and 4.4. From the tests results, the vertical stiffness values described above were calculated as $(K_v)_1$ = 21598.87 kN/m and $(K_v)_2$ = 20699.35 kN/m, respectively. These values correspond to the effective compression modulus of E_1 = 155.51 MPa and E_2 = 149.03 MPa, respectively. The corresponding vertical frequencies of vibration $(f_v)_1$ = 11.4Hz and $(f_v)_2$ = 11.2Hz, respectively, and are considered satisfactory values for seismic isolation application [7]. Accordingly, these bearings provide sufficient vertical stiffness for vertical pressure around the design value of 5MPa.

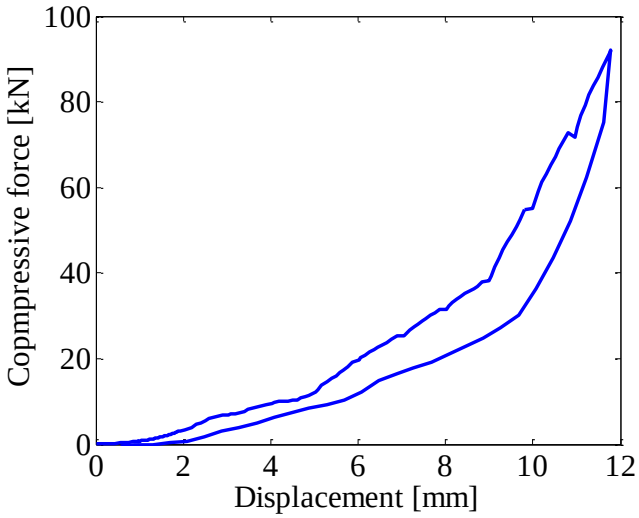

Figure 4.3 Load-deflection relationships (compressive load of 91.9kN)

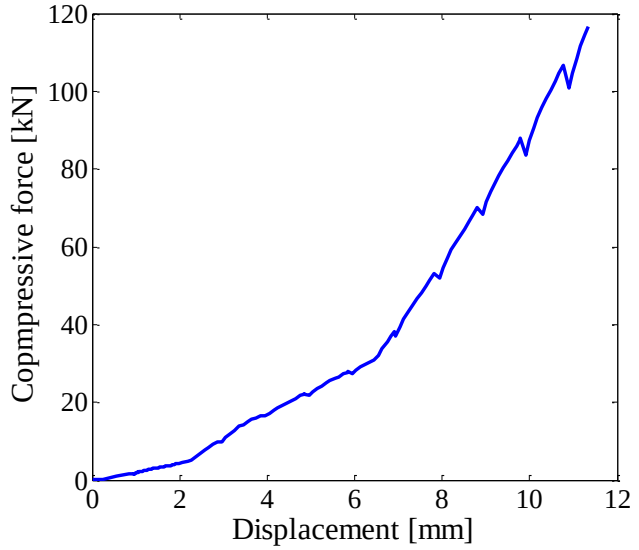

Figure 4.4 Load-deflection relationships (compressive load of 116.6kN)

4.2.2 Cyclic shear test

The cyclic shear test on bearings provides the reliable methods to determine the deformation characteristics and damping values of any isolation system. The static shear test was performed under horizontal displacement control. The layer-unbonded STRP-6 specimen bearing was tested in cyclic shear with three fully reversed cycles at four maximum shear displacement amplitudes of 12mm, 24mm, 36mm, and 48mm. The loading history in the cyclic shear test is presented in Fig. 4.5. These cycles were applied at a constant vertical pressure of 5 MPa. The load-displacement relationship is presented in Fig. 4.6.

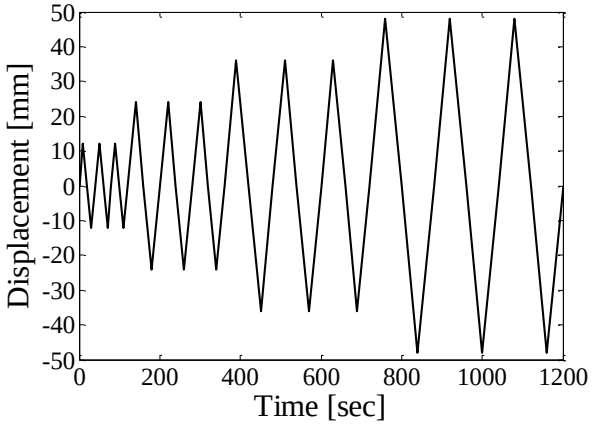

Figure 4.5 Input signal for cyclic shear tests

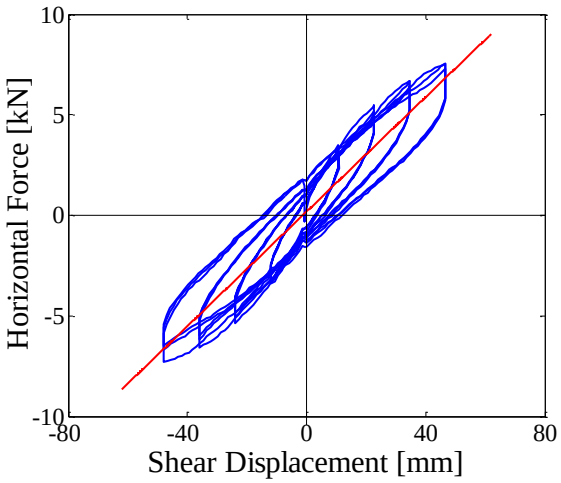

Figure 4.6 Load-displacement relationships in cyclic shear tests

4.2.3 Monotonic shear test

The purpose of the monotonic shear test was to evaluate the maximum shear deformation capacity and residual slip if any of the layer-unbonded STRP-6 bearing. The specimen bearing was tested at six maximum shear displacement amplitudes of 12mm, 24mm, 36mm, 48mm, 60mm, and 62mm. The loading history in the static monotonic shear test is shown in Fig. 4.7. These displacement amplitude cycles were applied at a constant vertical pressure of 5MPa. At the end of the maximum lateral displacement, gradual unloading was performed. During the complete experimental tests, no residual slip was observed. The load-displacement relationship in monotonic shear tests is shown in Fig. 4.8.

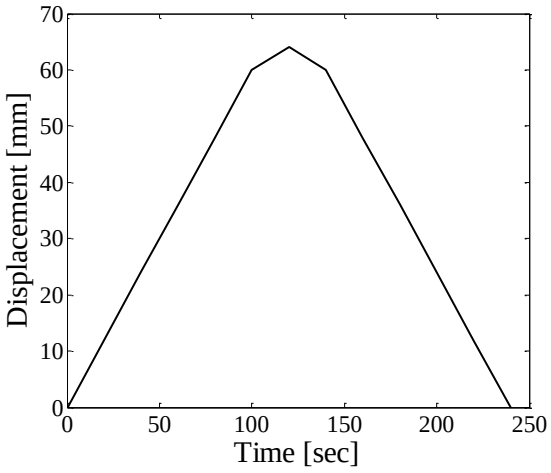

Figure 4.7 Input signal for monotonic shear test

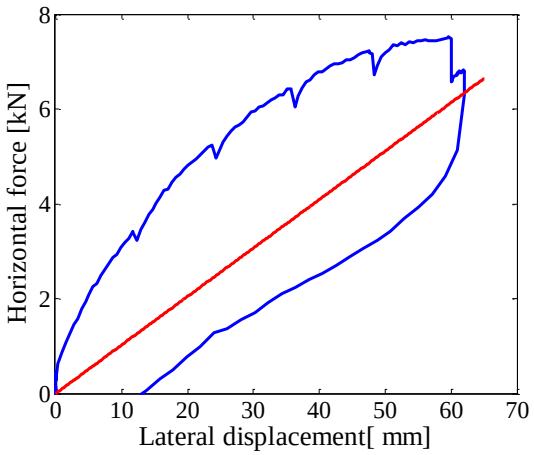

Figure 4.8 Load-displacement relationships in monotonic shear test

a)  b) 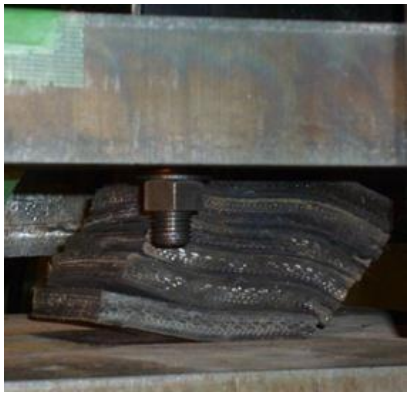

Figure 4.9 deformed states of layer-unbonded STRP-6 under constant vertical pressure of 5MPa at a) 80% and b) 103% shear deformation

Figure 4.8 has descending slope beyond 60mm lateral displacement; it indicates that the maximum shear deformation capacity of the layer-unbonded STRP-6 bearing is 60mm (100% shear strain).

4.2.4 Horizontal stiffness of STRP bearings

The effective horizontal stiffness of STRP-6 bearing corresponding to each load cycle of the test can be calculated based on the peak lateral force and peak lateral displacement as follows [4]:

$$K_{eff} = \frac{F^{+} - F^{-}}{\Delta^{+} - \Delta^{-}} \tag{4.1}$$

where F^{+}, F^{-}, Δ^{+} and Δ^{-} are the peak values of horizontal force and horizontal displacements, respectively, at the extremes of the cyclic displacement range. For the last cycle of the test, the effective horizontal stiffness of the first sample is 156.63kN/m. The average horizontal stiffness of the STRP bearings was evaluated using the least square fitting technique. Theoretical horizontal stiffness of the STRP-6 bearing was calculated using the conventional and established relationship. The maximum lateral displacements as well as average horizontal stiffness values of the layer-unbonded STRP-6 bearings are presented in Table 4.2.

Table 4.2 Horizontal stiffness of STRP bearing

Test No.	Sample	Hor. displacement (mm)	Hor. stiffness (kN/m)
1	STRP-6	48	142.48
2	STRP-6	62	102.20

The results of experimental test were used to calculate the effective horizontal stiffness at shear displacement amplitudes of 12mm, 24mm, 36mm and 48mm and are shown in Fig. 4.10. Due to the rollover deformation, the effective horizontal stiffness decreases with increase in lateral displacement which further elongates the period of the isolation system.

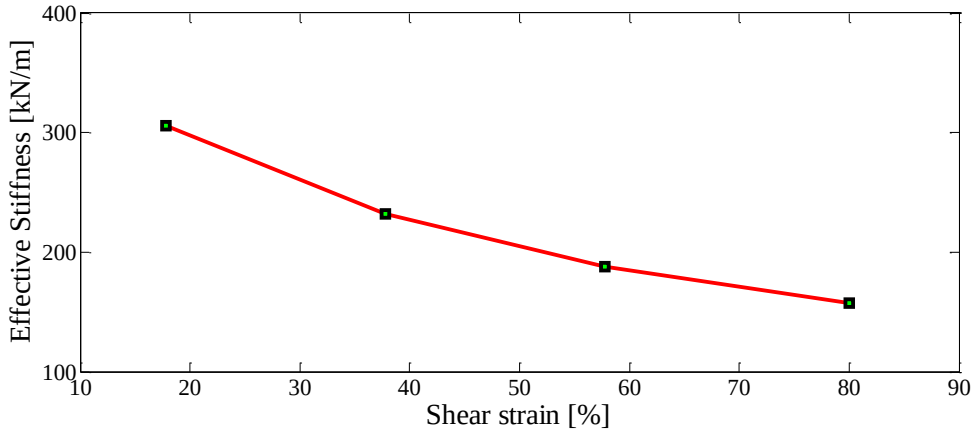

Figure 4.10 Relationship between effective stiffness and shear strain

4.2.5 Effective damping

The effective damping β_{eff} of an isolator shall be calculated for each cycle of loading by the Eq. (4.2) [4]:

$$\beta_{eff} = \frac{2}{\pi}\left[\frac{E_{loop}}{K_{eff}\left(\left|\Delta^{+}\right|+\left|\Delta^{-}\right|\right)^{2}}\right] \tag{4.2}$$

where E_{loop} is the energy dissipated per cycle of the loading, K_{eff} is the effective horizontal stiffness of the bearing.

Using the computed mechanical quantities of bearing mentioned in Eq. (4.2) for cyclic shear tests with maximum lateral displacement of 48mm which is the peak amplitude of lateral deformation of cyclic shear tests, the effective damping ratio was calculated as 0.12. This value is in a close agreement with the value obtained in the previous study [8]. The effective damping value is higher than the low damping natural rubber bearings which is usually in the range of 2 to 3 % of critical damping [2]. The relationship between shear strain and effective damping ratios is shown in Fig. 4.11 for entire range of lateral displacement.

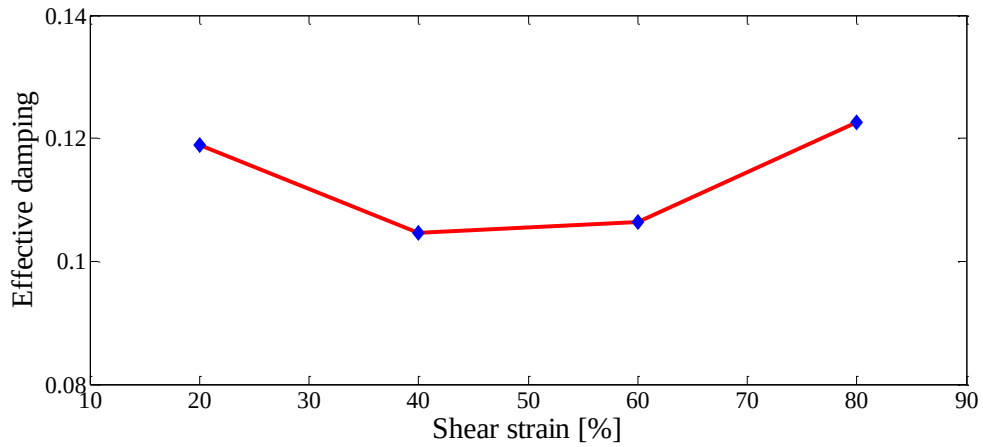

Figure 4.11 Relationship between effective damping and shear strain

The steel reinforcing cords are more flexible in tension than the individual filaments; therefore, they may stretch when the STRP bearing is loaded by the weight of a structure. On the other hand, they are completely flexible in bending, implying that the assumption for modeling steel laminated rubber bearing that plane sections remains plane after loading no longer holds [9]. In fact, when a STRP bearing is loaded in shear, a plane cross section is distorted. The layer-unbonded STRP-6 specimen bearing tests show that the energy dissipation is much larger than that of natural rubber (12% damping at 80% shear deformation). Therefore, when using STRP bearing for specified level of damping, use of additional damping enhancement mechanism can be avoided. The brief explanation about the damping phenomenon in STRP specimen is discussed in chapter 4.5.

4.3 Finite element analysis of layer-unbonded STRP

The FE analysis of the strip layer-unbonded STRP-6 bearing was carried out in order to assess the force-displacement relationship and to evaluate the stress state within the bearing. Although the shear deformation capacity of STRP bearing cannot be expected as much as steel laminated rubber bearing, properly layer-bonded STRP bearing is expected to provide more than 150% shear deformation capacity. The sketch of the deformation pattern of the layer-unbonded STRP bearing without connection system with support interfaces is shown in Fig. 4.12. The moment created by the offset of the resultant compressive force *P* balances the moment created by the shear force *V*. Due to this reason, no tension stresses are produced within the STRP bearing.

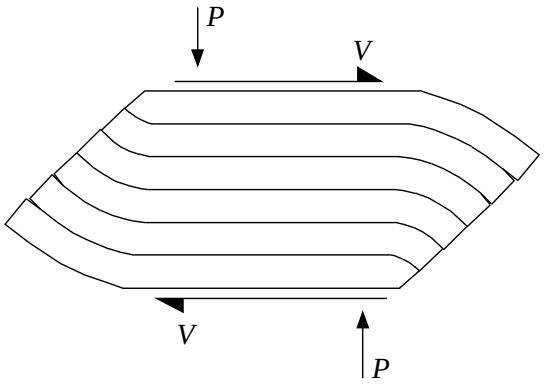

Figure 4.12 Free body diagram of laterally deformed layer-unbonded STRP bearing

4.3.1 Modeling of STRP bearings

4.3.1.1 Model of cord-rubber composite

The orientation of cord ply in a radial tire changes the tensile moduli of cords which show the complicated mechanics of anisotropy and nonlinearity. The establishment of appropriate numerical model of cord-rubber composite is one of the keys to determine whether the FE analysis result is rational and precise or not. There are two varieties of finite element model of

cord-rubber composite; namely, laminated shell model and rebar model. In the latter type of model, rebar and solid elements are used to describe the reinforcing cord and rubber, respectively. In this model, rubber element includes a single or multilayer reinforcing cord of different orientation as shown in Fig. 4.14. The solid and rebar elements select the same nodes and the additional degrees of freedom are not introduced. Thus, computing efficiency is not affected. This model can be used to describe small strain and large strain states of the reinforcing cord. The other benefit of using the rebar model is that the rebar element can be defined as any material property. On utilizing the rebar model, the rubber (host or matrix) and the reinforcing cord can be described by different stress-strain relationships. Thus, rebar model is very effective to simulate the material and geometrical nonlinearity of the cord-rubber composite.

4.3.1.2 Finite element mesh generation

The STRP that constitutes the rubber bearing is composed of a rubber body with embedded steel reinforcing cords. The bearing's physical and geometrical properties are given in Table 3.1. The FE analysis of the strip layer-unbonded STRP was conducted using commercially available general purpose finite element software MSC Marc 2010 [10]. The rubber was modeled using four-node, isoparametric quadrilateral elements coded for plane strain incompressible applications. This element is preferred over higher-order elements when used in simulating large deformation and contact analysis [11]. The reinforcing steel cords were modeled by using the isoparametric plane strain two-node line elements. These elements need to be used in conjunction with four-node plain strain continuum elements (host elements). These rebar elements have to be embedded into their corresponding solid elements representing the matrix materials.

The typical rebar element inserted into the rubber element is shown in Fig. 4.13 (a). Since the matrix element and the rebar element share the same nodal points, no additional degrees of freedom are introduced. The degrees of freedom of the nodes to be inserted are tied to the corresponding degrees of freedom of the host elements. When defining the material properties of the rebar layer, the reference plane or the edge of the rebar layer should be defined. In this model, the reference axis of rebar direction, the cross-section area of a single rebar, density/spacing of the rebar, angle of orientation with respect to the reference axis has to be defined.

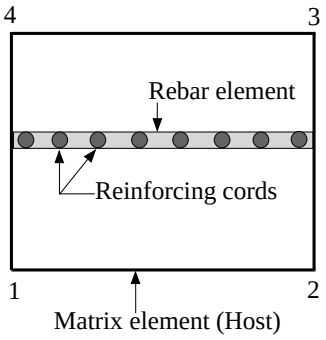

a)

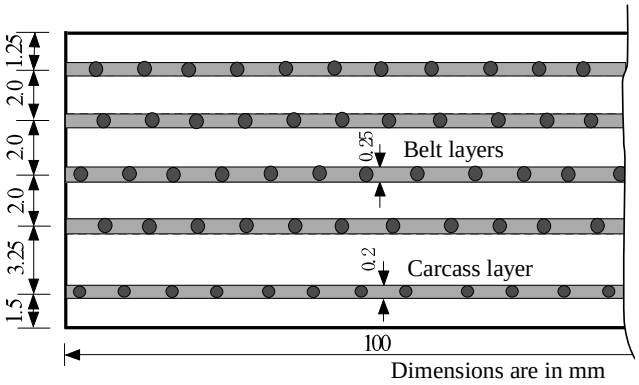

b)

Figure 4.13 a) Rebar elements and rubber element (host) b) position of steel reinforcing cords in a single layer of STRP

Figure 4.13 (b) shows the dimensions of a single layer STRP used in preparing the finite element model. In this figure, the indicated thickness of layer is the equivalent thickness defined by the total area of reinforcing cords divided by the width of the bearing. For the top and bottom layers, the edge length of the quadrilateral elements was selected to be approximately 0.4mm. The element edge length for intermediate layers was selected to be approximately 0.5mm. These modeling techniques were also used to model the steel reinforcing cords. There are total of 8750 quadrilateral elements and 1250 rebar elements in a single layer of STRP placed near the uppermost and lowermost support surfaces. The number of quadrilateral and rebar elements in the middle layers was reduced to 5800 and 1000, respectively. There are total of 47200 elements in a layer-unbonded STRP-6 model. The area of single steel reinforcing cord in carcass layers is $0.44mm^2$ while in the belt layer is $0.63mm^2$. The average spacing of the reinforcing cord is

about 0.4/mm.

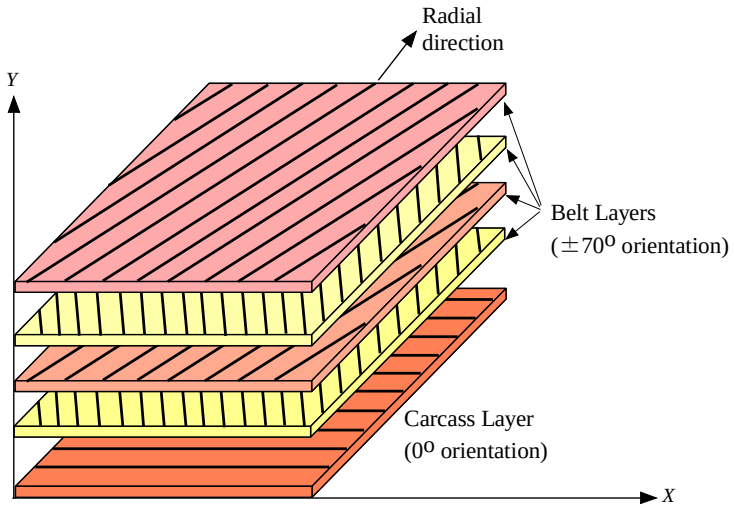

Figure 4.14 Layout of steel reinforcing cords in a single layer of STRP

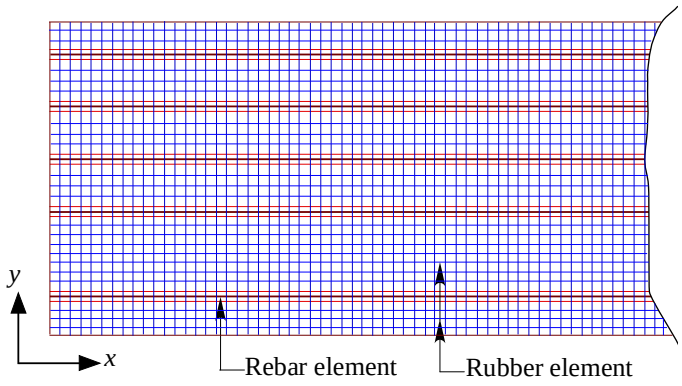

Figure 4.15 Typical finite element meshes

The orientation of the steel reinforcing cords of a radial tire were measured and verified by relevant literature [12]. The orientation of the individual layers with respect to the direction of the cords in the carcass layer is shown in Fig. 4.14. The orientation of the rebar direction was assigned as ± 70º for belt layers about the reference axis [12]. The typical finite element meshing for a single layer of STRP is shown in Fig. 4.15. The rubber is modeled as hyperelastic material model while the steel reinforcing cords in the finite element model is treated as a linear elastic isotropic material with material properties given in Table 3.1 and Table 3.2.

4.3.1.3 Boundary conditions

Two horizontal rigid bodies (lines) were defined at the top and bottom of the layer-unbonded STRP-6 model to represent the superstructure and substructure, respectively. In this model, the vertical and horizontal loads were applied on the top support; the top support was allowed to move in vertical and in horizontal directions while the bottom support was considered as a fixed support. These boundary conditions were exactly similar as were in the experimental tests. In this contact model, the contact between the supports and the STRP bearing was modeled by the Coulomb friction law with a coefficient of friction of 0.8. The coefficient of friction was selected such that no slips occur between the contact supports and the rubber. The contact in between the STRP layers was considered as a touching contact. The individual layers of STRP were modeled as deformable bodies with a local coefficient of friction of 0.95. The layer-unbonded STRP-6 bearing was not bonded to the top and bottom support surfaces and its rollover deformation was allowed. This means that when the compression contact stresses approach to zero, the nodal points were allowed to detach from the contact supports.

4.3.1.4 Constitutive model of rubber material

Generally, rubber material is thought to be an isotropic hyperelastic material. Due to this reason, the mechanics of behavior of rubber can be described in terms of strain energy density function. Among the various constitutive models, the Mooney-Rivlin model is commonly used to characterize the rubber material undergoing large strain [13]. This model is simplest hyperelastic model for elastomeric materials when material test data is insufficient. The Mooney-Rivlin material law is well suited for most practical applications involving cord-rubber composite [14]. This material model works with incompressible elastomer and strain up to 200%. The strain energy polynomial is expressed as:

$$W = \sum_{i,j=0}^{N} C_{ij} (I_1 - 3)^i (I_2 - 3)^j + \sum_{i=1}^{N} \frac{1}{D_i} (J_{el} - 1)^{2i} \tag{4.3}$$

In this finite element modeling, three-term Mooney-Rivlin strain energy density was used which is given in Eq. (4.4). The detail about the material constants is discussed in chapter 3.

$$W = C_{10}(I_1 - 3) + C_{01}(I_2 - 3) + C_{11}(I_1 - 3)(I_2 - 3) \tag{4.4}$$

4.3.2 Loads

To investigate the nonlinear behavior of the STRP bearing, the load was applied in an incremental manner. At the initial stage of the analysis, the target compressive load of 5MPa was applied in different incremental steps. Then the horizontal load was applied with the constant compressive load until a target lateral displacement was achieved. The target loads were selected such that 80% and 103% shear deformations in the bearing were achieved.

4.3.3 Finite element analysis

As the STRP bearing is not bolted between the superstructure and substructure, rollover deformation is allowed to take place in the bearing. When the rollover deformation occurs, one end of the bearing separates from the contact support while the other end is highly stressed as shown in Figs. 4.16 (a) and (b). To accurately simulate the STRP bearing, the size of the mesh at the corner region had to be made finer than the other areas when necessary.

The analysis is two-dimensional under the plane strain assumption. Unlike the other structural materials such as steel and concrete, the deformation of the rubber is relatively severe due to its low shear modulus value. Its large deformability together with its near-incompressibility makes rubber a major challenge for FE analysis. The large deformation that the rubber components experience can only be modeled with a finite strain formulation [15].

FE analysis using the standard lower-order isoparametric finite elements that have not been tailored for incompressibility analysis will produce extremely poor results [15]. More importantly, the pathological behavior called volumetric mesh-locking is likely to occur [16]. So-called mixed methods used in modern FE analysis of incompressible and nearly incompressible materials are based on the Hellinger-Reissner and Hu-washizu variational principles [10]. In the mixed methods, both stress and strains are treated as unknowns [17]. The results of FE analysis presented here are based on the widely popular mixed method proposed by Herrmann [18]. Figure 4.17 contains the shear strain distribution within the rubber layers at shear strain of 80% and 103%, respectively.

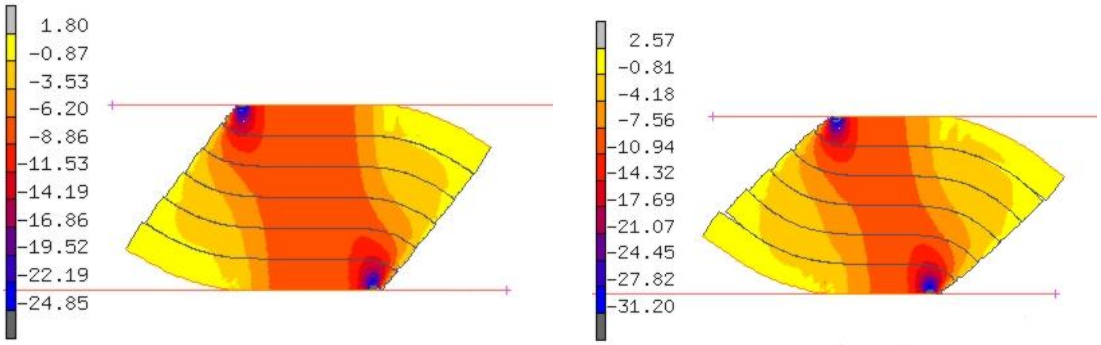

a) 80% shear deformation b) 103% shear deformation

Figure 4.16 Contour of normal stress S_{22} (MPa) in the rubber layers of the layer-unbonded STRP-6 bearing

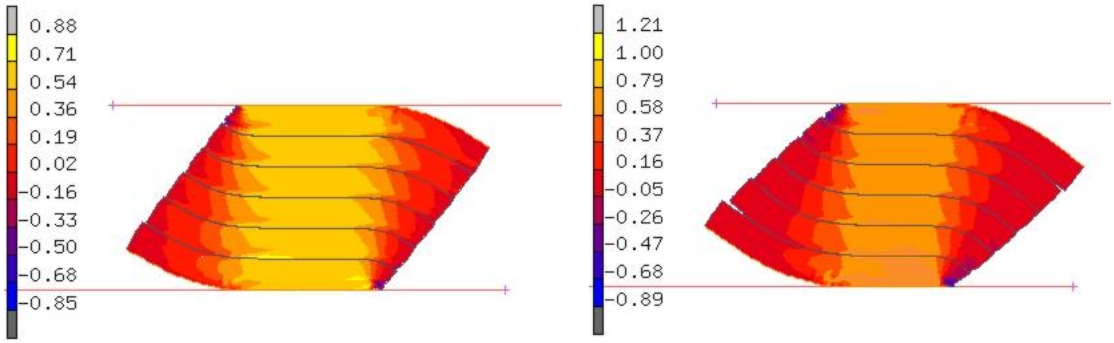

a) 80% shear deformation b) 103% shear deformation

Figure 4.17 Shear strain distribution within the layer-unbonded STRP-6 bearing

4.3.4 Results and discussion

The FE analysis was carried out on the strip layer-unbonded STRP-6 bearing whereas the experimental tests were conducted on a square layer-unbondedSTRP-6. The lateral load-displacement results obtained by FE analysis were multiplied by 100 in order to account for the100mm out of plane length of the square STRP-6 bearing. The lateral load-displacement relationship of the STRP bearing is nonlinear which is shown in Fig. 4.18.

Figure 4.18 shows the lateral load-displacement relationships for both the test and FE analysis of layer-unbonded STRP-6 bearings up to 80% and 103% lateral deformation, respectively. Due to the rollover deformation, the effective secant stiffness decreases with increase in lateral deformation. This results in natural period elongation which further increases the efficiency of the bearing, provided that lateral stability of the STRP bearing is maintained [3]. As seen in Figs. 4.18 (a) and (b), reasonable agreement is found between the experimental test and FE analysis results. However, it should be noted that for lower level lateral displacement, the horizontal force obtained by the FE analysis is noticed to be lower than the experimental test results in both the cases. The reason behind this can be the negligence of strain dependency of the steel reinforcing cords and rubber material [3].

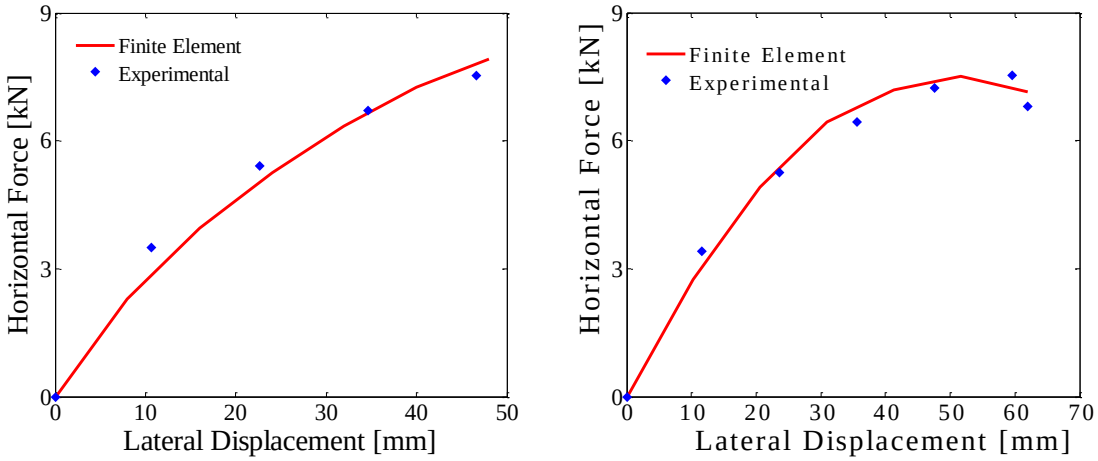

a) 80% shear strain b) 103% shear strain

Figure 4.18 Lateral load-displacement relationship of layer-unbonded STRP-6; comparison between experimental test and FE analysis results.

Figure 4.16 contains the distribution of normal stress in the vertical direction corresponding to 80% and 103% shear strain, respectively. As shown in these figures, as a result of rollover deformation, high levels of stresses are occurred at the corner regions, and tensile stress is not transferred to a laterally deformed STRP at the bearing's contact interfaces. As a result, no balancing moment develops at the top and bottom surfaces of a STRP bearing. As seen in Fig. 4.16 (a) and (b), the width of the compression column zone largely decrease when lateral displacement increases. The aspect ratio of STRP bearing in the present case is less than two (aspect ratio = 1.4, average shape factor = 10.4) which plays an important role in stability and

stress demand of the STRP bearing.

4.4 Role of aspect ratio

Unlike other elastomeric bearings which deforms without losing the contact with support surfaces, the STRP bearings in an unbonded application roll-off the contact supports during the lateral deformation. This phenomenon decreases the contact area which further governs the maximum shear deformation capacity of the bearing. The effect of aspect ratio in shear deformation capacity is studied by means of FE analysis. In this study, footprint dimensions of the bearing were increased without changing the total thickness of the STRP bearing. FE analysis of the STRP bearing with dimensions of 150×150×72mm (aspect ratio = 2.08, average shape factor = 10.4) and material properties given in Table 3.1 and Table 3.2 was carried out in order to investigate the effect of aspect ratio.

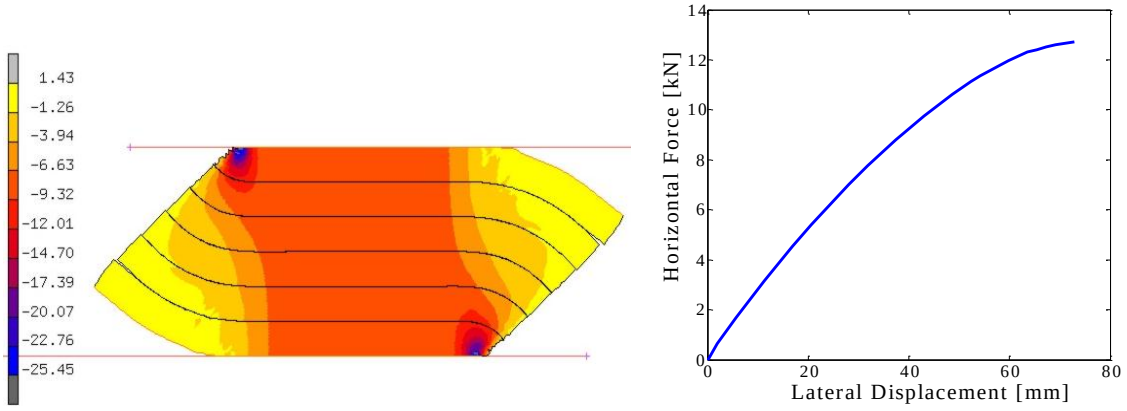

a) Normal stress S_{22} (MPa) distribution b) Load-displacement relationship

Figure 4.19 150×150×72mm layer-unbonded STRP bearing analysis results at 103% shear strain

FE analysis procedure is already discussed in the preceding section of this chapter. Constant vertical compressive load of 5MPa was applied in order to compare the results with that of the STRP-6 bearing. Figure 4.19 shows the vertical compressive stress as well as horizontal force-displacement relationship. As seen in Fig. 4.19 (a), the size of compression column zone is wider and the maximum stresses within the bearing are also lower than 100×100×72mm size

bearing shown in Fig. 4.16 (b). It also resulted in enhanced positive incremental force resisting capacity, which is one of the mandatory criteria for designing the seismic isolator [19]. The aspect ratio is one of the important factors that govern the maximum shear deformation capacity of the STRP bearings. In conclusion, it can be said that the aspect ratio plays a crucial role in shear deformation capacity and stability of the isolation bearings.

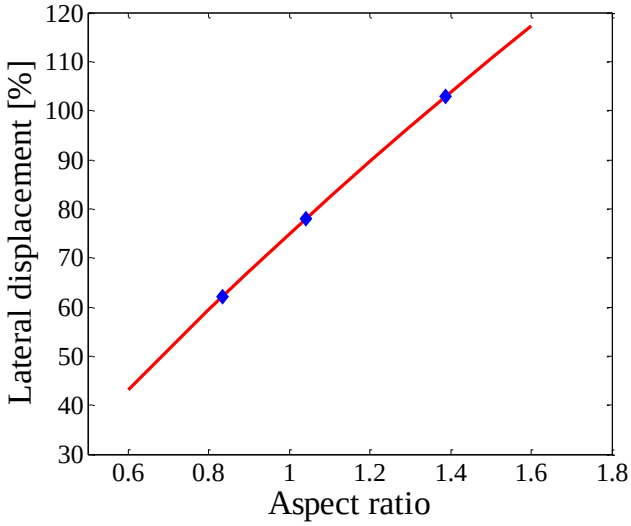

Figure 4.20 Variation of shear deformation capacity with aspect ratio of STRP bearings

The effect of thickness on maximum shear deformation capacity of the STRP bearing was studied by means of FE analysis. For this purpose, the FE analysis of eight and 10-layer STRP bearings were also carried out. In this analysis, only the thickness of bearing was increased without increasing the footprint dimensions. The results of the FE analysis are shown in Fig. 4.20, indicating that increasing the thickness of STRP bearing without increasing the aspect ratio sharply decreases the shear deformation capacity of the layer-unbonded STRP bearing.

4.5 Role of steel reinforcing cords in damping

The STRP bearing consists of steel reinforcing cords interleaved within the rubber body. Each layer of STRP consists of five such layers of steel reinforcing cords as shown in Fig. 4.14. Among these, each cords contents about five to fourteen filaments. The diameter of each filament is about 0.4mm in belt layers and 0.2mm in carcass layer. The steel reinforcing cords

are more flexible in tension than the individual filaments; therefore, they may stretch when the STRP bearing is loaded by the vertical axial load. On the other hand, they are completely flexible in bending, so the assumption made when modeling steel laminated rubber bearing that plane sections remains plane after loading no longer holds [9]. These cords are made from yarns (consisting of filaments), and forming helical path. The twist of the yarn is about two to four hundred rotations per meter of yarn length. When the cord is elongated, it contracts laterally and friction between filaments occurs [20]. The schematic representation of the applied and induced forces is shown in Fig. 4.21. In this figure, F represents the tensile force produce in cords, N represents the normal or applied compressive force and μ represents the coefficient of friction between the filaments. The hysteresis of a cord is necessary to improve the damping of the tire [20]. Steel reinforcing cords have such friction behavior. In addition, the adhesive which are used to bond the cords with elastomer improves the mechanical damping [21].

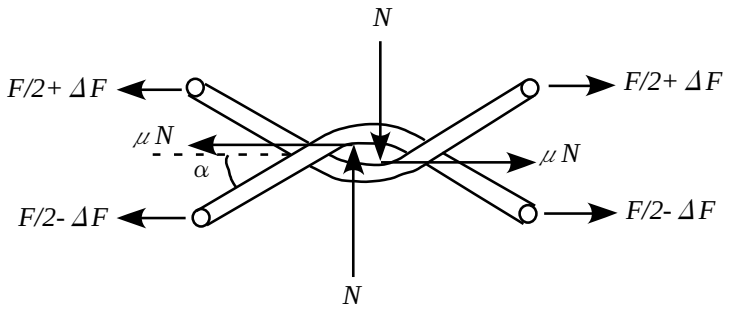

Fig. 4.21 Relative motion and friction forces

In fact, when a STRP bearing is loaded in shear, a plane cross section becomes curved. This leads to an unexpected advantage in the use of STRP bearing having steel reinforcing cords. When the bearing is displaced in shear, the tension in the cord strand produces a frictional damping that is due to individual filaments in the strand slipping against each other as discussed earlier. This energy dissipation in the steel reinforcing cords adds to that of the rubber. The tested STRP-6 bearings show that this energy dissipation is much larger (12% damping at 80% shear deformation) than that of natural rubber. Therefore, when using STRP bearing for specified level of damping, it is not necessary to use additional damping enhancement mechanism.

4.6 Natural period of isolation system

The natural period can be roughly estimated using the vertical pressure and the effective shear modulus given by Eq. (4.5) [19]:

$$T = 2\pi\sqrt{\frac{pt_r}{Gg}} \tag{4.5}$$

If the average pressure on STRP bearing p is assumed to be 5MPa, G = 0.89MPa, t_r = 72mm, and the period is evaluated as 1.27 sec. If the thickness is increased up to 120 mm with 10 layers STRP, the period becomes 1.65 sec. This suggests that if the period 1.65 sec is acceptable as the target value for design of isolated building structure, the STRP bearings would be adequate providing that the vertical pressure is 5MPa. Longer periods can be achieved by stacking more STRP layers one on top of another, although the stability of the bearing should be tested before their application. The time period mentioned here is considered as indicative value only, as the period is also related to the lateral displacements and code provisions [4].

4.7 Conclusion

This chapter describes about the investigation of a seismic isolation device using layer-unbonded STRP. The investigation was carried out by means of experimental test and FE analysis. The results of experimental test were used to compute the mechanical quantities of the bearings by employing code provisions. The force-displacement relationship obtained by FE analysis was compared with experimental test results. The findings obtained in this part of the study are summarized as below:

1. The vertical stiffness of the bearing is sufficient to withstand structural load of low-rise residential buildings as well as to prevent the rocking motion of the structure. An effective compression modulus of 155.5MPa at an axial pressure of 5MPa implies a vertical vibrational frequency of 11.4Hz which is sufficient for any seismic isolation application [7].

2. The ratio between vertical and horizontal stiffness is more than 150, so that the SRTP

bearings can be used as base isolation device [5].

3. The average horizontal stiffness computed by the cyclic shear test and monotonic shear test results show that the horizontal stiffness is decreased with increase in lateral displacement due to its unbounded application with the support surfaces. The monotonic shear test results indicate that the layer-unbonded STRP-6 bearings with geometrical properties given in Table 3.1 can be used to achieve 100% shear strain [6], beyond that layer separation occurs.

4. The damping ratio of the tested STRP bearings is found to be higher than the damping value of natural rubber bearings [2]. Therefore, when using STRP bearing for specified level of damping, use of additional damping enhancement mechanism can be avoided.

5. The finite element model is found to be almost accurate in simulating the STRP bearings as the force-displacement relationships in both the cases are in close agreement with the experimental test results.

6. The role of aspect ratio in shear deformation capacity and stability of STRP bearing is also studied by means of FE analysis. This part of study suggests that the proper aspect ratio should be maintained while designing the SRTP bearing.

7. The experimental test and FE analysis results suggest that there is possibility of using the STRP bearing as low-cost base isolation device.

8. This part of study also suggests for bonding the STRP layers in order to improve the shear deformation capacity.

9. Similar studies on layer-bonded STRP bearings with increased aspect ratio shall be the focus of further investigation.

References

[1] Hamid Toopchi-Nezhad, Michael J. Tait, Robert G. Drysdale. Testing and modeling of square carbon fiber-reinforced elastomeric seismic isolators. *Structural Control and Health Monitoring*, 2008, Vol. 15(6): 876-900.

[2] Farzad Naeim, James M. Kelly. Design of seismic isolated structures from theory to practice. John Willey and Sons, Inc. 1999.

[3] Hamid Toopchi-Nezhad, Michael J. Tait, Robert G. Drysdale. Bonded versus unbonded strip fiber reinforced elastomeric isolators: Finite element analysis. *Composite Structures*, 2011, Vol. 93 (2): 850-859.

[4] Uniform Building Code, Volume 2, Structural Design Requirements, 1997, Earthquake Regulations for Seismic Isolated Structure, Whittier, CA.

[5] Eurocode 8. Design of structures for earthquake resistance. 2004

[6] ASCE-7. Minimum design loads for building and other structures, ASCE/SEI 7-05. New York, American Society of Civil Engineers, 2005.

[7] James M. Kelly. Earthquake-resistant design with rubber. 2nd edition London, Springer-Verlag, 1997.

[8] Ahmet Turer, Bayezid Ozden. Seismic base isolation using low-cost Scrap Tire Pads (STP). *Materials and Structures*, 2008, Vol. 41 (5), pp: 891-908.

[9] James M. Kelly. Analysis of fiber reinforced elastomeric isolators. JSEE 1999, Vol. 2(1), pp: 19-34.

[10] MSC Software (2008r1), MSC Marc 2010 and MSC Marc Mentat 2010, Santa Ana, California

[11] MSC.Marc. Theory and user information, Vol. A Santa Ana, CA, MSC software Corporation; 2010

[12] J. Y. Wong. Theory of ground vehicle. 3rd edition, John Wiley and Sons, Inc., 2001.

[13] Aidy Ali, M. Hosseini and B. B. Sahari. A review of constitutive models for rubber-like materials. *American Journal of Engineering and Applied Science*, 2010, Vol. 3(1): 232-239.

[14] P. Helnwein, C. H. Liu, G. Meschke and H. A. Mang. A new 3-D finite element model for cord-reinforced rubber composites-Application to analysis of automobile tires. *Finite Elements in Analysis and Design*, 1993, Vol. 14(1), pp: 1-16.

[15] James M. Kelly, Dimitrios Konstantinidis. Low-cost seismic isolators for housing in highly-seismic developing countries. *10th World Conference on Seismic Isolation, Energy Dissipation and Active Vibrations Control of Structures*, Istanbul, Turkey, 2007,May 28-31

[16] MSC Software (2000) Nonlinear Finite Element Analysis of Elastomers, Whitepaper Santa Ana, California

[17] Zienkiewicz OC., Taylor R.L., Zhu J.Z. The finite element method: its basis and fundamentals, 6th edition, 2005. Oxford, Butterworth-Heinemann.

[18] L.R. Herrmann. Elasticity equations for incompressible and nearly incompressible materials by variational theorem. *AIAA Journal*, 1965, Vol. 3(10), pp: 1896-1900.

[19] James M. Kelly. Analytical and experimental study of fiber-reinforced strip isolators. PEER report 2002/11. College of Engineering, University of California, Berkeley.

[20] F. Böhm. Dynamic rolling process of tires as layered structures. *Mechanics of Composite materials*, 1996, Vol. 32(6), pp: 568-576.

[21] D. C. Prevorsek, R. K. Sharma. Role of adhesion in viscoelastic properties of rubber-tire cord composites. *Rubber Chemistry and Technology*, 1981, Vol. 54(1), pp: 72-90.

5

Experimental and analytical study of layer-bonded STRP bearings

This chapter explains about the fabrication process of layer-bonded STRP specimen bearings by applying adhesive. The objective of this part of study is to investigate the improvement on mechanical properties as well as shear deformation capacity of the layer-bonded STRP bearings. This chapter deals in details about the experimental test and FE analysis of layer-bonded STRP bearings. In addition, the chapter discusses about the recent practices of designed axial loads on elastomeric bearings and compares the results with the design practices to check the applicability of layer-bonded STRP for seismic isolation of structures.

5.1 Introduction

The study carried out on layer-unbonded STRP bearings suggests that the key parameters have to be improved; namely, bonding of STRP layers to prevent the layer separation and to maintain the proper aspect ratio. Ultimately, these parameters are responsible to achieve the target shear deformation capacity and to maintain the stability of the isolation system. Thus, in this part of study, the STRP layers were bonded using adhesive chemical and the aspect ratio was increased by decreasing the number of STRP layers. In this regard, the study on layer-bonded STRP bearings is one of the parts of study to develop low-cost seismic isolation system for application to seismic isolation of structures. The layer-bonded STRP specimen bearings were produced by stacking the STRP layers one on top of another with the application of adhesive chemical. The detail specimen preparation procedure is discussed in the subsequent chapter.

Similar methodology as used in chapter 4 was adopted to conduct the experimental test on

layer-bonded STRP specimen bearings. These types of bearings were tested for the case of unbonded application with the contact interfaces. The dowelled connection system in turn puts much lower demands on the internal bonding between the layers of STRP [1]. In an unbonded application, the layer-bonded STRP bearing is laterally deformed with its upper and lower faces roll-off the contact supports which in turn decreases the contact area. In the meantime, the decrease in contact area also affects the stability of the isolation system. This phenomenon should be carefully studied before the practical application of these types of seismic isolation bearings.

In this study, the results of experimental test and FE analysis conducted on layer-bonded square STRP-4 bearings are presented to investigate the improvement on performance of layer-bonded STRP bearings. The performance of layer-bonded STRP bearings is discussed in terms of shear deformation capacity and stability of the isolation unit. The experimental test results were used to compute the mechanical properties of the layer-bonded STRP bearings. These mechanical properties of the bearings were further compared with the relevant code provisions to check the viability of using the layer-bonded STRP as seismic isolation device [2], [3] and [4]. Finally, the discussion about the applicability of the STRP bearings for base isolation of structures is presented. In this section, brief discussion about the incurred cost of layer-bonded STRP bearings is also discussed.

5.2 Layer-bonded STRP specimen bearings

The detail steps about the fabrication of individual STRP specimens are discussed in chapter 3. The fabrication process of the layer-bonded STRP specimen bearings is described in this chapter. The tire product used for the preparation of STRP specimen samples was Bridgestone Tire, 385/65R22, 5.

5.2.1 Bonding of STRP layers

The bonding between rubbers to rubber is generally achieved by using either epoxy or urethane. For the bonding of vulcanized rubber surfaces, epoxy is generally used as adhesive, in addition to essential application of priming, for which the type of primer depends on the rubber material and type of epoxy to be used. In the particular case of study, Chemlok 7701 and Fusor 320/322

(Lord Corp.) were used as the primer and the epoxy adhesive, respectively.

The raw STRP samples taken from a tire were sanded using a belt sanding machine as shown in Fig. 5.2, so that smooth plain surfaces were obtained on the STRP samples. The sanded STRP surfaces must be cleaned to achieve proper good quality adhesion between the surfaces. Foreign materials such as dirt, oil, moisture, rust, loose particles and any contaminants, if they exist, have to be removed from the surface; otherwise, the adhesive will bond to these weak boundary layers rather than to the substrate. These treatments generally involve physical process, typically with a hard brush, chemical process to apply appropriate agent, or combination of both. The choice of surface treatment process, recommended by the adhesive supplier, depends on the adhesive to be used. The chemical treatment of the surfaces by applying the Chemlok 7701 primer with a brush allows the surface to be more easily wet, which improves compatibility with adhesive and environmental resistance, thus making the rubber surfaces more receptive to bonding. After the solvent flashes off in approximately five minutes, the treatment was assumed to be completed. The bonding between STRP samples was conducted immediately after the solvent has flashed off to achieve the best adhesion quality in creating layer-bonded STRP samples. The basic steps followed in the preparation of the layer-bonded STRP sample is shown in Fig. 5.1.

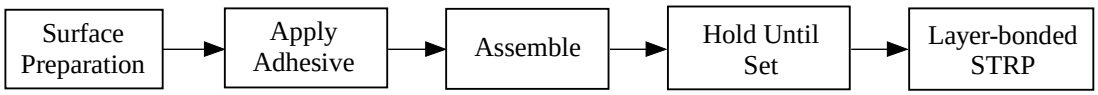

Figure 5.1 Basic steps involved in adhesive bonding of STRP layers

The Fusor 320/322 contains resin and hardener compounds. The adhesive was prepared by mixing equal amounts of Fusor 320 and 322 by volume, as recommended by the manufacturer for general purpose (temperature range between -40°c to 204°c) application. The prepared adhesive paste was applied on both sides of STRP surfaces using a spatula. The thickness of adhesive shall be around 0.5mm to achieve proper bonding. The STRP samples were assembled into a layer-bonded STRP so that no air is entrapped in the bonding interfaces, and pressure (about 0.2MPa) was applied to ensure good wetting of the adhesive on both surfaces. The layer-bonded STRP samples were placed undisturbed for 24 hours to achieve fully cured.

Figures 5.3 to 5.5 show the surface preparation, adhesive application and cured samples, respectively. The dimensions of the STRP specimen samples are shown in Table 5.1 while the physical properties are the same as given in Table 3.1 of chapter 3. The overall thickness of STRP-4, produced by bonding four layers STRP samples, is increased by 2mm due to the application of adhesive.

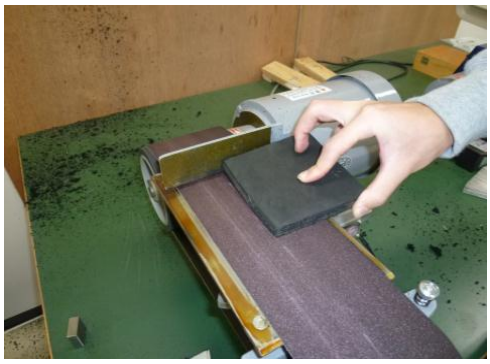

Figure 5.2 Sanding of layer is in progress

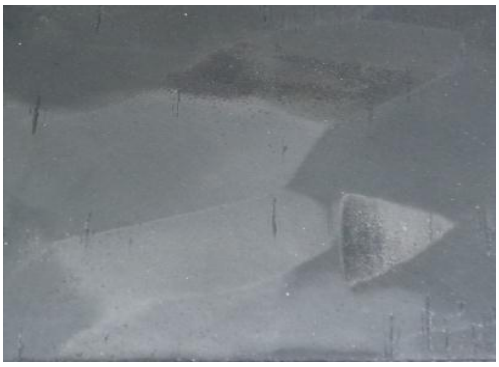

Figure 5.3 Surface treatment by primer

Figure 5.4 Adhesive on surface

Figure 5.5 Fully cured bonded STRP-4

Table 5.1 Geometrical properties of STRP bearings

Total thickness of STRP-4	= 48mm
Total thickness of rubber	= 40mm
Thickness increased by adhesive	= 2mm

5.3 Shear loading test

A shown in Fig.5.6, a series of shear loading tests of the layer-bonded STRP-4 specimens was conducted by applying horizontal force F_H under a vertical compression force P. Figure 5.7 shows the schematics of the test setup using three-dimensional loading equipment; two horizontal and one vertical loading, by means of nine servo-hydraulic actuators. The STRP-4 specimens were placed between the upper reaction frame and lower steel loading block as shown in Fig.5.6 (b). The vertical load was applied to the specimen by the vertical hydraulic actuator, with a maximum loading capacity of ±500kN and maximum displacement capacity of ±100mm, using a constant load control. The horizontal load was applied by imposing specified displacements by the horizontal hydraulic actuators with a load capacity of ±100kN and a maximum displacement capacity of ±100mm. The capacity of the testing equipment in all the three directions is presented in Table 5.2.

Table 5.2 Capacity of testing equipment

Actuator	Max. Displacement	Max. Load	Direction	Remarks
No.1	±100mm	±100KN	Horizontal	*Fx*
No.2	±100mm	±100KN	Horizontal	*Fy*
No.3	±100mm	±500KN	Vertical	*Fz*

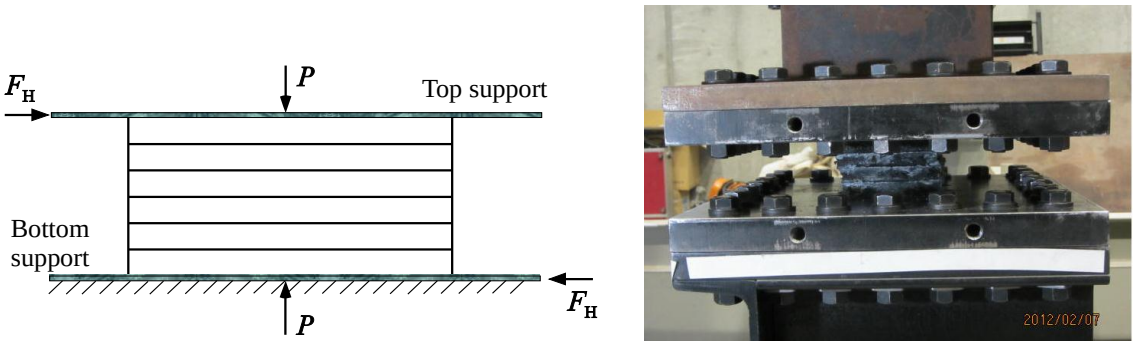

a) b)

Figure 5.6 a) Sketch of loading setup and b) photograph of layer-bonded STRP-4 specimen for unbonded application with contact interfaces

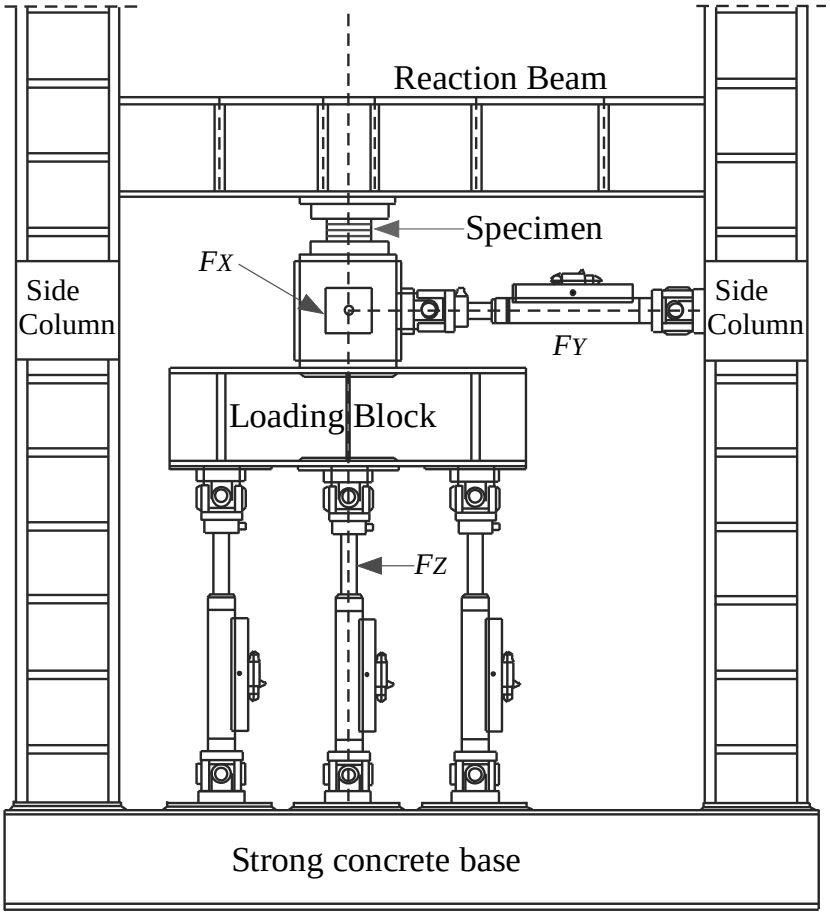

Figure 5.7 Schematics of test setup and instrumentation

5.3.1 Preliminary axial compression tests

In order to investigate the fundamental property of the layer-bonded STRP, two preliminary axial compression tests of the STRP-4 specimens were conducted. Results of the tests, ‘‘Test 1’’ and ‘‘Test 2’’ are described in this section.

5.3.1.1 Test 1

In Test 1, the initial condition was such that the sample was just made contact with the top and bottom support surfaces with zero vertical compression load. The vertical load was applied and

increased until 120kN, and then unloading was performed, and again the vertical load was increased up to 200kN. This is equivalent to 20MPa axial pressure on the STRP-4 specimen. The STRP-4 specimen did not show any sign of failure in Test 1. The force-displacement relationship obtained from Test 1 is shown in Fig. 5.8.

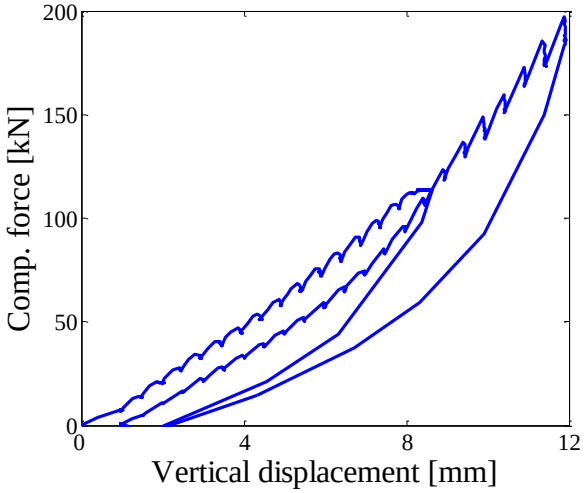

Figure 5.8 Vertical load-deflection relationships of layer-bonded STRP-4 bearing

5.3.1.2 Test 2

In Test 2, layer-bonded STRP-4 specimen bearing was tested in vertical compression, including a cyclic loading pattern at its maximum amplitudes. At the initial stage, the specimen was loaded up to an equivalent pressure of 13.7MPa and unloaded. Then the compressive load was increased to 200kN which is equivalent to 20MPa axial pressure on the SRTP-4 specimen. Starting from this loading condition, three fully reversed cycles with ±4MPa amplitude were performed. The loading history and force-displacement relationship in Test 2 is presented in Figs. 5.9 and 5.10, respectively.

The vertical stiffness of the bearings was determined using the load-deflection relationship of Fig. 5.10. For this purpose, least square fitting technique was used on the cyclic part of the load deformation curve. From the test results, the vertical stiffness values described above is calculated as $(K_v)_1$= 50.98 MN/m and $(K_v)_2$ = 56.417MN/m, respectively. These values correspond to effective compression modulus of E_1 = 244.7MPa and E_2 = 270.8MPa,

respectively. The corresponding calculated vertical frequencies of vibration $(f_v)_1$ = 17.43Hz and $(f_v)_2$ = 18.34Hz, respectively and are considered satisfactory values for any seismic isolation application [5].

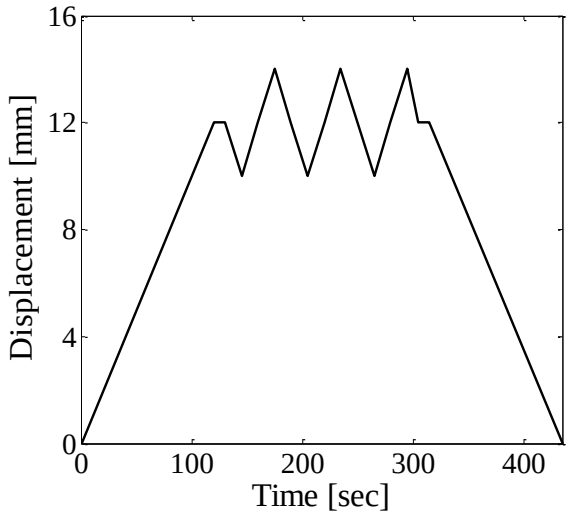

Figure 5.9 Input signal for cyclic compression test

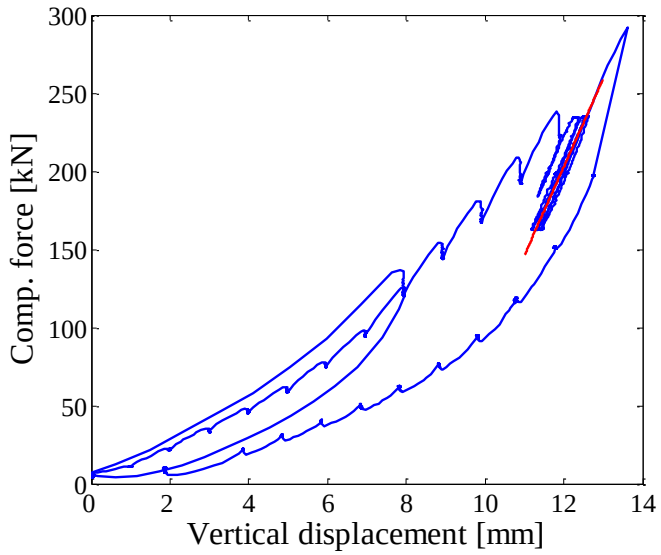

Figure 5.10 Load-deflection relationship in cyclic compression test

5.3.2 Cyclic shear tests

5.3.2.1 Test S1

In Test S1, layer-bonded STRP-4 specimen was tested in cyclic shear with three fully reversed cycles at three maximum shear displacement amplitudes of 20mm, 40mm and 60mm, at constant vertical pressure of 10MPa. The loading history in the horizontal shear test is shown in Fig. 5.11 and the force-displacement relationship obtained by Test S1 is presented in Fig. 5.12.

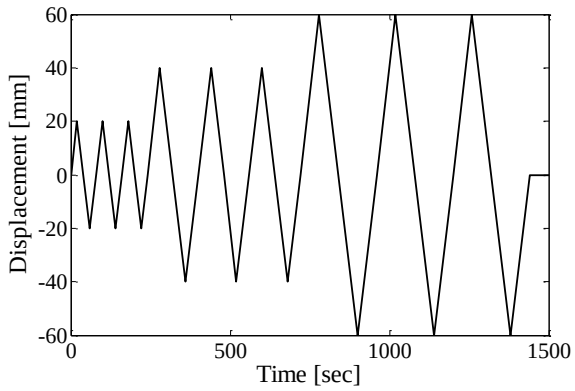

Figure 5.11 Input signal

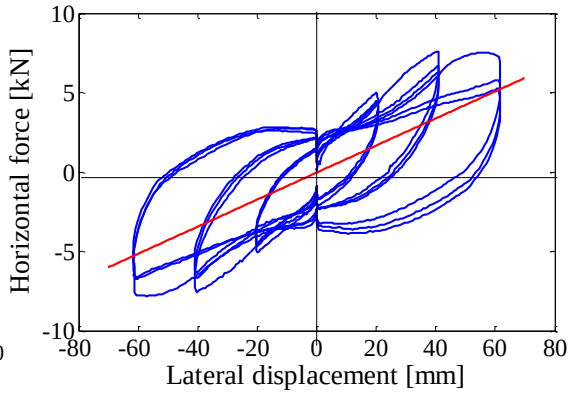

Figure 5.12 Load-displacement relationship

5.3.2.2 Test S2

In Test S2, layer-bonded STRP-4 specimen was tested in cyclic shear with three fully reversed cycles at four maximum shear displacement amplitudes of 15mm, 30mm, 45mm and 60mm, at a constant vertical pressure of 5MPa. The loading history in Test S2 is presented in Fig. 5.13. Figure 5.14 shows the force-displacement relationship obtained by Test S2. The deformed states of the specimen at different shear strain levels are shown in Fig. 5.15. Although noticeable slip can be seen in Fig.5.14 at the displacement amplitudes of 45mm, this phenomenon again disappears for a higher level of displacement amplitudes.

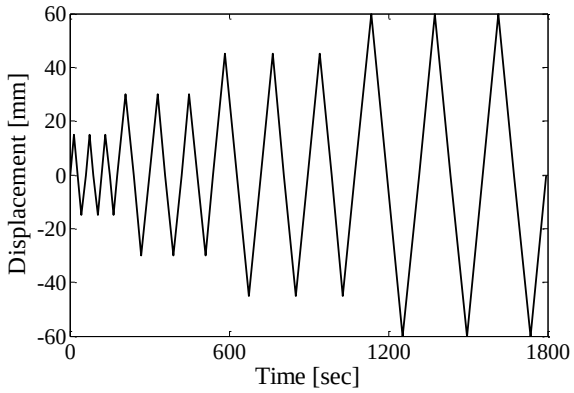

Figure 5.13 Input signal

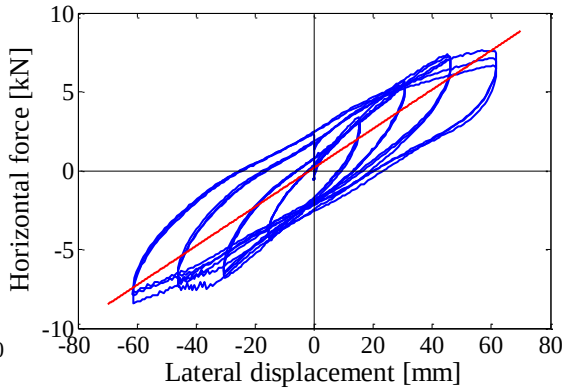

Figure 5.14 Load-displacement relationship

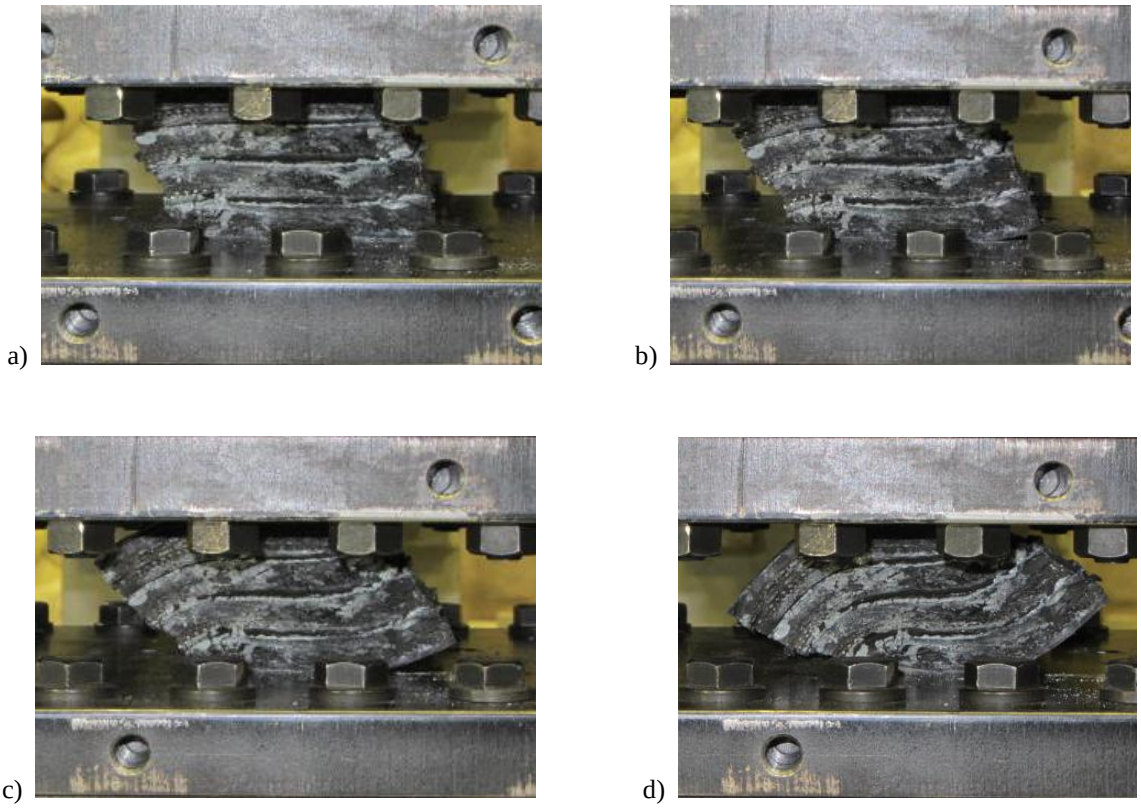

Figure 5.15 Deformed state of layer-bonded STRP-4 bearing under 5MPa vertical compressive pressure subjected to a) 37.5%, b) 75%, c) 112.5% and d) 150% shear strain

5.4 Horizontal stiffness of STRP bearing

The bearing's effective horizontal stiffness corresponding to each load cycle of the test can be calculated based on the peak lateral load and peak lateral displacement as follows [2]:

$$K_{eff} = \frac{F^+ - F^-}{\Delta^+ - \Delta^-} \tag{5.1}$$

where F^+, F^-, Δ^+ and Δ^- are the positive/negative peak values of horizontal loads and horizontal displacements, respectively, at the extremes of the cyclic displacement range. For the last cycle of the tests, the effective horizontal stiffness of the STRP-4 specimen with 10MPa and 5MPa axial pressure at 150% shear strain is 127.4kN/m and 132.3kN/m, respectively. The average horizontal stiffness of the STRP isolators was evaluated using the least square fitting technique. The maximum lateral displacements as well as average horizontal stiffness values of layer-bonded STRP bearings are shown in Table 5.3. From Table 5.3, it can be seen that the average horizontal stiffness decreases with increase in axial pressure for equal level of horizontal displacement.

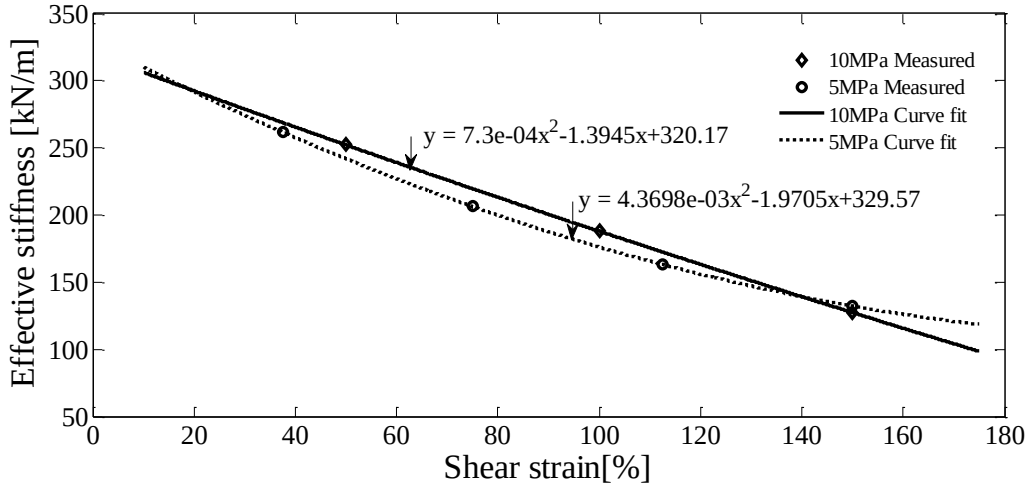

Figure 5.16 Variation of effective stiffness with shear strain of layer-bonded STRP-4 at various axial pressures

The results of experimental test are used to determine the effective horizontal stiffness at the

maximum shear displacement amplitudes. Due to the rollover deformation, the effective horizontal stiffness decreases with increase in lateral displacement which further elongates the period of the isolation system. Figure 5.16 shows that the variation of the stiffness can be approximated as a linear function for a larger axial pressure (10MPa) whereas the variation is nonlinear for lower axial pressure (5MPa).

Table 5.3 Average horizontal stiffness of layer-bonded STRP bearings

Test No.	Sample	Axial pressure (MPa)	Hor. displacement (mm)	Horizontal stiffness (kN/m)
Test S1	STRP-4	10.0	60	85.3
Test S2	STRP-4	5.0	60	124.0

5.5 Effective damping of STRP bearing

The effective damping β_{eff} of an isolator shall be calculated for each cycle of the loading by the formula [2]:

$$\beta_{eff} = \frac{2}{\pi}\left[\frac{E_{loop}}{K_{eff}\left(\left|\Delta^{+}\right|+\left|\Delta^{-}\right|\right)^{2}}\right] \tag{5.2}$$

where E_{loop} is the energy dissipated per cycle of the loading, K_{eff} is the effective horizontal stiffness.

Using the quantities for 60mm lateral displacement as the peak amplitude, the average effective damping ratio for axial pressure of 10MPa and 5MPa are calculated as 0.18 and 0.15, respectively. When axial pressure drops to 3.3MPa, the average effective damping ratio is approximately 0.11. These effective damping ratios are slightly higher than the effective damping ratio obtained from layer-unbonded STRP specimen tests (0.12 at 80% shear strain with the axial pressure of 5MPa). The damping ratio also depends on axial pressure on the STRP specimens. The effective damping ratio is evidently higher than the natural rubber bearings for which the equivalent damping is usually 2 to 3 % of critical damping [6]. The

relationship between shear strain and effective damping is shown in Fig. 5.17 for the entire range of lateral displacement.

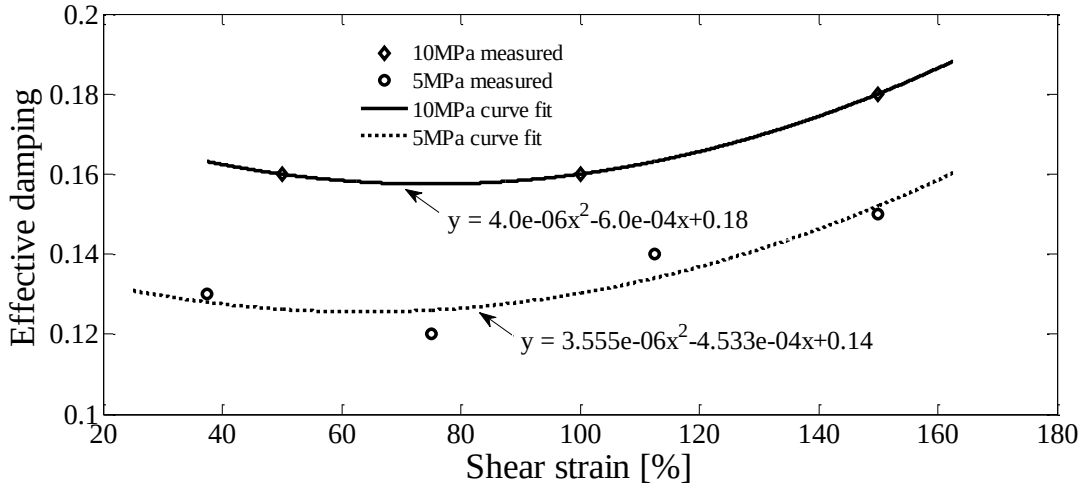

Figure 5.17 Variation of effective damping ratio with shear strain

The test result shows that the adhesive bonding is sufficiently strong to withstand the shear strain of 150%. The tests conducted with larger axial pressure (10MPa) and with low axial pressure (3.3MPa) show that the layer-bonded STRP specimens are especially suitable for lightly loaded building structures. Figure 5.16 shows that the horizontal effective stiffness of the layer-bonded STRP specimen significantly reduces as the horizontal displacement increases. This phenomenon can be attributed to the unbonded contact condition of the layer-bonded STRP specimen with the top and bottom support interfaces. The decrease in horizontal stiffness consequently increases the isolation period, provided that the stability of the isolation bearing as well as whole building structure is maintained. Figure 5.17 reveals that the effective damping value also depends on the axial pressure as well as horizontal displacement.

Figure 5.18 clearly shows that the force displacement relationship of 5MPa axial pressure has positive incremental force resisting capacity up to 60mm which is equivalent to 150% shear strain based on the thickness of rubber. From this figure, it can be concluded that the 10MPa axial stress can be applied to achieve 100% shear strain, beyond this the STRP bearing is considered as unstable [2] and [4]. The stability of the STRP bearings can be enhanced by increasing the footprint area of the bearings. In the meantime, it should be ensured that the bearings should be in compression. This is considered as mandatory condition in case of dowelled connection system with support interfaces.

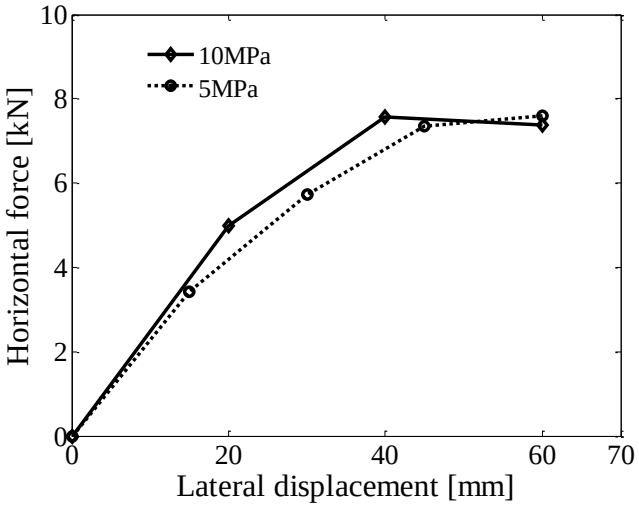

Figure 5.18 Comparison of force-displacement relationships for various axial pressures

5.6 Finite element analysis of layer-bonded STRP bearings

The FE analysis of a strip layer-bonded STRP-4 specimen was carried out to assess the force-displacement behavior and to evaluate the stress state within the specimen when it is used as seismic isolator. The sketch of the deformation pattern of the layer-bonded STRP as a seismic isolator with unbonded application between the superstructure and substructure is shown in Fig. 5.19. In this case, the moment created by the offset of the resultant compressive force P balances the moment created by the shear force V, no or negligible tensile stresses are produced within the STRP isolator.

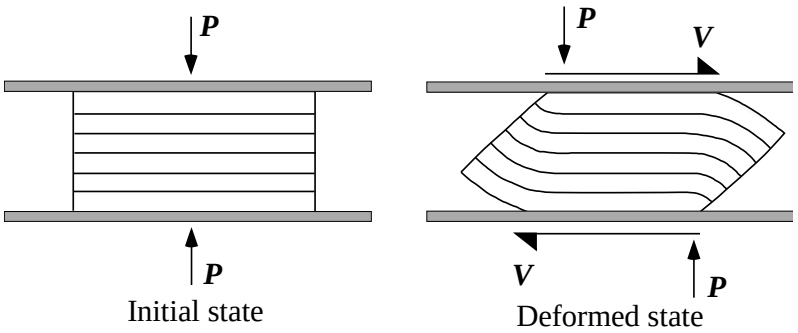

Figure 5.19 Free body diagram of laterally deformed layer-bonded STRP bearing

5.6.1 Modeling of layer-bonded STRP

5.6.1.1 Finite element model of cord-rubber composite

The STRP that constitutes the bearing is composed of a rubber body with embedded steel reinforcing cords. The bearing's physical properties are given in Table 3.1 of chapter 3 and geometrical properties are given in Table 5.1. FE analysis of the strip layer-bonded STRP-4 was conducted using commercially available general purpose finite element software MSC Marc 2010 [7]. The detail description about the finite element model of cord-rubber composite is presented in chapter 4.

5.6.1.2 Finite element mesh generation

The rubber was modeled using four-node, isoparametric quadrilateral elements coded for plane strain incompressible applications. This element is preferred over higher-order elements when used in simulating large deformation and contact analysis [8]. The reinforcing steel cords were modeled by using the isoparametric plane strain two-node line elements. These elements need to be used in conjunction with four-node plain strain continuum elements (host elements). These rebar elements have to be embedded into their corresponding solid elements representing the matrix materials. Since the matrix element and the rebar element share the same nodal points, no additional degrees of freedom are introduced. The degrees of freedom of the nodes to be inserted are tied to the corresponding degree of freedom of the host elements. The rebar model allows that the rubber and the steel reinforcing cords are described by different stress-strain constitutive relationships. When defining the material properties of the rebar layer, the reference plane or the edge of the rebar layer should be defined. In this model, the reference axis of rebar direction, the cross-section area of a single rebar, density/spacing of the rebar, angle of orientation with respect to the reference axis were defined.

For the top and bottom layers, the edge length of the quadrilateral elements was selected to be approximately 0.4mm. The element edge length for intermediate layers was selected to be approximately 0.5mm. These modeling techniques were also used to model the steel reinforcing cords. There are 8750 quadrilateral elements and 1250 rebar elements in a single layer of STRP

placed near the uppermost and lowermost support interfaces. The number of quadrilateral and rebar elements in the middle layers was reduced to 5800 and 1000 respectively. There are total of 33600 elements in a layer-bonded STRP-4 model. The area of single steel reinforcing cord in carcass layers is 0.44mm^2 while in the belt layer is 0.63mm^2. The spacing of the steel reinforcing cords is about 0.4/mm. The orientation of the individual layers with respect to the direction of the cords in the carcass layer is shown in Fig. 4.14 of chapter 4. The orientation of the rebar direction was assigned as ± 70º for belt layers about the reference axis [9]. The dimensions and modeling of single layer STRP used in FE model is shown in Fig. 5.20. The rubber is modeled as hyperelastic material model while the steel reinforcing cords in the finite element model is treated as a linear elastic isotropic material with material properties given in Table 3.1 of chapter 3. The typical matrix element and rebar element is shown in Fig. 4.13 and typical finite element meshes is shown in Fig. 5.20 (b).

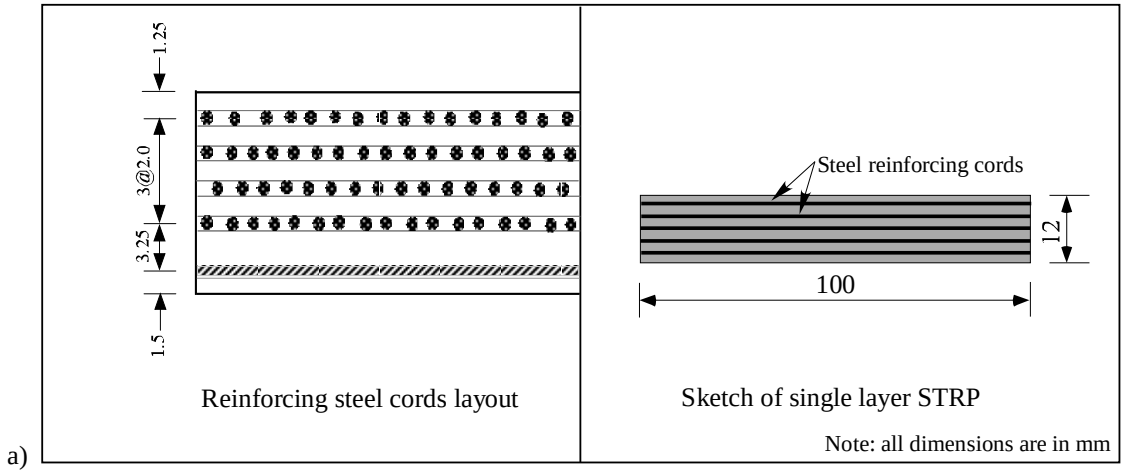

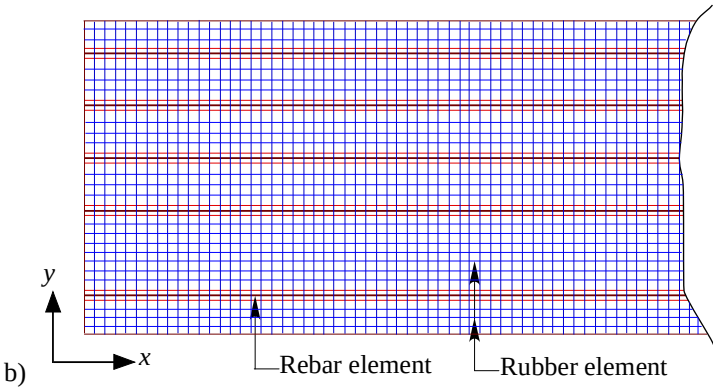

Figure 5.20 a) Dimensions and b) finite element mesh in a layer of STRP

5.6.1.3 Boundary conditions

Two horizontal rigid bodies (lines) were defined at the top and bottom of the STRP bearing to represent the superstructure and substructure, respectively. In this model, the vertical as well as horizontal loads were applied on the top support; the top support was allowed to move in vertical as well as in horizontal directions while the bottom support was considered as a fixed support. The boundary conditions were selected to represent the experimental setup. In this contact model, the contact between the supports and the layer-bonded STRP bearing was modeled by the Coulomb friction law with a coefficient of friction as 0.8. The coefficient of friction was selected such that no slips occur between the contact supports and the rubber. In this contact model, the shear force is transmitted through a Coulomb friction mechanism, while the normal force is transmitted across the link. The individual layer of layer-bonded STRP was modeled as glue contact. In this contact model, the degrees of freedom of the contacting nodes are tied. This contact model prevents any detachment or slip between the individual layers of layer-bonded STRP by constraining the nodal points in the directions normal and tangential to the touching surfaces. Due to the unbonded application with support interfaces, when the compression contact stresses approach to zero, the nodal points were allowed to detach from the contact supports.

5.6.1.4 Constitutive model of rubber material

Elastomeric materials are characterized by hyperelastic material model. Due to this reason, the mechanics of behavior of elastomeric material can be described in terms of strain energy density function. There are varieties of strain energy density functions proposed by different researchers are available, among those models, Mooney-Rivlin model is commonly used to characterize the rubber material undergoing large strain [10]. This model is simplest hyperelastic model for elastomeric materials when material tests data is insufficient. The Mooney-Rivlin material law is well suited for most practical applications involving cord-rubber composite [11]. In the current modeling, three-term Mooney-Rivlin strain energy density model was used which is given in Eq. (5.3). The detail about the material constants is discussed in chapter 3.

$$W = C_{10}(I_1 - 3) + C_{01}(I_2 - 3) + C_{11}(I_1 - 3)(I_2 - 3) \tag{5.3}$$

5.6.2 Loads

In the analysis, loads were applied to the model in an incremental manner in order to capture the nonlinear behavior of the cord-rubber composite. At the initial stage of the analysis, the target vertical load corresponding to compressive pressure of 5MPa or 10MPa was applied in different incremental steps. Then the horizontal load was applied with the constant compressive load until a target lateral displacement was achieved. The target lateral load was selected such that 150% shear deformation in the layer-bonded STRP-4 is achieved.

5.6.3 FE analysis of layer-bonded STRP

The FE analysis of layer-bonded STRP was carried out for the case of application unbonded with the support surfaces. This type of seismic isolation system allows for rollover deformation to take place in the layer-bonded STRP used as the isolator. When the rollover deformation occurs one end of the isolator separates from the contact support while the other end is highly stressed as shown in Figs. 5.21 (a) and 5.22 (a). The corresponding shear strain distribution within the rubber layer of layer-bonded STRP is shown in Figs. 5.21 (b) and 5.22 (b), respectively.

The analysis was two-dimensional under the plane strain assumption. The low value of shear modulus of rubber causes the deformation pattern relatively severe as compared with other materials like steel and concrete. Its large deformability together with its near-incompressibility makes rubber a major challenge for finite element analysis. The large deformation that the rubber components experience can only be modeled with a finite strain formulation [1]. The FE analysis using the conventional lower-order isoparametric finite elements not tailored for incompressibility analysis produces extremely poor results [1] occasionally involving the volumetric mesh-locking [12]. The mixed methods, in which both stress and strains are treated as unknown, are used in modern FE analysis of incompressible and nearly incompressible materials [13]. The results of finite element analysis presented in this chapter are based on the widely popular mixed method proposed by Herrmann [14].

In large deformation analysis of elastomeric materials, two equivalent methods may be used: the total Lagrangian method and updated Lagrangian method. In the total Lagrangian approach, the

equilibrium is expressed with the original undeformed state as the reference; in the updated Lagrangian approach, the current configuration acts as the reference state [8]. Generally, elastomeric materials undergo very large deformation under shear loading. In this case, it is necessary to update the orientation of the local coordinate system based on the deformed configuration of the element during the analysis. Due to this reason, updated Lagrangian approach is used in the FE analysis of layer-bonded STRP.

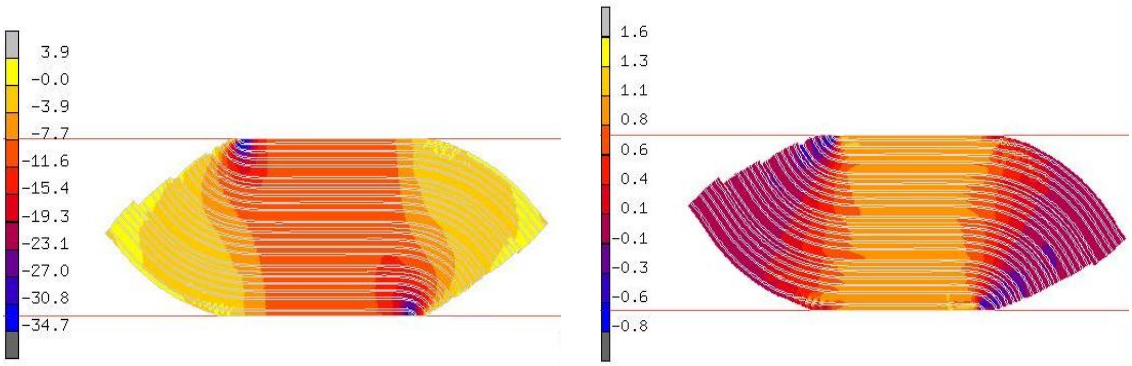

a) Contour of normal stress S_{22} (MPa) b) Shear strain distribution

Figure 5.21 Normal stress and shear strain distribution in the rubber layers of layer-bonded STRP-4 bearing under vertical compressive pressure of 5MPa

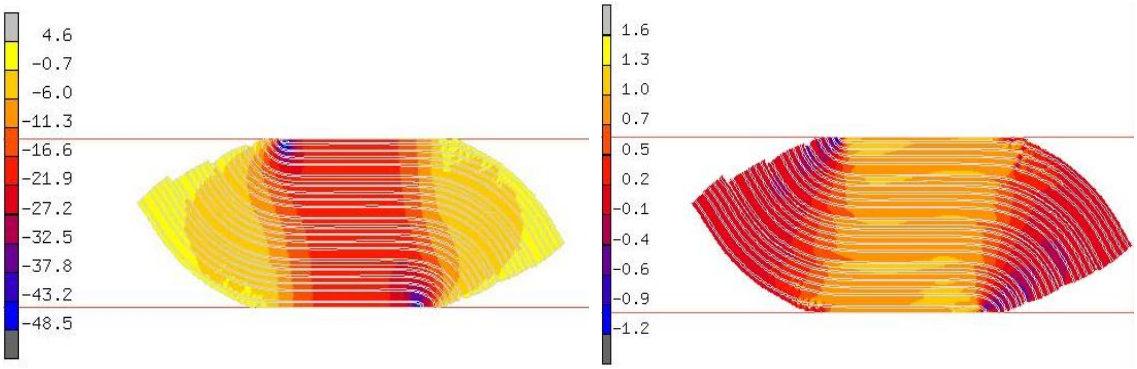

a) Contour of normal stress S_{22} (MPa) b) Shear strain distribution

Figure 5.22 Normal stress and shear strain distribution in the rubber layers of the layer-bonded STRP-4 bearing under vertical compressive pressure of 10MPa.

In 2D finite element model, for each rubber element, local axes can be denoted by axis 1 and

axis 2 which are parallel and perpendicular to the orientation of the carcass layer, respectively. The normal stress S_{11} acts parallel to the orientation of steel reinforcing cords in carcass layer while normal stress S_{22} acts perpendicular to the reinforcing cords in carcass layer. Due to the unbonded application with support interfaces, the STRP is allowed to roll-off of the contact supports which results in shifting the line of action of vertical load resultant, at each contact surface as shown in Fig. 5.19. As a result, no balancing moment develops at the top and bottom surfaces of layer-bonded STRP. The lower level of tension stress S_{22} as shown in Fig. 5.21(a) and 5.22(a) in the layer-bonded STRP prevents the peeling of STRP layers at extreme shear deformation level. The compression zone is responsible to carry the vertical compressive load. As shown in Fig. 5.21 and 5.22, the bonding between the layers of STRP is sufficiently strong in transmitting the stresses and to prevent the tangential motion between the layer-bonded STRP.

For the efficient operation of elastomeric isolator, the shear strain in the rubber material must be extremely large [15].The shear strain in layer-bonded STRP is approximated as 1.5 and the maximum shear strain is in reasonable agreement with the maximum values given in Fig. 5.21(b) and 5.22(b).

5.6.4 FE analysis results and discussion

The FE analysis was carried out on the strip layer-bonded STRP-4 model whereas the experimental tests were conducted on a square layer-bonded STRP-4 specimen. The lateral load-displacement relationship of the layer-bonded STRP is nonlinear as shown in Figs. 5.23 and 5.24. These figures contain lateral load-displacement relationships for the tests and the FE analysis of layer-bonded STRP-4 up to 150% shear strain. As shown in Figs. 5.23 and 5.24, reasonable agreement between the experimental test and FE analysis results can be found. However, it should be noted that for a higher level of lateral displacement, the horizontal force obtained by the FE analysis is noticed to be higher than the experimental test results in both cases. Figure 5.25 contains lateral load-displacement relationships obtained by FE analysis of layer-bonded STRP-4 up to 150% shear deformation for different axial pressures.

Figures 5.21 (a) and 5.22 (a) show the distribution of normal stress (22-component) corresponding to 150% shear deformation in the layer-bonded STRP-4 for 5MPa and 10MPa axial pressures, respectively. As seen in Figs. 5.21 (a) and 5.22 (a), as a result of rollover deformation, high level stresses are induced at the corner region, while the stresses are relatively

lower in the other region. Almost negligible tensile stresses are transferred to a laterally deformed STRP at the isolator's contact supports. As a result, no balancing moment develops at the top and bottom surfaces of a STRP bearing. The stability of the bearing entirely depends on the contact area between the bearing and the support surfaces at its maximum shear deformation level.

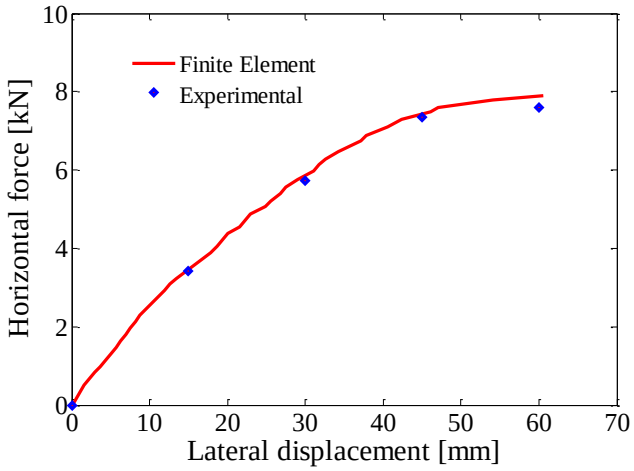

Figure 5.23 Load-displacement relationship of layer-bonded STRP-4 bearing with 5MPa axial pressure; comparison between experimental and FE analysis results

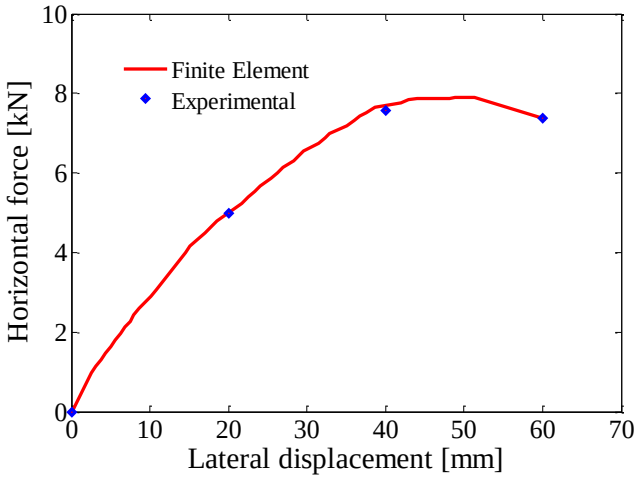

Figure 5.24 Load-displacement relationship of layer-bonded STRP-4 bearing with 10MPa axial pressure; comparison between experimental and FE analysis results

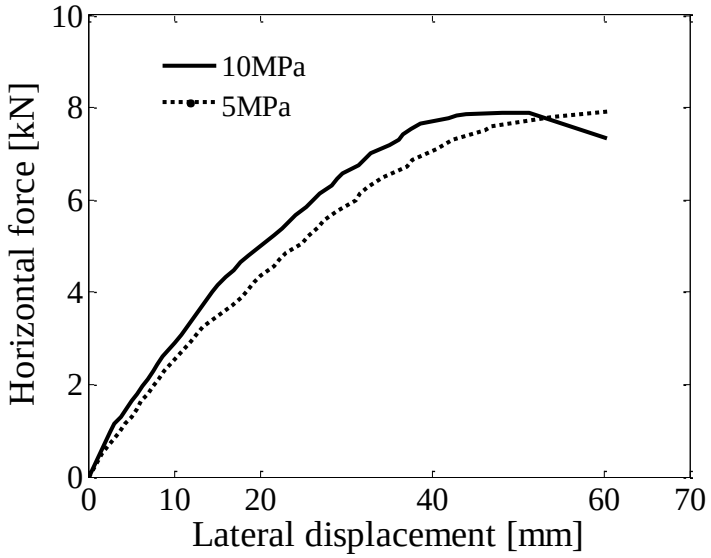

Figure 5.25 Load-displacement relationship of layer-bonded STRP-4 bearing obtained by FE analysis with different axial pressures

5.7 Discussion on applicability of layer-bonded STRP bearings

The isolation bearings are generally used at axial pressure levels ranging from 5 to 7MPa [5]. The compressive stress on isolators was between 3 and 8MPa in the early years in Japan [16]. Due to the improved performance of the isolators, the compressive pressure is increased to 7-13MPa for natural rubber bearings and 5-10MPa for high damping rubber bearings [16]. These isolators are generally adopted in multi-story building structures where the anticipated compressive load is much larger than the residential building. The average axial load on each of the columns of a three-story reinforced concrete building is estimated as 330kN. The expected average axial pressure on layer-bonded STRP bearings is about 3.3-7.5MPa in order to achieve 150% shear strain, as demonstrated by the test and analysis in the previous sections. The analytical study on stability of bonded STRP isolators [17] reveals that the layer-bonded STRP can provide positive force resisting capacity up to 150% shear strain when loaded with axial pressure of 8.6MPa. In this regards, the layer-bonded STRP can serve the purpose of base isolators for low-rise residential buildings. An interesting factor, however, is the level of damping shown by the STRP bearings. Figure 5.18 shows that the equivalent damping ratio that

depends on the shear strain amplitude is always greater than 0.10 in any case. It is a favorable aspect of the use of layer-bonded STRP as seismic isolators to conform isolation design philosophy to reduce the seismic demand using the effect of energy dissipation mechanism of the spectrum system.

The production cost of a single layer of STRP is about 12 dollars. The total cost including adhesive chemical of a layer-bonded STRP-4 specimen is about 68 dollars in Japan. Similar type of specimen can be produced in developing countries in the order of one fifth of the cost of Japan. The most important features of these types of bearings are the domestic production, they do not have steel end-plates and no extra cost is required for connection system with support interfaces. However, their cost is in the hundreds of dollars as compared to the cost of commercially available seismic isolators in the thousands of dollars.

5.8 Conclusion

Experimental tests as well as FE analysis were conducted on layer-bonded STRP bearings intended to be used as seismic isolators. The layer-bonded STRP used in this study were produced by applying adhesive on the interfaces between the individual layers of STRP. The aim of the study was to investigate the behavior of layer-bonded STRP in static compression and in cyclic shear loading and to discuss about the feasibility of the application to seismic isolators. The results of shear loading test are used to compute the mechanical properties of the layer-bonded STRP bearing. Two different levels of axial loads were applied during the shear loading tests and FE analysis to investigate the load-displacement behavior of the layer-bonded STRP. During the shear deformation, none of the samples show layer separation. This result indicates that the bonding agent is sufficiently strong in transmitting the shear forces. The results of shear loading test and FE analysis are compared in terms of load-displacement behavior and found to be in close agreement.

The properties of layer-bonded STRP are further compared with the relevant code provisions in order to identify the viability of the proposed base isolation system. The key findings obtained in this part of the study are listed as below:

1. The axial load carrying capacity of the layer-bonded STRP bearing is comparable with those of commercially available elastomeric bearings.

2. The vertical stiffness of the layer-bonded bearing is 56.417MN/m which is sufficient to withstand structural load of low-rise residential buildings and to prevent the rocking motion of the structure. An effective compression modulus of 270.4MPa at an axial pressure of 5MPa implies a vertical vibrational frequency of 18.4Hz. The vertical vibrational frequency is sufficient for seismic isolation purpose [5].

3. The ratio between vertical and horizontal stiffness is greater than 150 in any case so that the layer-bonded STRP-4 bearing can be considered as base isolation device [3].

4. The layer-bonded STRP bearings provide positive incremental force resisting capacity up to shear strain level of 150% when loaded with 5MPa axial pressure which is one of the characteristic properties of the seismic isolation device [4].

5. The test results with different axial pressures indicate that the shear deformation capacity is sharply reduced when loaded with larger axial pressures.

6. The damping ratio of the layer-bonded STRP bearings is in agreement with the first part of the study and is found dependent on axial pressures.

7. In conclusion, the performance of layer-bonded STRP bearing is improved and the mechanical properties are comparable with those of commercially available elastomeric bearings.

8. Identification of dynamic response characteristic of layer-bonded STRP bearing shall be the focus of further investigation.

References

[1] James M. Kelly, Dimitrios Konstantinidis. Low-cost seismic isolators for housing in highly-seismic developing countries. 10th *World Conference on Seismic Isolation, Energy Dissipation and Active Vibrations Control of Structures*, Istanbul, Turkey, 2007,May 28-31

[2] Uniform Building Code, Volume 2, Structural Design Requirements, 1997, Earthquake Regulations for Seismic Isolated Structure, Whittier, CA.

[3] Eurocode 8. Design of structures for earthquake resistance. 2004.

[4] ASCE-7. Minimum design loads for building and other structures, ASCE/SEI 7-05.

New York, American Society of Civil Engineers, 2005.

[5] James M. Kelly. Earthquake-resistant design with rubber. 2nd edition London, Springer-Verlag, 1997.

[6] Farzad Naeim, James M. Kelly. Design of seismic isolated structures from theory to practice. John Willey and Sons, Inc. 1999.

[7] MSC Software (2008r1), MSC Marc 2010 and MSC Marc Mentat 2010, Santa Ana, California.

[8] MSC.Marc. Theory and user information, Vol. A Santa Ana, CA, MSC software Corporation; 2010.

[9] J. Y. Wong. Theory of ground vehicle. 3rd edition, John Wiley and Sons, Inc., 2001.

[10] Aidy Ali, M. Hosseini and B. B. Sahari. A review of constitutive models for rubber-like materials. *American Journal of Engineering and Applied Science*, 2010, Vol. 3(1), pp: 232-239.

[11] P. Helnwein, C. H. Liu, G. Meschke and H. A. Mang. A new 3-D finite element model for cord-reinforced rubber composites-Application to analysis of automobile tires. *Finite Elements in Analysis and Design*, 1993, Vol. 14(1), pp: 1-16.

[12] MSC Software (2000) Nonlinear Finite Element Analysis of Elastomers, Whitepaper Santa Ana, California.

[13] Zienkiewicz OC., Taylor R.L., Zhu J.Z. The finite element method: its basis and fundamentals, 6th edition, 2005. Oxford, Butterworth-Heinemann.

[14] L.R. Herrmann. Elasticity equations for incompressible and nearly incompressible materials by variational theorem. *AIAA Journal*, 1965, Vol. 3(10), pp: 1896-1900.

[15] Hamid Toopchi-Nezhad, Michael J. Tait, Robert G. Drysdale. Bonded versus unbonded strip fiber reinforced elastomeric isolators: Finite element analysis. *Composite Structures*, 2011, Vol. 93 (2), pp: 850-859.

[16] Peng Pan, Dan Zamfirescu, Masayoshi Nakashima, Nariaki Nakayasu, Hisatoshi Kashiwa. Base-isolation design practice in Japan: Introduction to the post Kobe approach. *Journal of Earthquake Engineering*, 2005, Vol. 9(1), pp: 147-171.

[17] Huma Kanta Mishra, Akira Igarashi. Experimental and analytical study of scrap tire rubber pad for seismic isolation. World Academy of Science, Engineering and Technology, Issue 62, (*Proc. International Conference on Earthquake and Structural Engineering 2012*): 202-208, February 19-21, 2012, Kuala Lumpur, Malaysia.

6

Design of STRP bearings, numerical modeling and validation by pseudodynamic test

This chapter describes about the design and modeling of individual STRP bearings as well as building structure. The analytical results are verified by conducting pseudodynamic tests. The aim of this chapter is to discuss about the dynamic response of the proposed base isolation system. Further, the pseudodynamic test results are compared with numerical simulation results in order to evaluate the seismic performance of the base isolation system.

6.1 General

In this part of study, seismic response of the base isolated building using STRP bearings is carried out. Initially, analytical modeling of the bearings including building is carried out and then the results are verified by conducting pseudodynamic tests. The fabrication procedure of the specimen bearings used in the pseudodynamic test is discussed in chapter 5.

6.2 Building model

The building considered in this study is a three-story reinforced concrete frame structure with brick masonry infill walls as shown in Fig. 6.1. The building is 7.85m by 11.25m in plan and 9.0m in height. All the columns are of square cross sections of 300mm and all the beams are of 230mm in width and 350mm in depth. A floor slab has to be added at the ground level to

provide physical separation between the substructure and superstructure. The superstructure was designed for the fixed base building without considering the isolation system. The building structure was designed on stiff soil site with seismic zoning factor of 1.0. During the design of fixed base building, the infill walls were not included to be the part of the lateral force resisting system.

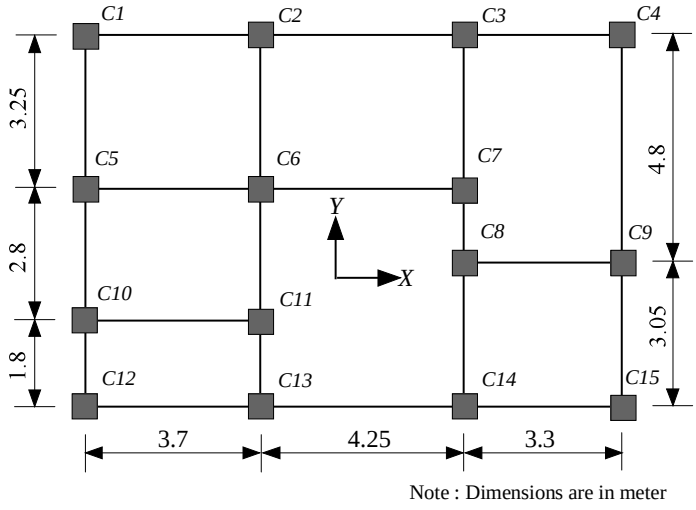

Figure 6.1 Building plan along with layout of STRP bearings

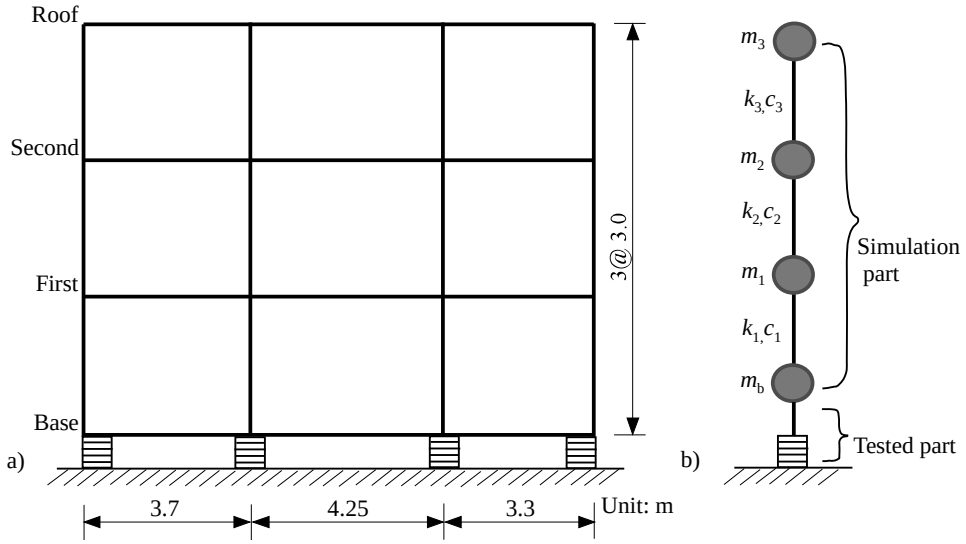

Figure 6.2 Base isolated building a) basic dimensions b) division into simulation and experimental part

6.3 Design of STRP bearings

The detail about the layer-bonded STRP bearings fabrication process and experimental test has been described in chapter 5. Total of 15 STRP bearings placed under each of the columns has to carry the total load of the building. These STRP bearing are not bolted with the substructure and superstructure but are simply placed between the support surfaces.

The principal design requirements of the rubber bearings are

1. bearing should provide required horizontal stiffness in order to achieve the desired horizontal frequency of the isolation system
2. vertical stiffness should be large enough so that the amplification of motion in the vertical direction is avoided as well as the rocking of the isolated structure is minimized.
3. bearing should control the maximum shear strain under the designed earthquake without failure
4. damping of the bearing should be sufficient to keep the displacements within the acceptable limits.

The detail design procedure is outlined below:

1. The vertical compressive load *W* is calculated using the Eq. (6.1) [1].

$$W = 1.2DL + 1.0LL + |EL| \tag{6.1}$$

where *DL* is the dead load of the structure, *LL* is the 25% live load, |*EL*| is the absolute value of earthquake load.

The design parameters are set according to the experimental tests and analytical study conducted on the STRP isolator. The maximum allowable axial pressure p, shear strain λ, horizontal frequency f_h, maximum shear displacement capacity δ and shear modulus G of the isolator has to be decided. The required area A of the square bearings can be computed by dividing the total load by the nominal axial pressure.

2. The total thickness t_r of the bearing is computed using the Eq. (6.2) [2]

$$t_r = \frac{Gg}{p}\frac{1}{(2\pi f_h)^2} \tag{6.2}$$

where g is the acceleration due to gravity.

3. The shape factor S of the bearings is computed using the expression given in Eq. (6.3). For this purpose average thickness of rubber layers is calculated.

$$S = \frac{Loaded}{force - free}\frac{area}{area} \tag{6.3}$$

4. The vertical load carrying capacity P of the square bearing is computed by the Eq. (6.4) [3]

$$P = \frac{GA}{\left(\frac{1.92kt_r/l}{S\sqrt{3}}\right) - \left(\frac{1.064}{S(S+2)}\right)} \tag{6.4}$$

where k is the effective length factor and is dependent on the connection of isolator between the support interfaces. In practical rubber bearings, the upper plate is usually not constrained horizontally and the critical load will be reduced by a factor of 2 so that the ratio between P and W must be substantially greater than 2 for stability [2].

5. The compression modulus E_c of the bearing is computes by

$$E_c = nGS^2 \tag{6.5}$$

where n is the factor that depends on the shape of the rubber bearing, for square shape the value of n is 6.73 [4].

6. The initial horizontal stiffness is computed using the Eq. (6.6) and is dependent on lateral displacement.

$$K_h = \frac{GA}{t_r} \tag{6.6}$$

7. The vertical stiffness of the bearing is calculated using the value of compression modulus, footprint area of bearing and rubber thickness.

$$K_v = \frac{E_c A}{t_r} \tag{6.7}$$

8. The ratio between vertical and horizontal stiffness must be greater than 150 for practical seismic isolation device [18].

9. The vertical frequency of vibration is computed as

$$6.73S^2 = \left(\frac{f_v}{f_h}\right)^2 \tag{6.8}$$

Generally, the vertical frequency of vibration is in the range of 8-12Hz for base isolation purpose [23]

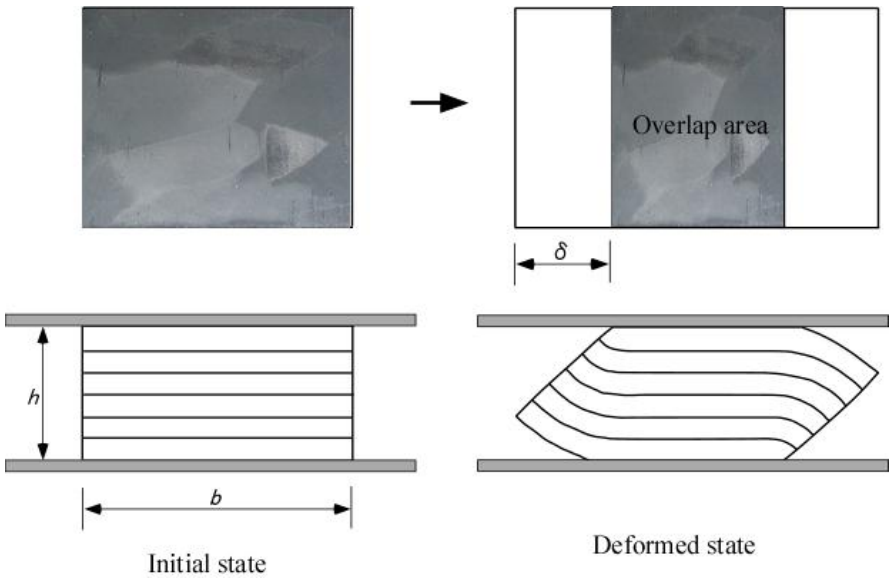

Figure 6.3 Lateral deformation pattern of layer-bonded STRP bearing

Figure 6.1 shows the layout of STRP bearings within the building. The additional structural requirement is the monolithic beam slab system added to provide rigid diaphragm action. Due to

this reason, while comparing the cost of base isolated and fixed base building, the additional structural requirement cost shall be considered in base isolation system cost.

The designed axial load on each bearing is presented in Table 7.4. Axial compressive load on each STRP bearings varies from 177.5kN to maximum of 619.9kN. The material properties of the STRP bearing cannot be altered so that each bearing were design 300mm square in size with overall thickness of 150mm. The thickness of bearings was computed to achieve the MCE risk level displacement with shear strain of 1.66 (based on the thickness of rubber). The total thickness of isolator is equivalent to twelve individual layers of STRP.

Depending on the capacity of the testing equipment available, only 1/3 scale model specimen samples were fabricated. In many engineering application, the design of civil structures has been verified by using experimental methods, in which small scale models have been frequently used because of limited capacity of testing facilities and economic reasons. While preparing these small scale models, the similitude law shall be used for analogizing prototype structure accurately with small scale models. The application of similitude law to design small scale models depends on the aim and methodology of the tests. With regard to dynamic problem, when the three basic dimensions of mass M , length L and time T are selected, other variables are derived from them [6]. The similitude law used in pseudodynamic tests is presented in Table 6.1.

Table 6.1 Scaling law for dynamic model

Physical Quantity	Dimension	Scale factor
Length	L	s
Time	T	s
Mass	M	s^3
Velocity	LT^{-1}	1
Acceleration	LT^{-2}	s^{-1}
Displacement	L	s
Force	MLT^{-2}	s^2
Stiffness	MT^{-2}	s

The layer-bonded STRP bearing having physical dimensions of 100×100×50 mm (STRP-4) including adhesive thickness were produced as shown in Figs. 6.4.

Figure 6.4 Photograph of layer-bonded STRP-4 specimen bearings

6.4 Quasi-static test

6.4.1 Loading system

Three dimensional schematic view of loading system which was used to carryout quasi-static and pseudodynamic tests is shown in Fig. 6.5. This loading system consists of one, three and five actuators in x, y and z directions, respectively. In all the directions, one actuator is pin connected between the reaction frame and rigid loading block. These three actuators namely; Fx, Fy and Fz are used to apply displacement and force in respective directions. Beside these actuators, four actuators are used to constraint the rotation about x and y axis and remaining two actuators are used to constraint the rotation about z axis. The specimen bearing is placed between the two steel plates to represent the superstructure and substructure, respectively. The specimen is placed without any fastening system with support surfaces as shown in Fig.6.3. The capacity of the loading system is presented in Table 5.2.

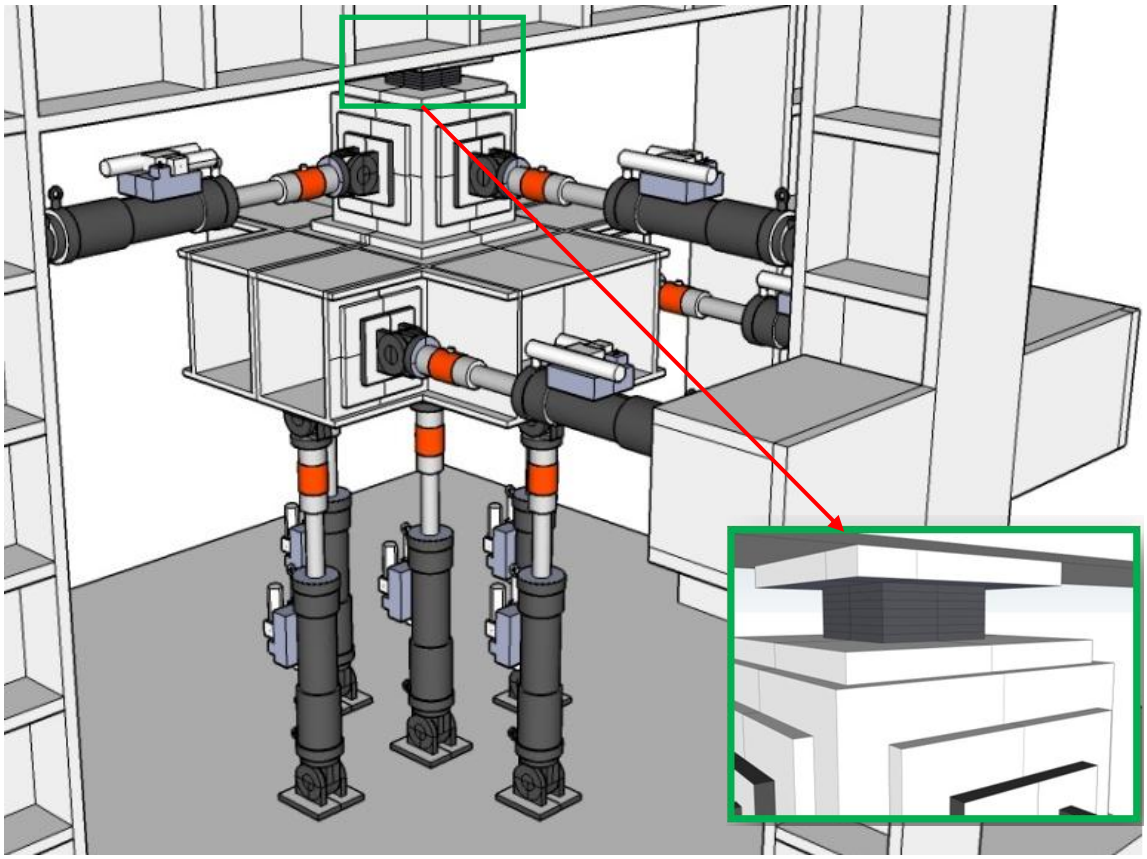

Figure 6.5 Schematic view of loading system

6.4.2 Tests procedure

Prior to pseudodynamic loading test, two quasi-static cyclic loading tests were performed to clarify the fundamental properties of the STRP bearing. Constant vertical axial pressure of 10MPa and 5MPa was applied for these two tests called as QS10 and QS5 hereafter, respectively. The specimens were loaded vertically with a constant load by load controlled vertical actuator Fz , and a series of horizontal cyclic displacements were applied by horizontal actuator Fx . Here, the function of horizontal actuator Fy is to constraint the out of plane movement of the loading system.

For the QS10, 1/3 scale model bearing was tested in cyclic shear with three fully reversed cycles at three maximum shear displacement amplitudes of 20mm, 40mm and 60mm which correspond

to shear strain of 50%, 100% and 150% respectively. Similar methodology was followed for the QS5 but the test was conducted with reduced displacement amplitudes. The specimen was tested in cyclic shear with three fully reversed cycles at four maximum shear displacement amplitudes of 15mm, 30mm, 45mm, and 60mm which correspond to shear strain of 37.5%, 75%, 112.5% and 150%, respectively. The test results of QS10 and QS5 were used to compute the mechanical properties of the specimen bearings including stiffness and damping ratios.

6.4.3 Parameters identification

The effective damping ratio of the tested layer-bonded STRP bearing was computed using the previously tested STRP bearings. Figure 6.6 contains the relationship between effective damping and shear strain for different levels of axial pressures. The predicted effective damping values for the 3.3MPa axial pressure at 100% shear strain is about 0.11. Similar methodology was adopted to predict the effective stiffness of the tested bearings. Figure 6.7 contains the relationship between effective stiffness (effective shear modulus) and shear strain for different levels of axial pressures. The predicted effective stiffness for 3.3MPa axial pressures at 100% shear strain is about 171kN/m. The numerical analysis was carried out using the computed damping ratio and effective horizontal stiffness.

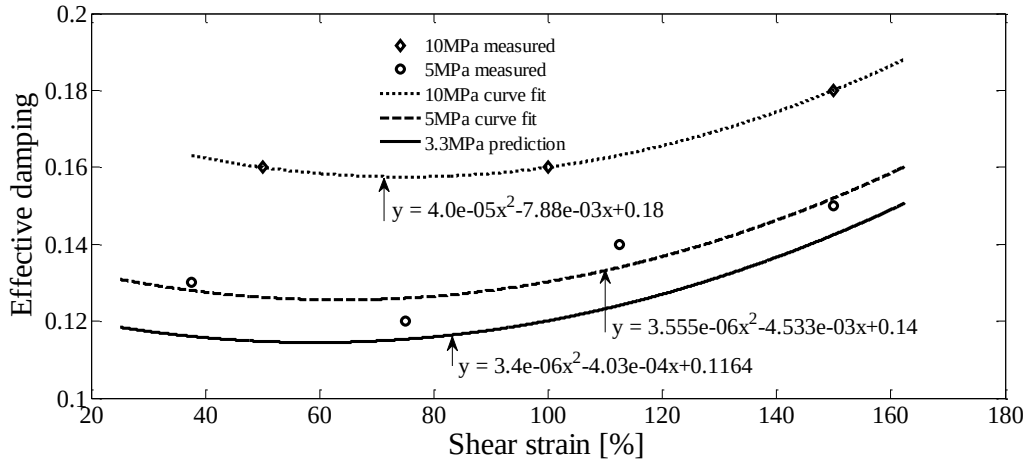

Figure 6.6 Relationship between effective damping and shear strain for different levels of axial pressures

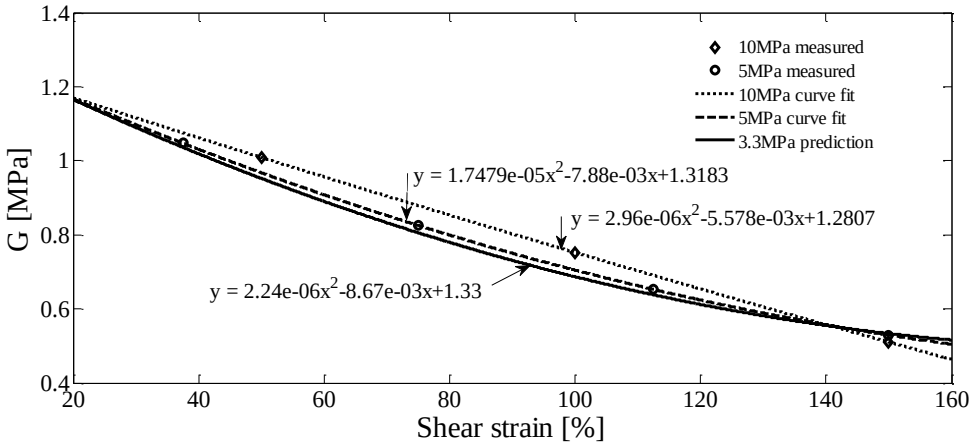

Figure 6.7 Relationship between effective stiffness and shear strain for different levels of axial pressures

6.5 Numerical simulation

6.5.1 General

The essential basis of seismic isolation is to support a structure providing a horizontal flexibility. This gives overall structure a longer effective period and low accelerations and inertia forces generated by earthquakes. The horizontal forces generated by typical design earthquakes are greatest on structures with low flexibility and low vibration damping. The seismic forces on such structures can be greatly reduced by supporting the structure on mounts which provide horizontal flexibility and high vibration damping. For most structures, vertical seismic loads are relatively unimportant in comparison with horizontal seismic loads. Therefore, the main seismic attack on structure is the set of horizontal inertia force acting on the structural masses, these forces being generated as a result of horizontal ground accelerations.

The effects of an earthquake on a building depend not only on properties of the earthquake ground motion but also on the dynamic characteristics of the building. For seismic isolation of buildings, it is necessary to include the flexibility of the structures itself and the interaction between the dynamics of structure and the dynamics of the isolation system. Hence, dynamic analyses are required in order to be able to predict the response of structures subjected to

dynamic loading. In these analysis methods, the real structures are represented by appropriate analytical models which can be described mathematically.

The complexity of an analytical model is determined by the real structural properties and behavior it must represent. For most building structures, a lumped mass model usually with the whole story mass lumped at the floor level is generally all that is required. Therefore, the lumped mass model is used in this study because the mass of the system is assumed to be represented by a finite number of point masses.

6.5.2 Equations of motion

If the dynamic loading is a known function of time, then a deterministic method for solving the equations of motion can be applied. The equation of motion for a multi degree of freedom (MDOF) structure subjected to a time varying load can be written as

$$[M]\{\ddot{v}\}+[C]\{\dot{v}\}+[K]\{v\}=\{P(t)\} \tag{6.9}$$

where M, C and K are the mass, damping and stiffness matrices, $\{\ddot{v}\}$, $\{\dot{v}\}$ and $\{v\}$ are the accelerations, velocities and displacements of the structures and $\{P(t)\}$ is the time varying loading on the structure.

For a multistory building, it is reasonable to lump the mass of the structure at certain nodes at which the translational degree of freedom are defined. In this case, the lumped mass matrix has a simple diagonal form. The off-diagonal terms of this matrix vanish since an acceleration of any mass point produces an inertia force at that point [7]. It is also usually assumed, in most building analysis, that the mass remains constant with time. The stiffness of the structure has a major effect on the design of multistory building. The stiffer the structure the shorter the natural periods of free vibration and the smaller the displacements under the earthquake excitation. The possible change of the structural stiffness due to inelastic or nonlinear actions within the structural components should be calculated during the dynamic analysis. The direct stiffness method [8] can be used to assemble the stiffness matrix of individual members into the global stiffness matrix of the structure.

It must be noted that the use of linear viscous damping is a mathematical convenience. The

assumption of linear viscous damping which provides the simplest mathematical model of damping that is directly proportional to the velocity [9]. If a deterministic nonlinear time history analysis is used, the damping matrix is usually assumed to be a combination of the mass and stiffness matrices, thus

$$[C] = \alpha[M] + \beta[K] \tag{6.10}$$

where the coefficient α and β are specified or computed by specifying the fraction of critical damping at two mode numbers. The damping of the superstructure was considered as stiffness proportional damping with viscous damping ratio of 0.05.

In Eq. (6.9), the displacements are the total displacements of the structure measured from some fixed reference point. Usually most engineering calculations are relative displacement $\{x\}$, i.e. displacement of the structure with respect to its foundation. As illustrated in Fig. 6.8, the total displacement $\{v\}$, can be represented by a combination of this relative displacement $\{x\}$ and the ground displacement $x_g(t)$.

$$\{v\} = \{x\} + \{r\}x_g(t) \tag{6.11}$$

where $\{r\}$ is the displacement of the structure due to a unit ground displacement, then substituting Eq. (6.11) into Eq. (6.9) leads to

$$[M]\{\ddot{x}\} + [C]\{\dot{x}\} + [K]\{x\} = \{P(t)\} - [M]\{r\}\ddot{x}_g(t) - [C]\{r\}\dot{x}_g(t) - [K]\{r\}x_g(t) \tag{6.12}$$

Given the ground acceleration $\ddot{x}_g(t)$, this will have to be integrated with respect to time to give $\dot{x}_g(t)$ and $x_g(t)$. If the ground displacement history $x_g(t)$ is known it will have to be differentiated with respect to time to give the velocity and acceleration histories of the ground. If the ground motion is considered to be uniform over the site i.e. travelling wave effect are not considered and the foundation is considered to undergo a rigid body displacement, then Eq. (6.12) may be considerably simplified [10].

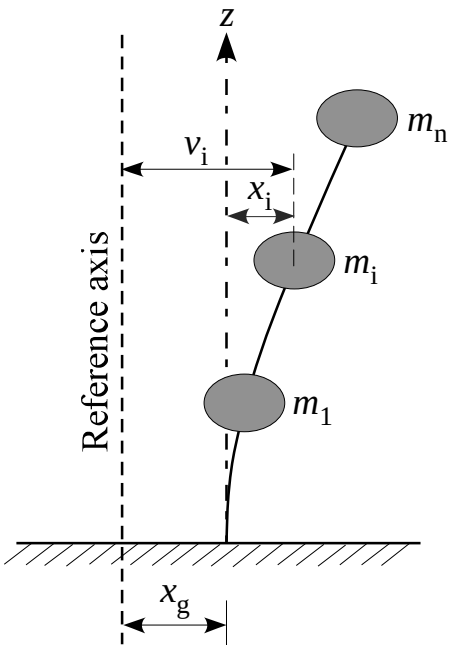

Figure 6.8 Relative and total displacements of a multistory structure with rigid translation

For a rigid body displacement, no forces are generated within the structure. This is a necessary property of any member or structure stiffness matrix.

$$[K]\{r\} = \{0\} \tag{6.13}$$

If the usual assumption that the damping forces are considered to be only due to relative velocities is made then,

$$[C]\{r\} = \{0\} \tag{6.14}$$

Eq. (6.12) becomes

$$[M]\{\ddot{x}\} + [C]\{\dot{x}\} + [K]\{x\} = \{P(t)\} - [M]\{r\}\ddot{x}_g(t) \tag{6.15}$$

If $\{P(t)\}$ is equal to $\{0\}$, then the term $-[M]\{r\}\ddot{x}_g(t)$ can be treated as the effective earthquake

load. The negative sign has little significance in earthquake response analysis and often ignored. However, it is important if total displacement or accelerations are required such as in the computation of floor acceleration spectra.

A ductile structure, at the design level of response, is no longer linearly elastic and thus the principle of superposition is no longer valid and modal analysis methods are not applicable [11]. The inelastic methods of dynamic analysis are usually based on deterministic time history analysis of the structure subjected to known ground motion. To deal with nonlinearity, a step by step integration technique of solving the equations of motion is required for the dynamic analysis. In this method, an actual or artificial earthquake accelerogram is applied to the base and the corresponding response history of the structure during the applied motion can be computed step by step by taking account any changes of the structural properties at each prescribed time interval.

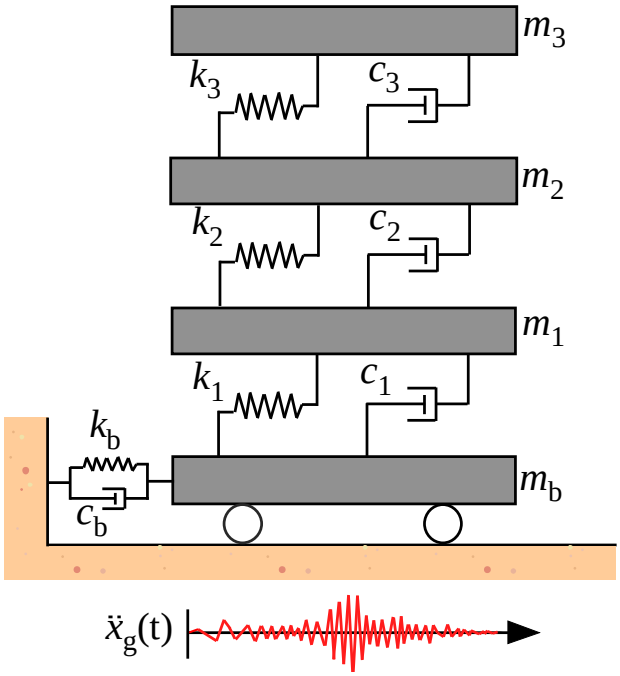

Figure 6.9 Lumped mass model of a three-story building isolated by STRP bearings

6.5.3 Time stepping method

The well-known Newmark β method has been used with β =1/6 and γ =1/2. As per

Newmark β method, the time stepping method is based on the following equations [11].

$$\dot{x}_{i+1} = \dot{x}_i + \left[(1-\gamma)\Delta t\right]\ddot{x}_i + (\gamma\Delta t)\ddot{x}_{i+1} \tag{6.16}$$

$$x_{i+1} = x_i + (\Delta t)\dot{x}_i + \left[(0.5-\beta)(\Delta t)^2\right]\ddot{x}_i + \left[\beta(\Delta t)^2\right]\ddot{x}_{i+1} \tag{6.17}$$

The parameters β and γ define the variation of acceleration over a time step and determine the stability and accuracy characteristics of the method. These two equations combined with the equilibrium Eq. (6.15) at the end of the time step, provide the basis for computing x_{i+1}, $\dot{x}_{i+1}$ and $\ddot{x}_{i+1}$ at time $i+1$ from the known x_i, $\dot{x}_i$ and $\ddot{x}_i$ at time i. Generally iteration is required to implement these computations because the unknown $\ddot{x}_{i+1}$ appears in the right side of Eq. (6.16) and Eq. (6.17).

6.5.4 Simulation method

The numerical simulation work was carried out using Matlab/Simulink platform [12]. The inelastic load-deformation behavior of STRP bearing was considered similar to equivalent linear model and the seismic response performance was evaluated by the MODF model shown in Fig. 6.9. The hysteretic behavior of the seismic isolation bearing is modeled as linear spring and viscous damping based on the force-displacement relationship obtained from the previous quasi-static tests on similar type of bearings. The mass and stiffness properties of the building are presented in Table 6.2.

Table 6.2 Mass and stiffness properties of base isolated structure

Floor level	Mass (ton)	Horizontal stiffness (kN/mm)
Base	85.0	5.5
First	127.6	87.1
Second	127.6	87.1
Roof	108.2	87.1

6.6 Pseudodynamic test

6.6.1 Introduction

Before the application of isolation system in real building structures, it is essential to know how the base isolated building with STRP bearings responds to dynamic loadings. When the response characteristics of a structural system are not well understood or difficult to model numerically, physical testing provides the only accurate way to analyze the dynamic response of the structure [13]. The two main methods currently used to test the structures under the influence of dynamic loadings are the shake table test and pseudodynamic test method [14]. Small scale model of structure have to be used in shake table test because of the limited size and capacity of the available shake tables and therefore it is often difficult to investigate the behavior of full scale structures. The other problem associated with reduced scale model is that the scale effect which may causes the misleading of the test results [15]. According to Krawinkler et al. (1988) [15], it is by no means an easy task to scale down the prototype properties properly. The pseudodynamic testing approach can be used to avoid the limitations of shake table tests along with scale effects for evaluating the performance of large scale structures under earthquake loads. And it is always not necessary to test the complete structure: an experimental test on a small part of the structure can provide a better understanding of the whole structural response [16]. Pseudodynamic testing method combines the merits of both the computer modeling and physical testing methods.

A critical nonlinear structural element that cannot be modeled satisfactorily namely the experimental part is tested physically while the remainder of the structure that can be modeled with confidence namely the simulation part is modeled in a finite element program. This substructuring technique is a combination between simulation and experimental test on a subpart of the structure which can be regarded as the better understanding of the entire structural response [16]. In pseudodynamic tests, the mass, damping and external excitation matrices of both the experimental and simulation part are assumed to be known in the dynamic equilibrium equation of motion. Therefore, the restoring force matrix is the only unknown that needs to be acquired in order to solve the governing equation of motion. The restoring force of the simulation part can be calculated using any of the programming software, but the restoring force of the experimental part is not easy to acquire satisfactorily using the computer program due to

the uncertainties associated with the material and geometrical nonlinearities and therefore, it needs to be acquired by performing physical tests [13]. To obtain the restoring force of the experimental part, hydraulic actuators are used to apply the target displacements to the experimental specimen through controller. The restoring force of the experimental specimen can be recorded from the load cell of the actuators during the experimental test. The restoring force matrices of the experimental and simulation part can be integrated in parallel into dynamic equation of equilibrium of the entire structure [17].

After acquiring the restoring force matrix of the entire structure, different numerical integration scheme can be employed to solve the equations of motion. The choice of numerical time integration depends on the numerical integration step size to be chosen. In this work, Newmark-β method is employed. The pseudodynamic tests can be categorized into two types namely: conventional pseudodynamic test and real-time testing. In real-time testing, the actuators move very fast as the ground motion of realistic earthquake. On the contrary, in conventional pseudodynamic test, the target displacement is quasi-statically applied to the experimental specimen over a greatly expanded time scale. In pseudodynamic test of multi degree of freedom (MDOF) systems, the entire structure is divided into simulation and experimental subparts. The experimental part is physically tested and the simulation part is evaluated utilizing the computer program.

In this study, a three-story reinforced concrete frame building was modeled using the method outlined above. The model was represented by three degrees of freedom structure with mass assumed to be lumped at each floor level and the lateral stiffness of each story represented by elastic shear spring. With an additional degree of freedom assigned for the base isolation floor, the structure was modeled as four degrees of freedom (4MDOF) system. The base isolation system was considered as experimental part while the superstructure was considered as simulation part as shown in Fig. 6.2 (b). In this study, the sample specimen STRP bearings were designed according to the steps as outlined [2], [1] and [4]. Only 1/3 scale model of the STRP bearings were fabricated due to the capacity of the available testing equipment. In order to evaluate the seismic performance of base isolated building using STRP bearings, El Centro NS component of 1940 Imperial Valley earthquake record was selected in the present test. Two levels of seismic excitations were used in order to identify the seismic performance of the base isolated building. For this purpose, the original peak ground acceleration values were multiplied by 1.0 and 1.5, respectively. The pseudodynamic test results were compared with numerical simulation results in order to validate the simulation results. The test results were further

compared with the numerical simulation results for fixed base building to evaluate the seismic response performance of the purposed base isolation system.

6.6.2 Control system

The control system shown in Fig. 6.10 was used to conduct the substructure pseudodynamic tests in this study. This control system consists of (a) test control PC equipped with AD/DA interfaces, (b) a loading system control PC, (c) a digital servo controller with instrumentation panel and (d) the aforementioned hydraulic pump loading system. The test control PC conducts numerical time integration of the equations of motion and is connected with the servo controller.

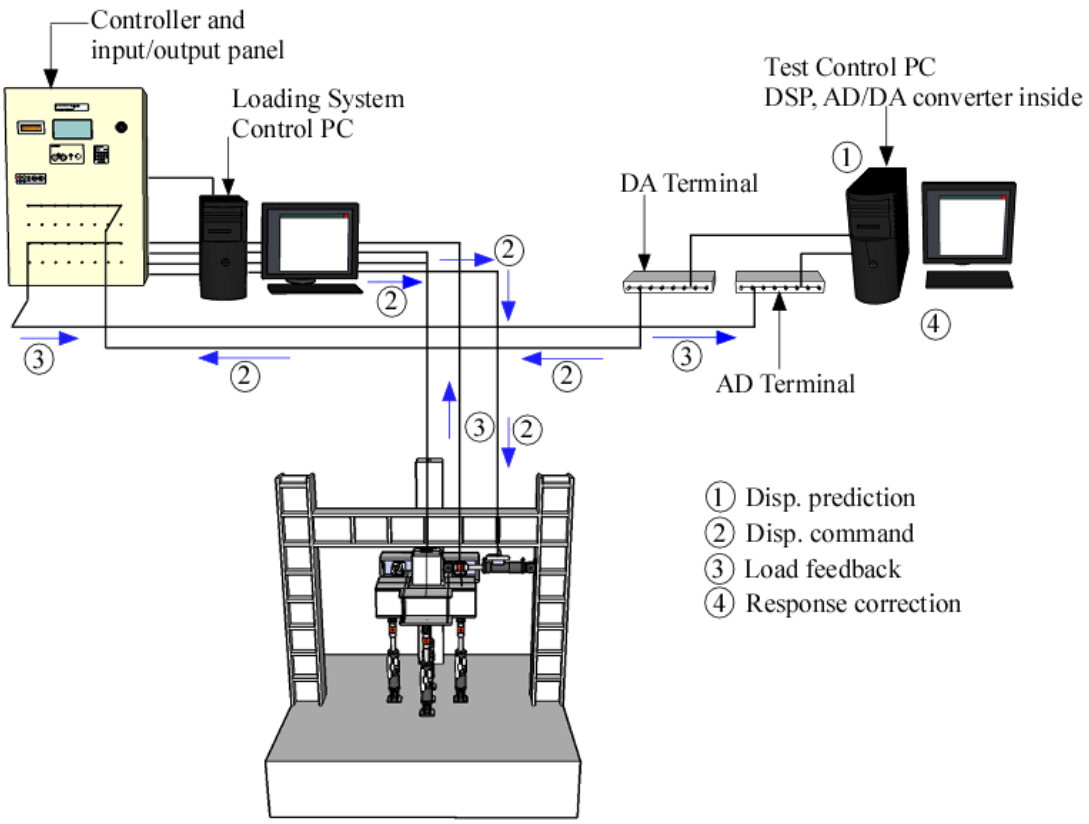

Figure 6.10 The control system for pseudodynamic test

6.6.3 Algorithm of pseudodynamic test

A time domain numerical integration following prediction-correction procedure was built inside the operation PC. This procedure is based on the well-known Newmark-β method. For each integration time step, the prediction displacement $\{\tilde{x}_{n+1}\}$ can be completely calculated without any feedback load information using the following equations.

$$\{\tilde{x}_{n+1}\} = \{x_n\} + \{\dot{x}_n\}\Delta t + 0.5\{\ddot{x}_n\}\Delta t^2 + \beta\left[\hat{M}\right]^{-1}\{\hat{f}\}\Delta t^2 \tag{6.18}$$

$$\left[\hat{M}\right] = [M] + 0.5[C]\Delta t + \beta[K]\Delta t^2 \tag{6.19}$$

$$\{\hat{f}\} = [M]\{\Delta\ddot{z}_{n+1}\} - \Delta t([C] + 0.5\Delta t[K])\{\ddot{x}_n\} - \Delta t[K]\{\dot{x}_n\} \tag{6.20}$$

where M, C and K represent the mass, damping and elastic stiffness matrices of numerical model, respectively. $\{x\}$, $\{\dot{x}\}$ and $\{\ddot{x}\}$ present the response displacement, velocity and acceleration vector, respectively. $\{\ddot{z}\}$ represents the input acceleration vector of ground motion, the subscript n and n+1 represent the previous and current steps, respectively, Δt represents the incremental time interval of each loading step, β is the Newmark integration coefficient and β =1/6 is used in this study.

In this study, the whole building structure is considered as multi degrees of freedom (MDOF) system. The deformation of the isolation floor is set as the displacement of the first degree of freedom system $\{x\}_1$. Therefore, only the first element of predicted displacement vector $\{\tilde{x}_{n+1}\}_1$ is necessary to load the specimen. After loading the predicted displacement $\{\tilde{x}_{n+1}\}_1$, the feedback restoring force f_{n+1} is used to build a correction force increment vector $\{\Delta f_c\}$, which is the difference between restoring force based on elastic stiffness and actual loading. The correction force incremental vector for isolation floor can be expressed by Eq. (6.21).

$$\{\Delta f_c\}_1 = f_{n+1} - f_n - k_1\left(\{\tilde{x}_{n+1}\}_1 - \{x_n\}_1\right) \tag{6.21}$$

where f_n is the restoring force of experimental substructure in previous step, k_1 is the elastic stiffness of shear spring 1 in MDOF model. Using this correction force increment

vector Δf_c, the corrected response displacement, velocity and acceleration $\{x_{n+1}\}$, $\{\dot{x}_{n+1}\}$ and $\{\ddot{x}_{n+1}\}$ can be computed using the Eqs. (6.22)-(6.24).

$$\{x_{n+1}\} = \{\tilde{x}_{n+1}\} - \beta\left[\hat{M}\right]^{-1}\{\Delta f_c\}\Delta t^2 \tag{6.22}$$

$$\{\dot{x}_{n+1}\} = \{\dot{x}_n\} + 0.5\left(\{\ddot{x}_n\} + \{\ddot{x}_{n+1}\}\right)\Delta t \tag{6.23}$$

$$\{\ddot{x}_{n+1}\} = \{\ddot{x}_n\} + \left[\hat{M}\right]^{-1}\left(\{\hat{f}\} - \{\Delta f_c\}\right) \tag{6.24}$$

Accordingly, the procedure used to calculate the response at time $(n+1)\Delta t$ can be outlined as below:

I. Calculate the prediction response displacement vector $\{\tilde{x}_{n+1}\}$ for entire structural model using the Eq. (6.18)
II. Apply the predicted displacement of the experimental substructure $\{\tilde{x}_{n+1}\}$ as target displacement command to the loading system.
III. Measure the feedback restoring force f_{n+1} from the experimental substructure
IV. Calculate the corrected response displacement $\{x_{n+1}\}$ using the Eq. (6.22). If the correction part $\beta\left[\hat{M}\right]^{-1}\{\Delta f_c\}\Delta t^2$ is small enough then proceed to the next step otherwise substitute $\{x_{n+1}\}$ as predicted displacement $\{\tilde{x}_{n+1}\}$ and go back to step II.

The convergence tolerance is dependent on the finite resolution of the control and measuring devices. There are merits and demerits of using small and large convergence tolerance limit. The convergence tolerance limit has to be chosen to fulfill the requirements of the tests. In these tests, the displacement and force tolerances were set as 0.1mm and 0.1kN, respectively based on the displacement and force resolution capacity of the load cell.

6.6.4 Pseudodynamic test program

For the purpose of pseudodynamic tests, a seismic loading of 1.0 time and 1.5 times that of El Centro Earthquake record were applied consecutively to the building model. The acceleration time history of El Centro earthquake is shown in Fig. 6.11.

In this study, the pseudodynamic tests of STRP specimen bearing were conducted under constant vertical axial pressure of 3.3MPa. The seismic response of the prototype model obtained by pseudodynamic tests were compared with the numerical simulation results in terms of top floor absolute acceleration, top floor drift, bearing's displacement and base shear transmitted to the superstructure. Figures 6.12 (a) and (b) show the force displacement relationship of the bearing obtained from pseudodynamic tests under 100% and 150% El Centro record excitation for a shear strain level of 70% and 100%, respectively. The corresponding deformed state of the STRP bearing is shown in Figs 6.13. Figure 6.14 contains the photograph showing the overview of the test setup including loaded specimen.

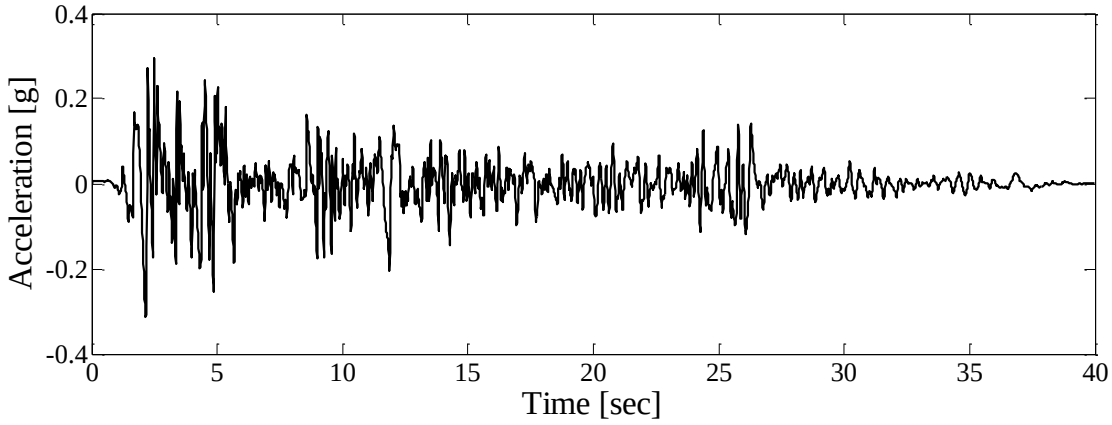

Figure 6.11 Input accelerogram (El Centro 1940 NS component, PGA = 0.313g)

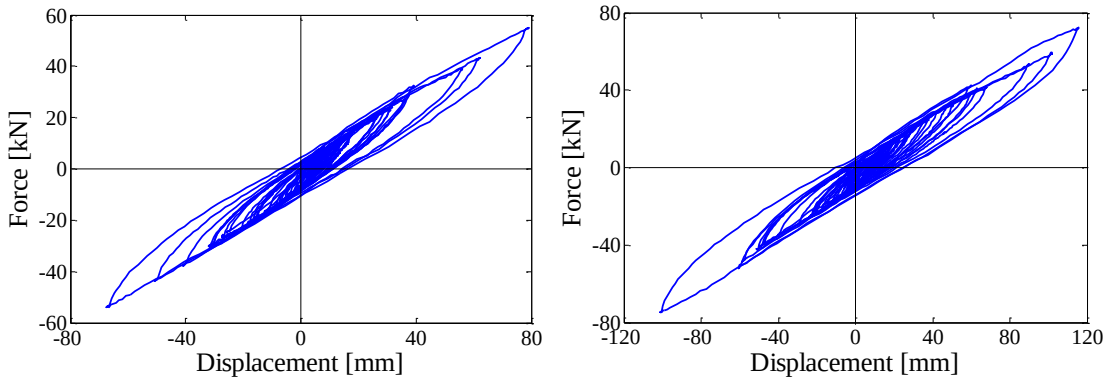

a) 100% El Centro record input b) 150% El Centro record input

Figure 6.12 Force-displacement relationship of STRP bearing

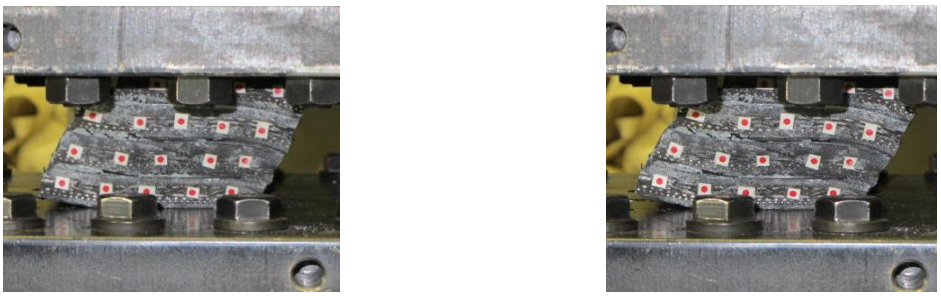

a) 70% shear strain b) 100% shear stain

Figure 6.13 Photographs showing deformed state of 1/3 scale model STRP bearing

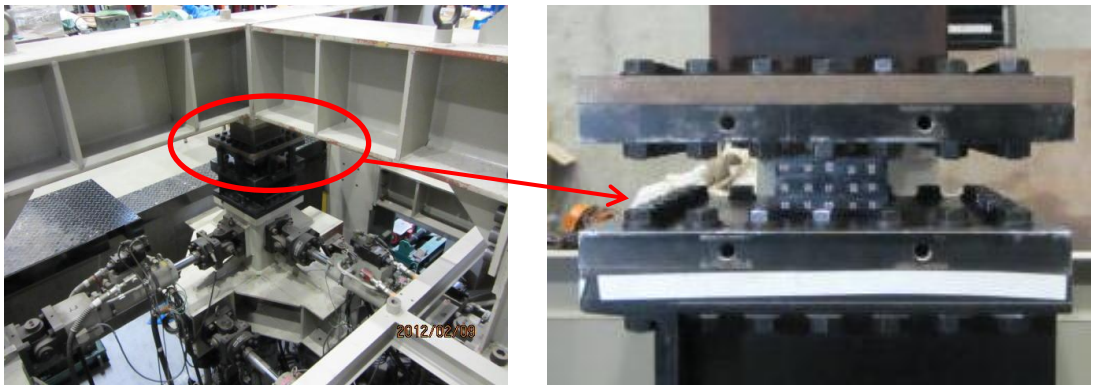

Figure 6.14 Overview of pseudodynamic test setup

6.7 Comparison of results

The pseudodynamic test results as well as numerical simulation results due to El Centro NS component of 1940 Imperial Valley Earthquake excitation are presented. In numerical simulations reported herein, the stiffness of the STRP bearing was identified by quasi-static cyclic tests as described earlier. Figures 6.15 (a) and (b) show the comparison between numerical simulation and pseudodynamic test results in terms of force-displacement relationships. From these figures, it can be seen that, there is close agreement between numerical simulation and pseudodynamic test results.

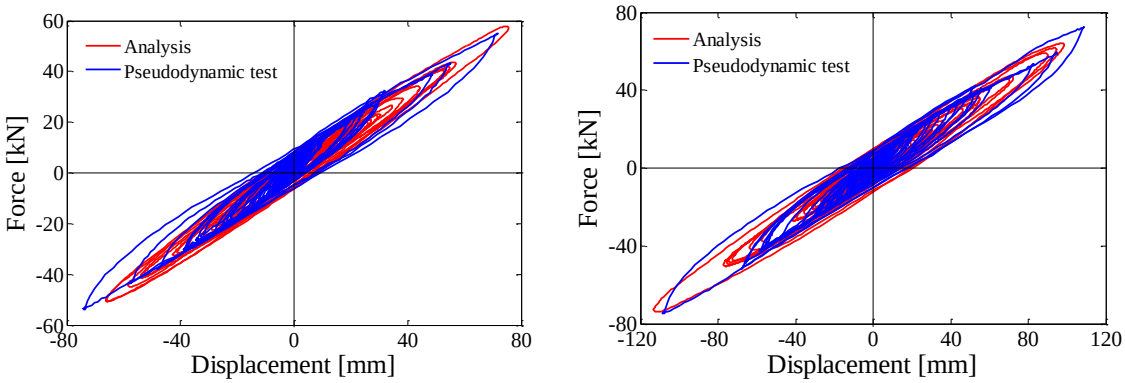

a) 100% El Centro record input b) 150% El Centro record input

Figure 6.15 Force-displacement relationship of STRP bearing; comparison between pseudodynamic test and numerical simulation results

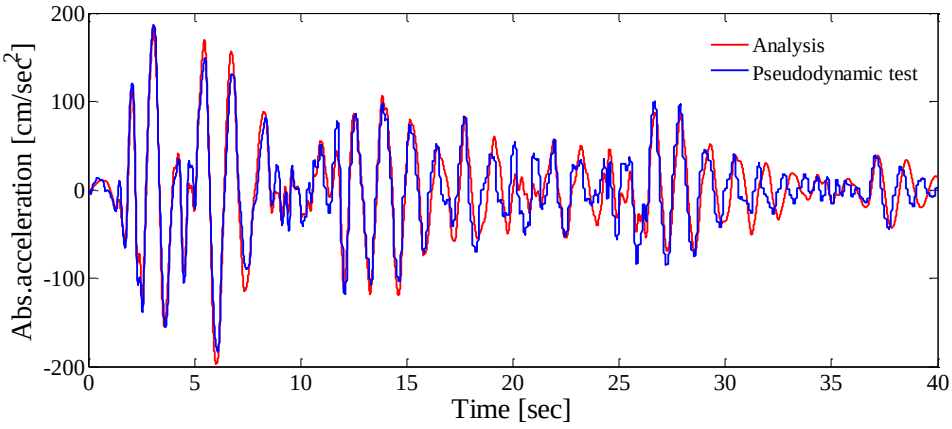

Figure 6.16 Top floor absolute acceleration produced by100% El Centro record input

Table 6.3 Floor drifts due to different levels of seismic excitations

	Floor drifts (mm)			
	100% El Centro input		150% El Centro input	
Floor level	Pseudodynamic test	Simulation	Pseudodynamic test	Simulation
First	7.9	7.9	10.4	12.10
Second	5.1	5.24	6.9	7.87
Roof	2.3	2.44	3.1	3.64

The comparative values of floor drifts obtained by numerical simulation and pseudodynamic tests are presented in Table 6.3. From the Table 6.3, it can be seen that the floor drifts obtained by numerical simulation and pseudodynamic tests are almost equal for 100% El Centro record excitation while we increase the excitation acceleration by 1.5, the difference is noticeable. Similar situation can be seen in case of top floor absolute acceleration which is presented in Table 6.4. The top floor absolute acceleration time histories are also presented in Figs. 6.16 and 6.18. Figure 6.17 shows the floor displacement profile obtained by the pseudodynamic test. These results indicate that the equivalent linear elastic-viscous damping model over-estimate the displacement demand which can be considered appropriate for preliminary analysis and design of STRP isolators.

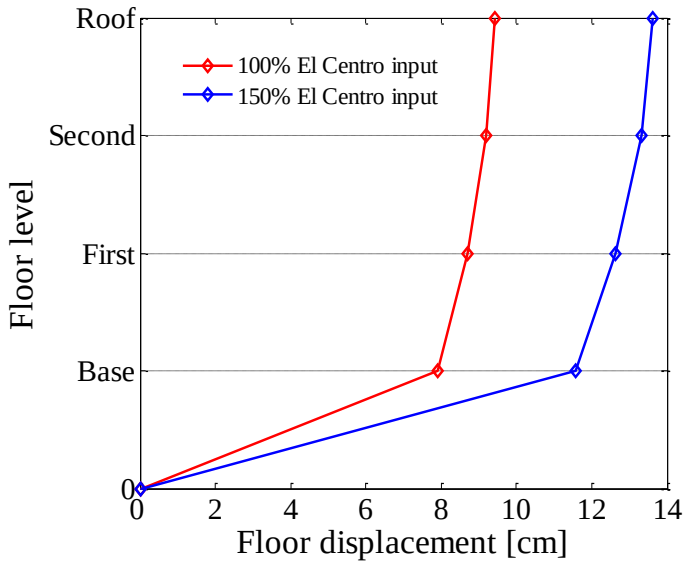

Figure 6.17 Comparison of floor displacements profile for different input amplitude level

Table 6.4 Maximum absolute floor acceleration from different methods (cm/sec^2)

	Method	Base	First	Second	Roof
	El Centro 100%				
1.	Pseudodynamic test	164.0	172.0	183.0	187.0
2.	Numerical Simulation	175.8	187.5	193.7	197.1
	El Centro 150%				
1.	Pseudodynamic test	224.0	236.0	249.0	255.0
2.	Numerical Simulation	263.7	281.10	290.6	295.6

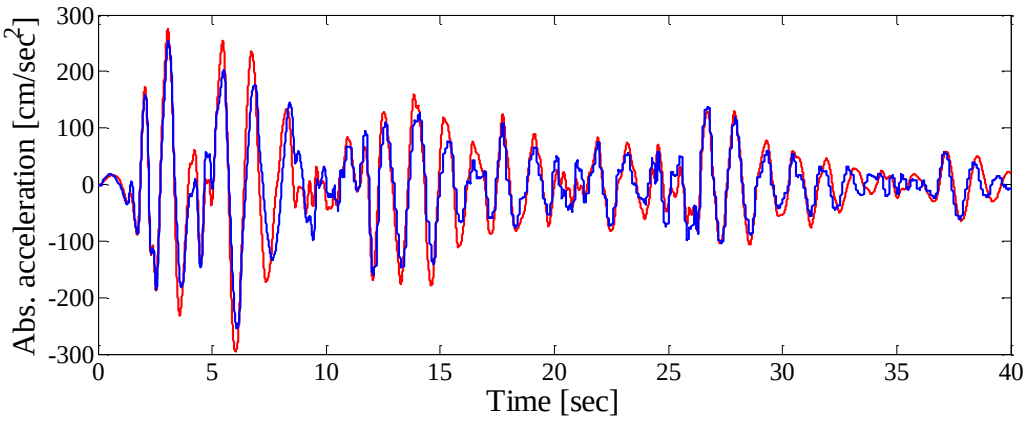

Figure 6.18 Top floor absolute acceleration produced by150% El Centro record input

The maximum responses obtained by numerical simulation are found to be in reasonable agreement with pseudodynamic test results. It can be seen that, the difference between the pseudodynamic test and simulation results is increased for increased in excitation accelerations. The maximum difference is found for roof level absolute acceleration which is about 15% higher than the pseudodynamic test results. From the Tables 6.3 and 6.4, it can be concluded that the simulation results are slightly higher than the pseudodynamic test results in all the cases.

6.8 Seismic performance evaluation

The pseudodynamic test results were further compared with numerical simulation results of fixed base building. The seismic performance of the base isolated building was evaluated in terms of absolute acceleration, drift and base shear. These quantities were evaluated only for higher level of seismic excitation. An important parameter for the evaluation of performance of base isolation system is the peak inter-story drift. In this case, the reduction on top floor inter-story drift is about 81% and which is within the limit of $0.02/R_I$ as set forth in UBC 1997 [1]. Another important parameter of seismic performance is the top floor absolute acceleration. The reduction on top floor absolute acceleration is about 80%. The base shear transmitted to the superstructure for fixed base and base isolated cases are 3740kN and 1124kN, respectively. This results show that the reduction of base shears due to incorporation of base isolation is about 70% of the fixed base building.

In the absence of experimental test results of fixed base building, only the simulation results

were compared with pseudodynamic test results. When we compare the results of base isolated building, it can be concluded that, on an average, numerical simulation predicts 15% higher top floor drifts and 13% higher top floor absolute accelerations. On incorporation of these variations, one can conclude that the reduction on top floor drifts, top floor absolute accelerations and base shear are 66%, 67% and 70%, respectively. The comparative response quantities are presented in Figs. 6.19-6.21. The comparison of floor drifts for fixed base and base isolated building produced by seismic excitations of 100% and 150% El Centro earthquake is also shown in Fig. 6.22.

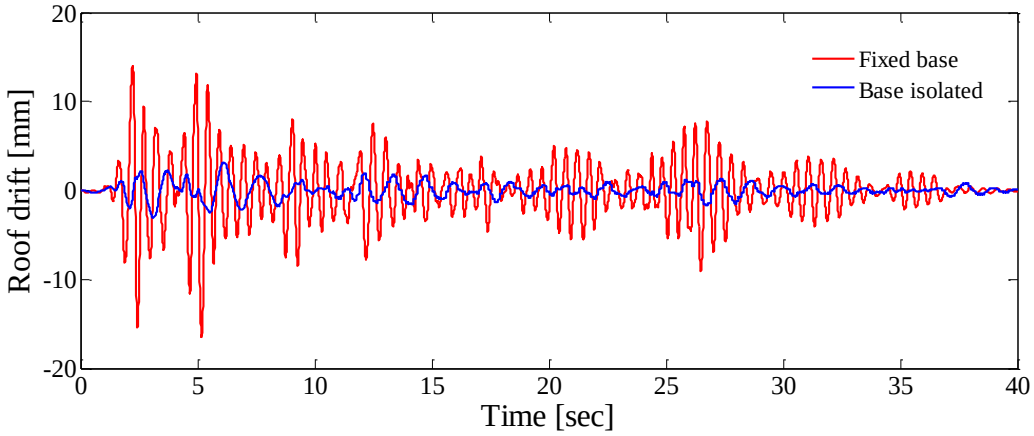

Figure 6.19 Top floor drift: comparison between numerical analysis of fixed base case and pseudodynamic test of base isolation case

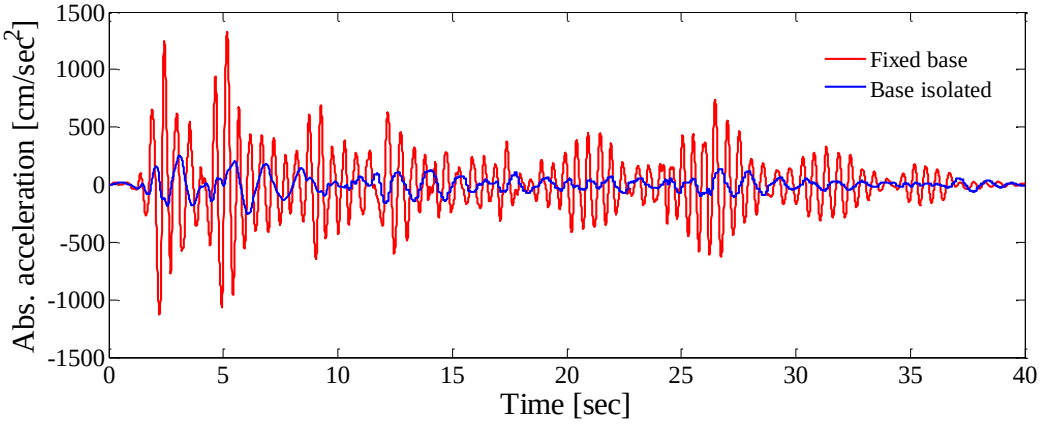

Figure 6.20 Top floor absolute acceleration: comparison between numerical analysis of fixed base case and pseudodynamic test of base isolation case

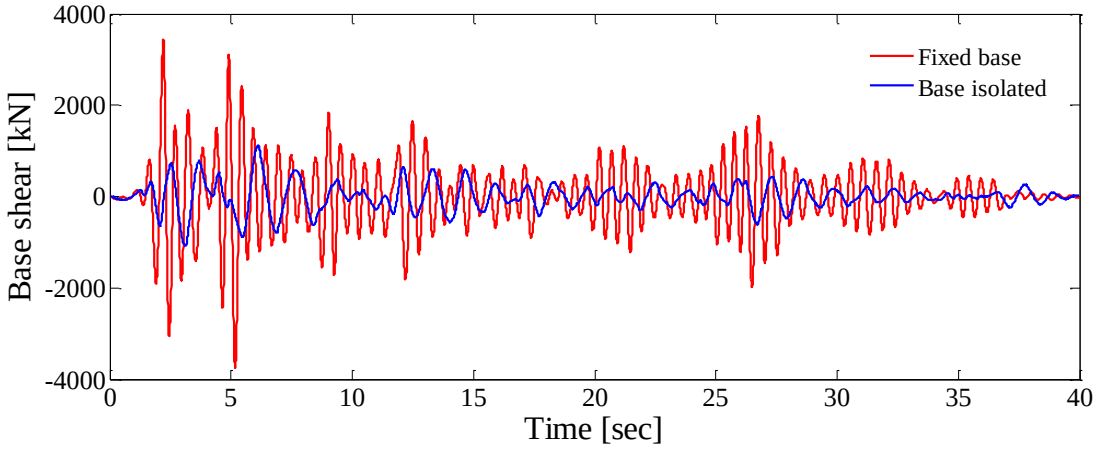

Figure 6.21 Base shear: comparison between numerical analysis of fixed base case and pseudodynamic test of base isolation case

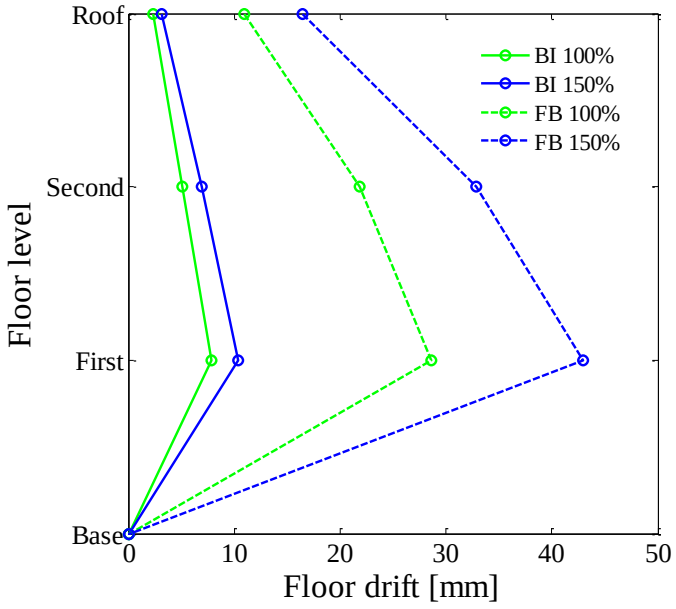

Figure 6.22 Floor drift profile in fixed base and base isolation cases under 100% and 150% El Centro NS record input

6.9 Conclusion

As a part of the development of a low-cost seismic isolation system, seismic performance of a

building with layer-bonded STRP bearings is verified by means of pseudodynamic tests in this study. Although accurate numerical modeling of the dynamic behavior of tire rubber pads by analytical methods is difficult, dynamic response of the base isolation system as well as seismic performance of a three story base isolated building using STRP isolators can be evaluated while avoiding the problems associated with shaking table tests.

The seismic isolation bearings used in this study were produced by using scrap tire rubber. Due to the capacity of testing equipment available, only $1/3$ scale model specimen isolators were used in the pseudodynamic test. The mechanical properties of the tested isolators were determined by conducting quasi-static cyclic loading tests. The superstructure was modeled as linear elastic structure while the nonlinearities were assumed to be concentrated in the STRP isolators. Seismic performance of the base isolated building was evaluated for two levels of seismic excitation: the El Centro record scaled with 100% and 150% amplitudes corresponding to the PGA values of 0.313g and 0.47g, respectively.

The main findings of the study are summarized as below:

1. The comparison between pseudodynamic test and analytical results show that the maximum seismic responses are in reasonable agreement.

2. The maximum base displacement produced by 150% El Centro record excitation is within the acceptable limit of the base isolation system.

3. The response absolute accelerations of top floor are 0.19g and 0.26g for input excitation of 0.313g and 0.47g, respectively. In this regards, one can conclude that the reduction of accelerations due to incorporation of base isolation is about 40% and 45 % for 100% and 150% El Centro inputs, respectively.

4. The reduction on top floor inter-story drift is about 66% and the top floor drifts are within the limit of $0.02/R_I$ [1].

5. Further comparison with simulation results of fixed base building shows that the reduction on top floor absolute acceleration is about 67% of the fixed base building.

6. The reduction on base shear transmission to the superstructure is about 70% of the fixed base building.

7. These results indicate that the proposed base isolation system using STRP bearings is

attractive alternative to the commercial isolation system. It can also be concluded that the pseudodynamic tests can be considered as appropriate method to evaluate the seismic responses of base isolated building.

References

[1] Uniform Building Code, Volume 2, Structural Design Requirements, 1997, Earthquake Regulations for Seismic Isolated Structure, Whittier, CA.

[2] S. K. Jain and S. K. Thakar. Quasi-static testing of laminated rubber bearings. *Journal of the institution of engineers* (India), Civil Engineering Division, 2003.

[3] John F. Stanton, Glen Scroggins, Andrew W. Taylor, Charles W. Roeder. Stability of laminated elastomeric bearings. *Journal of Engineering Mechanics*, 1990, Vol. 116(6), pp: 1351-1371

[4] James M. Kelly. Earthquake-resistant design with rubber. 2nd edition London, Springer-Verlag, 1997.

[5] Y.J. Arditzoglou, J. A. Yura and A. H. Haines. Test methods for elastomeric bearing on bridges. Research Report 1304-2, Texas Department of Transportation.

[6] Nam-Sik Kim, Ji-Ho Lee and Sung-Pil Chang. Equivalent multi-phase similitude law for pseudodynamic test on small scale reinforced concrete models. *Engineering Structures*, 2009, Vol. 31 (4), pp: 834-846.

[7] Ray W. Clough, Joseph Penzien. Dynamics of Structures, Computers & Structures Inc., Third Edition, 2003, chapter 10, pp: 184-185.

[8] Franklin Y. Cheng. Matrix analysis of structural dynamics: Applications and earthquake engineering, Marcel Decker, Inc., 2001, chapter 4, pp: 203.

[9] Franklin Y. Cheng. Matrix analysis of structural dynamics: Applications and earthquake engineering, Marcel Decker, Inc., 2001, chapter 1, pp: 33-34.

[10] T. K. Datta. Seismic analysis of structures, John Wiley & Sons (Asia) Pte. Ltd., 2010, chapter 3, pp: 110.

[11] Anil K. Chopra. Dynamics of structures: Theory and application to earthquake engineering, Pearson Education, Inc., 2007, chapter 5, pp: 174.

[12] Matlab software (R2007a), The MathWorks.Inc.

[13] Juan E. Carrion, B.F. Spencer Jr. and Brian M. Philips. Real-time hybrid testing of a semi-actively controlled structure with an MR damper. *American Control Conference*,

2009, USA.

[14] A. P. Darby, A. Blakeborough and M. S. Williams. Real-time substructure tests using hydraulic actuator. *Journal of Engineering Mechanics*, 1999, Vol. 125 (10), pp: 1133-1139.

[15] Helmut Krawinkler. Scale effects in static and dynamic model testing of structures. *Proceedings of Ninth World Conference on Earthquake Engineering*, 1988, Japan.

[16] A. Souid, A. Delaplace, F. Ragueneau and R. Desmorat. Pseudodynamic testing and nonlinear substructuring of damaging structures under earthquake loading. *Engineering Structures*, 2009, Vol. 31 (5), pp: 1102-1110.

[17] Stephen A. Mahin and Pui-shum B. Shing. Pseudodynamic method for seismic testing. *Journal of Engineering Structures*, 1985, Vol.111 (7), pp: 1482-1503.

[18] Eurocode 8. Design of structures for earthquake resistance. 2004.

7

Design displacements and seismic performance of a base isolated building with STRP bearings considering bidirectional seismic effects

This chapter intends to describe the design of isolation system and seismic performance evaluation of a three-story reinforced concrete frame structure isolated with STRP bearings. For this purpose, detail procedure to determine the seismicity of the site and selection and scaling of the ground motion records is presented. The dynamic response of the building under bidirectional seismic excitations is investigated by performing nonlinear time history analysis. In addition, the displacement responses of lumped mass modeled is compared with the displacement responses obtained by nonlinear time history analysis.

7.1 Introduction

The base isolation system, used to provide certain degree of flexibility in the structure in order to reduce the seismic demand instead of increasing the earthquake-resistant capacity of the structure is becoming an attractive alternative to the conventional earthquake-resistant design methods.

This study is an effort towards the extension of this efficient earthquake-resistant technology to common public and private residential buildings in developing countries. To fulfill this demand, the isolation system should be simple, easily available and affordable to general public as well

as effective in reducing the seismic demand on structures. As a feasibility study, this part of the study is extremely important to evaluate the dynamic behavior of the base isolated building under bidirectional seismic excitations.

This part of study includes the development of appropriate elastic response spectra to match the seismic scenario of the site and dynamic analysis of the building. In this study, the same building as used in chapter 6 is used which is a three-story moment resisting reinforced concrete frame structure with brick masonry infill walls. The architectural plan of the building along with layout of the STRP bearings is shown in Fig. 6.

Nepal Building Code (NBC 1994) [1] was originated from a study performed by BECA Worley International Consultants Ltd., New Zealand in 1994. The country is divided into different seismic zone with seismic coefficient given in country's map as contour lines. The NBC 1994 has only inelastic response spectra for three different site soil categories with site soil category type I as rock site. The NBC 1994 does not permit time history analysis and there is no provision for base isolation system. This situation needs to adopt the appropriate code provisions from other country relevant to the seismic scenario of the site with provisions of elastic response spectra applicable for the design of base isolation system. Due to this reason, the seismic isolation provisions were adopted from Uniform Building Code (UBC 1997) [2].

The study focuses on the analysis of the isolated building for two different earthquake risk levels. Three dimensional nonlinear direct integration time history analysis and two dimensional lumped mass model analysis are carried out. The analysis results are compared with the design displacement of the isolation system.

7.2 Seismic scenario of the site

The building considered in this study was constructed in Kathmandu, Nepal. The site is located with seismic zoning factor of 1.0. The soil site was considered as subsoil category II as per NBC 1994. The site soil category is considered as similar to soil category D as mentioned in UBC 1997. The seismic demand on fixed base building was calculated according to NBC 1994. However, since the code has no provisions for the design of seismic isolated structures, provisions from UBC 1997 were used. The elastic response spectra were evaluated for two different risk levels as mentioned in UBC 1997. The first one is the Design Basis Earthquake

(DBE), namely 10% probability of exceedance in 50 years (475 years return period) and another is Maximum Considered Earthquake (MCE), namely 2% probability of exceedance in 50 years (2475 years return period). Figure 7.1 shows the recommended 5% damped site specific elastic response spectra for two different risk levels.

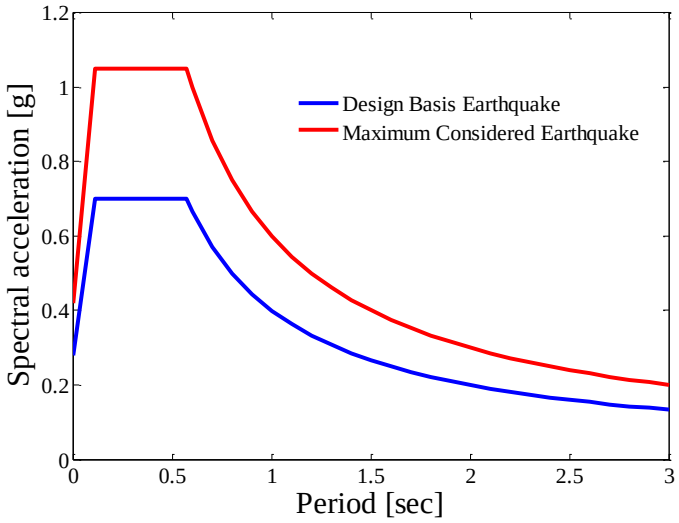

Figure 7.1 Design site response spectra for two levels of earthquakes

7.3 Design displacement of isolation system

There are total of 15 STRP bearings under each of the columns of the building. The deformation pattern of the unbonded application of STRP bearing is shown in Fig 6.3. Due to this connection system, there should not be local uplifting of the superstructure so that the axial pressure should always be compressive in order to active as base isolation unit.

The target isolation period was determined by considering the stability of the isolation system. Increasing the time period will increase the horizontal displacement which ultimately forces to increase the thickness of the isolator. Increasing the thickness of isolator adversely affects the stability of the whole isolation system. The target isolation period was set to 1.8 seconds so that the resultant displacement can be achieved with minimum numbers of STRP layers. In other words, the target period cannot be taken higher value for lightly loaded structures [3]. The target period is greater than three times the fixed based period of the building.

The experimental study conducted on 1/3 scale model of STRP bearing suggests that the damping ratio is about 0.11. The design displacement of the isolation system is 140mm and 210mm for the DBE and MCE risk levels, respectively. The spectral displacements were calculated using the Eq. (7.1) [4]

$$S_D = \frac{S_A}{\omega^2} \tag{7.1}$$

where S_D is spectral displacement, S_A is the spectral acceleration and ω is the circular frequency of the base isolation system. In addition the damping correction factor was calculated as given in Eq. (7.2) [5]

$$\eta = \sqrt{\frac{10}{(5+\zeta)}} \tag{7.2}$$

where η is damping correction factor and ζ is the viscous damping ratio (%)

7.4 Design of superstructure

The case study building is a regular structure with height less than 40m. The design base shear V was calculated as given by Eq. (7.3) [1]

$$V = CZIKW_t \tag{7.3}$$

where C is the basic seismic coefficient, Z is the seismic zone factor, I is the importance factor, K is the performance factor and W_t is the seismic weight of the structure. The seismic weight of the structure including 25% of the live load is about 4396kN. All the coefficients given in Eq. (7.3) are unity except basic seismic coefficient *C*.

The fundamental period T_t of the fixed base structure was determined by using the Eq. (7.4) given in NBC 1994 and is equal to 0.31 second. The fixed base fundamental period calculated as per the properties of the building is about 0.51 seconds.

$$T_t = 0.06H^{3/4} \tag{7.4}$$

where H is the height of the building in meter.

From Fig.7.2, the seismic coefficient for subsoil type II for fundamental period of 0.31 second is obtained as 0.08.

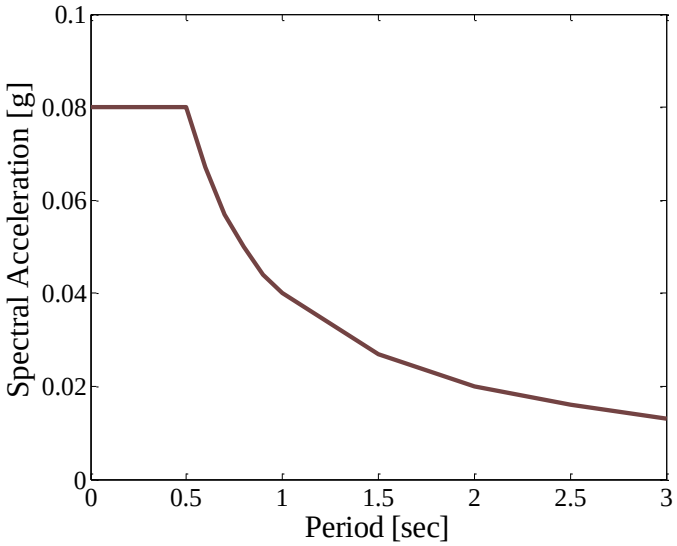

Figure 7.2 Inelastic response spectra for stiff soil

The NBC 1994 design response spectra has reduced ordinates to account for the ductility behavior of the building structure. This is equivalent to the reduction factor R value given in UBC 1997. The value of R for special moment resisting concrete frame is about 8.5. In this case, the elastic response spectra ordinate comes out to be 0.68g. The design base shear computed according to the NBC 1994 was 352kN. The structural elements of the building and the infill brick masonry walls were designed with the relevant code provision set forth in NBC 1994. The designed nominal compressive strength of the concrete was 20MPa. Deformed bars of different diameter with yield stress of 415MPa were used.

7.5 Ground motion records and scaling

In the absence of recorded strong ground motion data within the country, recorded ground motion data of the past earthquakes around the world were selected to represent the seismicity of the site. The possible option could be to generate the artificial earthquake compatible with

design response spectra but this needs reliable seismic source mechanism data. A total of eight strong ground motion records from eight earthquakes were selected [6]. The selected records content peak ground acceleration ranging from 307cm/sec^2 to 884.8cm/sec^2 and magnitude ranging from 6.33 to 7.62. Each set of the records with two orthogonal horizontal components were used to analyze the base isolated building. The selected earthquake records have different seismic characteristic like, magnitude, frequency content, recoding site, distance and source mechanism. In this regards, these records are assumed to represent the building site. The selected strong ground motion records with scaling factor are presented in Table 7.1.

Table 7.1 Selected earthquake records and scaling factors

Earthquake	Mag.	Depth (km)	Station	component	PGA (gal)	Multipliers	
						DBE	MCE
Duzce Turkey	7.14	10.0	Duzce	DZC180	341.4		
11/12/99				DZC270	524.8	0.6125	0.9187
Imperial Valley	6.95	8.8	El Centro	ELC180	307.0	1.1978	1.7968
05/19/40			station # 9	ELC270	210.9		
Imperial Valley	6.53	10.0	El Centro Array	E07140	331.6		
10/15/79			#7	E07230	454.2	0.4827	0.7241
Kobe	6.9	17.9	KJMA	KJM000	805.4	0.4343	0.6515
01/16/1995				KJM090	587.6		
Loma Prieta	6.93	17.5	Saratoga Aloha	STG000	502.2	0.6096	0.9144
10/18/89			Ave	STG090	317.8		
Northridge	6.69	17.5	Sylmar- Olive	SYL090	592.5		
01/17/94			View Med FF	SYL360	826.9	0.3119	0.4679
Victoria Mexico	6.33	11.0	6604 Cerro Prieto	CPE315	575.8		
09/06/1980				CPE045	609.2	1.3078	1.9617
Chi Chi Taiwan	7.62	6.8	CWB 99999	CHY080E	710.2		
09/20/99			CHY080	CHY080	884.8	0.3271	0.4906

The selected strong motion records were scaled for two seismic risk levels. For the purpose of scaling of the ground motion records, 5% damped elastic spectra were constructed. The scaling of the ground motion records was done by matching the S_A of the strongest components from each pair of records with the target S_A of the response spectra at the designed period of 1.8 seconds [7]. The selected ground motion records representing the site response spectra for each seismic risk levels were obtained by using acceleration spectra fitting and scaling technique.

The scale factors were computed for two seismic risk levels and are presented. The 5% damped scaled elastic spectra are shown in Figs. 7.3 and 7.4 for BDE and MCE risk level, respectively.

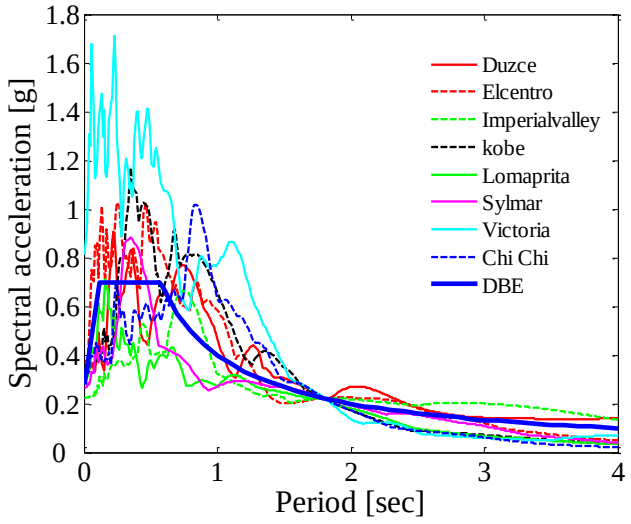

Figure 7.3 Scaled elastic response spectra of selected earthquake records for DBE

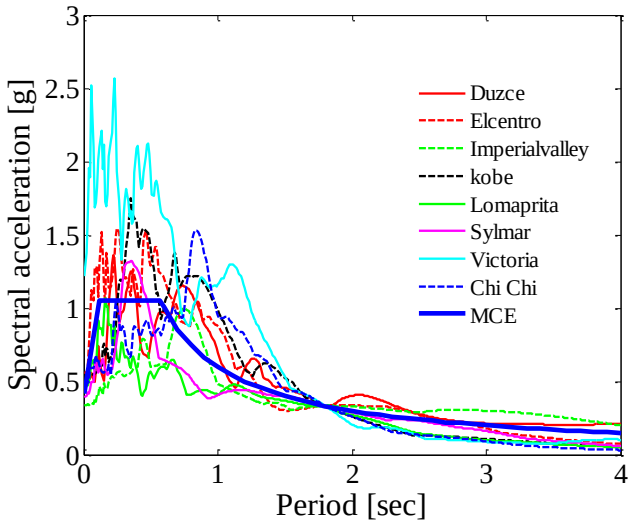

Figure 7.4 Scaled elastic response spectra of selected earthquake records for MCE

The averages of the square root of sum of squares (SRSS) of the 5% damped spectrum of the scaled horizontal components were constructed. The time histories were so scaled that the average value of SRSS should not fall below the 1.3 times the 5% damped spectrum of the DBE

(or MCE) by more than 10% within the period range $0.5T_{eff}$ to $1.25T_{eff}$ [2]. The average SRSS of scaled time histories and 1.3 times the DBE is presented in Fig. 7.5.

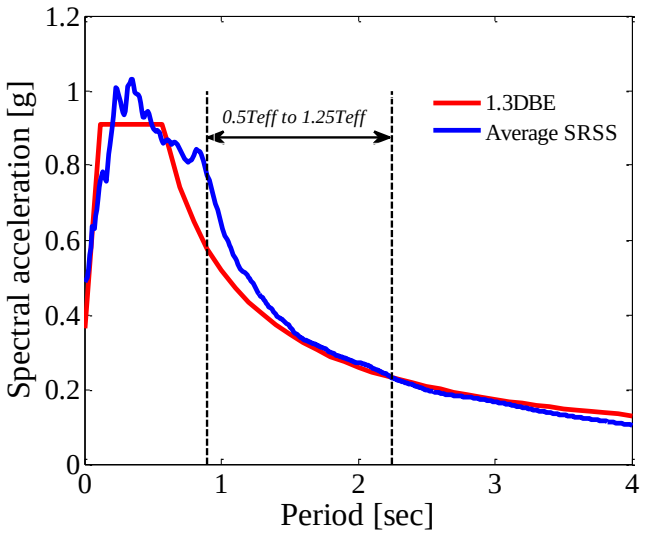

Figure 7.5 Comparison of the average SRSS of all the scaled pairs of time histories with 1.3 times the design basis earthquake

7.6 Modeling of isolated building and STRP bearings

A base isolation system at the ground floor level separates the substructure and superstructure. Time history analysis was performed by using the computer program SAP2000 [8]. The building was modeled as 3-D bare frame model and all the weight of the infill brick masonry walls was applied as distributed loads on the corresponding beams. This assumption shall be valid as the infill walls were not considered to account the lateral load resisting system during the design of fixed base building. In addition, the building was modeled as lumped mass model. The model was represented by three degrees of freedom structure with mass assumed to be lumped at each floor level and the lateral stiffness of each story represented by elastic shear spring. With an additional degree of freedom assigned for the base isolation floor, the structure was modeled as four degrees of freedom (4MDOF) system. For this purpose, a computer program was coded in Matlab/Simulink [9]. The properties of reinforced concrete frame members were assigned exactly the similar properties that were used to design the fixed base

building.

The mechanical properties of the STRP bearings were computed by experimental test conducted on 1/3 scaled model. The details about the experimental tests are already discussed in chapter 5. The mechanical properties of the full scale STRP bearings were computed by applying the similitude law as discussed in chapter 6.

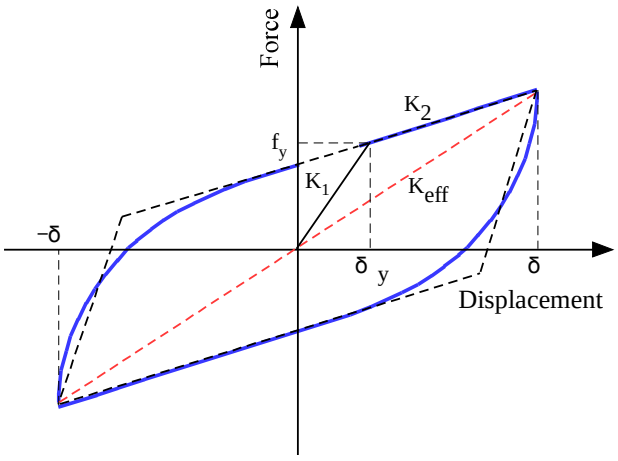

Figure 7.6 Idealized force-displacement relationship

Usually, the practical isolators are modeled by bilinear model based on the parameters mentioned hereafter [10]. The stiffness parameters K_1, K_2, δ_y and f_y were idealized to be equivalent to the equivalent stiffness and viscous damping value for a target displacement of δ shown in Fig. 7.6. The horizontal effective stiffness K_{eff} of the STRP bearing is the horizontal stiffness to achieve the target isolation period. Post yield stiffness K_2 was computed with yield stiffness ratio equal to 0.1. The response quantities calculated using this method almost represents the equivalent viscous modeling of the rubber bearing as shown in the Fig.7.6. The nonlinear direct integration time history analysis performed based on the presented method has close agreement with the equivalent viscous damping modeling.

7.7 Nonlinear time history analysis

The horizontal stiffness is dependent on axial pressure and shear strain, due this reason the

horizontal stiffness was distributed to each STRP bearing proportionally to the nominal axial pressure it carries. The gross section properties were used to compute the natural period and mode shapes of the fixed base building. The natural periods of fixed base building corresponding to different modes of vibration were computed as 0.51, 0.45, 0.39 corresponding to first mode, second mode and rotational mode, respectively. This analysis concludes that the fundamental period of the superstructure is sufficiently far apart from the design period (1.8 seconds) of the base isolated building.

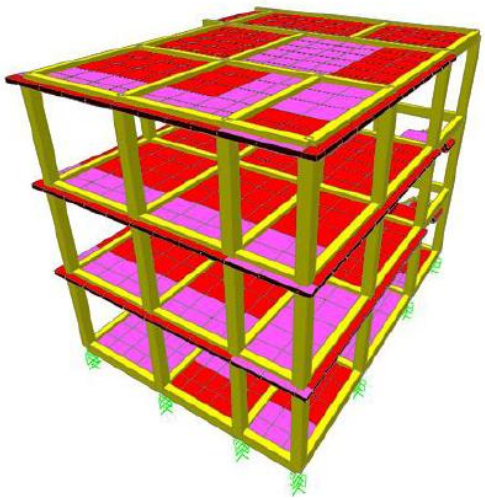

Figure 7.7 Three-dimensional model of base isolated building

The nonlinear direct integration time history analysis was performed with stiffness proportional damping. The isolation modes have period of approximately 1.8 seconds, and the superstructure periods range from approximately 0.23 to 0.004 second (from fourth mode to end). In nonlinear direct integration time history analysis, it is difficult to define the damping that will produce 5% damping in all modes and nearly zero damping for the first three modes which are associated with the isolation system. In this analysis, the mass proportional damping was set to zero and stiffness proportional damping was calculated as 0.0286. Two orthogonal horizontal components of earthquake motions as presented in Table 7.1 were applied simultaneously. The response of the base isolated building was evaluated for the most critical combination.

7.8 Seismic performance evaluation

The seismic response of the base isolated building was evaluated for two seismic risk levels

specified in UBC 1997; namely, DBE and MCE. It is expected that the building should remain elastic for code prescribed DBE but minimal structural damage to lateral load resisting system is permitted. The building should resist the MCE which is assumed to be the upper bound earthquake without collapse. Moderate level of damage is expected either on lateral load resisting system or in non-structural elements. In addition, there should be enough seismic gaps (moat) between the neighbor buildings and base isolated building to accommodate the maximum isolator displacement produce by MCE level earthquake. The seismic performance evaluation criterions are the top floor absolute accelerations, top floor drifts, maximum base displacement, base shear and axial pressure variation on each STRP bearing.

The absolute acceleration produced by all the earthquake records including average is presented in Figs. 7.8 and 7.9 along x and y-directions, respectively. The maximum top floor absolute accelerations produced by Chi Chi earthquake record in x-direction is 2.82m/sec^2 and the maximum top floor absolute acceleration produced by Sylmar earthquake record in y-direction is 3.78m/sec^2. These values were used to normalize the maximum floor accelerations. The variation of absolute acceleration is very small except the results produced by Chi Chi in x-direction and Sylmar earthquake in y-direction. The top floor average absolute acceleration is about 3.3m/sec^2, which is equivalent to one third of the absolute acceleration of the equivalent fixed base building.

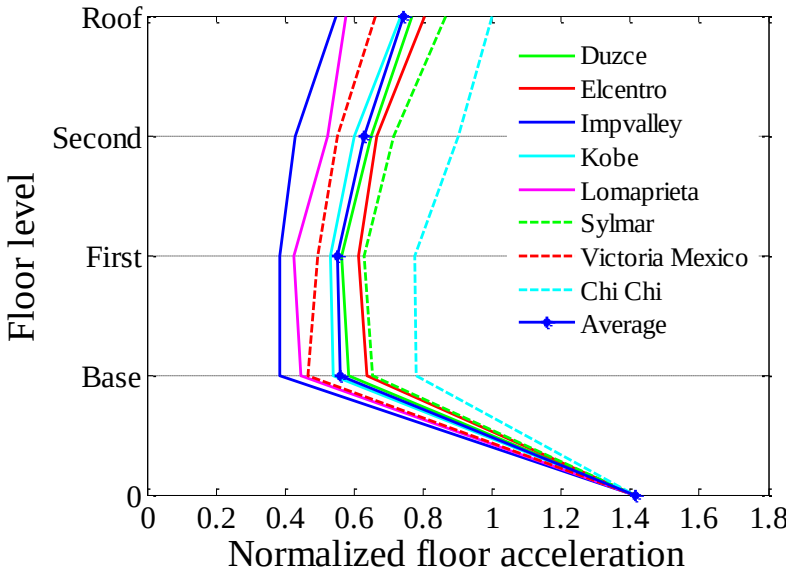

Figure 7.8 Normalized maximum absolute floor accelerations in x-direction for MCE

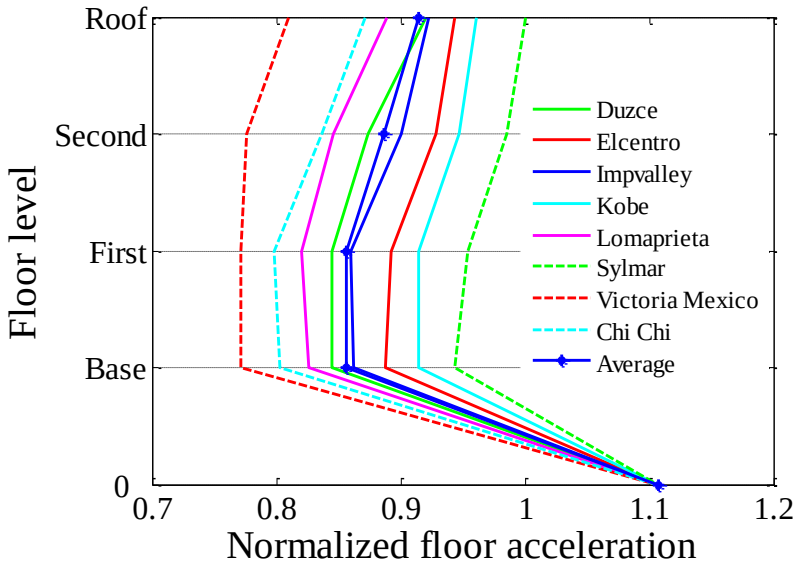

Figure 7.9 Normalized maximum absolute floor accelerations in y-direction for MCE

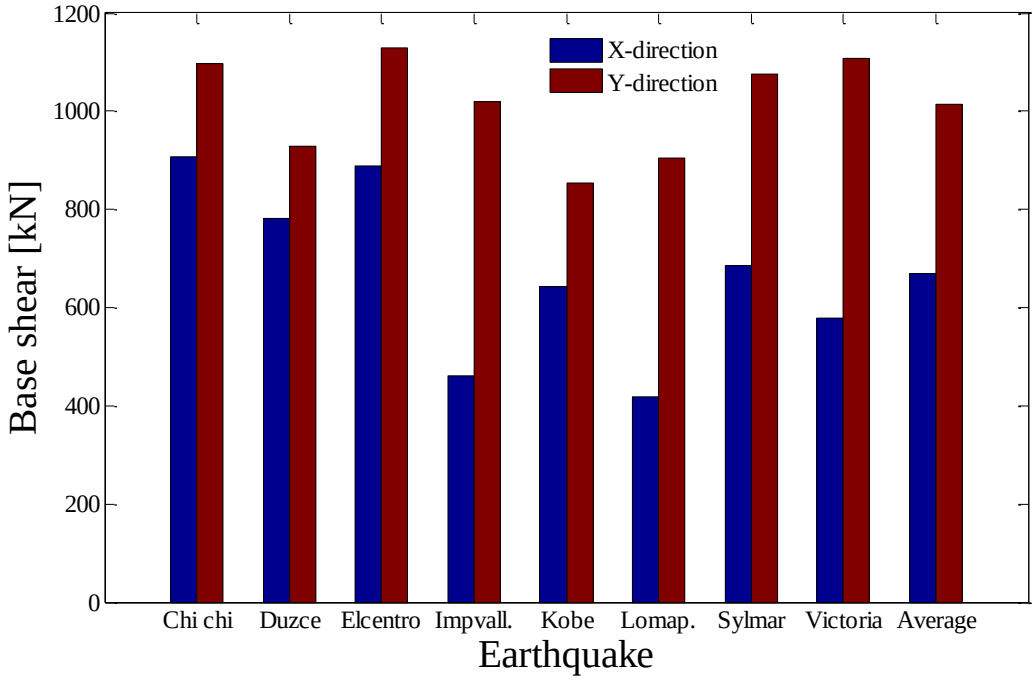

Figure 7.10 Maximum base shear transmitted to the superstructure along x and y-directions for MCE risk level

The maximum base shear in either direction was evaluated at the base isolation level for each of

the earthquake records. The base shears results obtained by time history analysis is presented in Fig. 7.10 in both the directions. The maximum MCE base shear forces transmitted to the superstructure was obtained by El Centro earthquake which is about 1130kN. Similarly, the minimum base shear transmitted to the superstructure was produced by Kobe earthquake input which is about 855kN. The average MCE base shear transmitted to the superstructure is 1015kN. This value is equivalent to the elastic seismic coefficient of 0.24g. The maximum DBE base shear transmitted to the superstructure was obtained by Victoria earthquake record which is 830.8kN. The average DBE base shear force transmitted to the superstructures is 671kN. This value is equivalent to the elastic seismic coefficient of 0.15g. These results indicate that the base isolation is effective and none of the earthquake records produce base shear forces more than the design elastic seismic coefficient for both the risk levels. The average base shear force transmitted to the superstructure is about 1078kN by using the shear type lumped mass model. This value is quite close to the average value obtained by nonlinear time history analysis.

The maximum MCE floor displacements for each of the earthquake records in x and y-directions are presented in Fig. 7.11 and Fig.7.12, respectively. The maximum responses were obtained by making square root of sum of square (SRSS) which is 100/100 rule mentioned in UBC 1997, and are presented in Table 7.3. The average maximum base displacement is well below the design displacement of 210mm. Except Chi Chi and El Centro earthquake records, the SRSS displacements are well below the MCE level design displacement. The average SRSS displacement for MCE risk level is 184mm which is less than the design displacement of 210mm.

The floor drift for MCE risk level are presented in Table 7.2. The average floor drifts for MCE risk level on either direction are less than the maximum permissible limit of $0.02/R_I$. Table 7.3 also contains the bearing displacement for all the earthquake records using lumped mass model. The bearing displacement produced by Victoria earthquake record is higher than the design displacement as well as the displacement obtained by time history analysis for MCE risk level. The average bearing displacement obtained by lumped mass model is about 164mm which is less than the design displacement as well as displacement obtained in time history analysis.

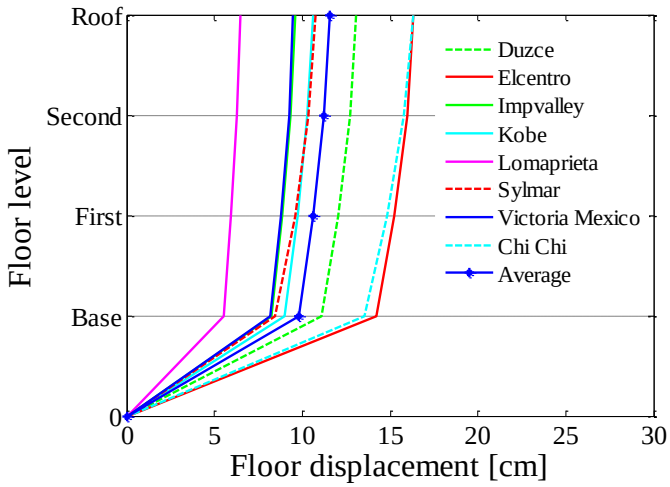

Figure 7.11 Maximum floor displacements in x-direction for MCE

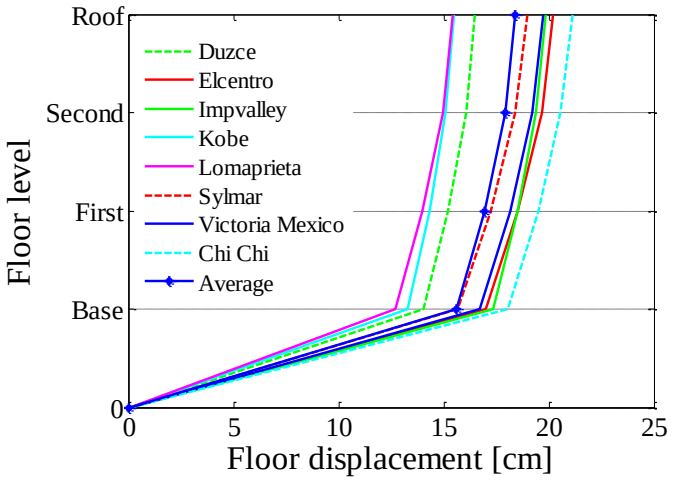

Figure 7.12 Maximum floor displacements in y-direction for MCE

Table 7.2 Average floor displacement and story drift for MCE (mm)

Story	Height	X-direction			Y-direction		
	(m)	Displacement	Drift	Ratio	Displacement	Drift	Ratio
Roof	3.0	116	3.0	1/1000	184	5.0	1/600
Second	3.0	113	7.0	1/428	179	10.0	1/300
First	3.0	106	8.0	1/375	169	13.0	1/230
Base	-	98	-	-	156	-	-

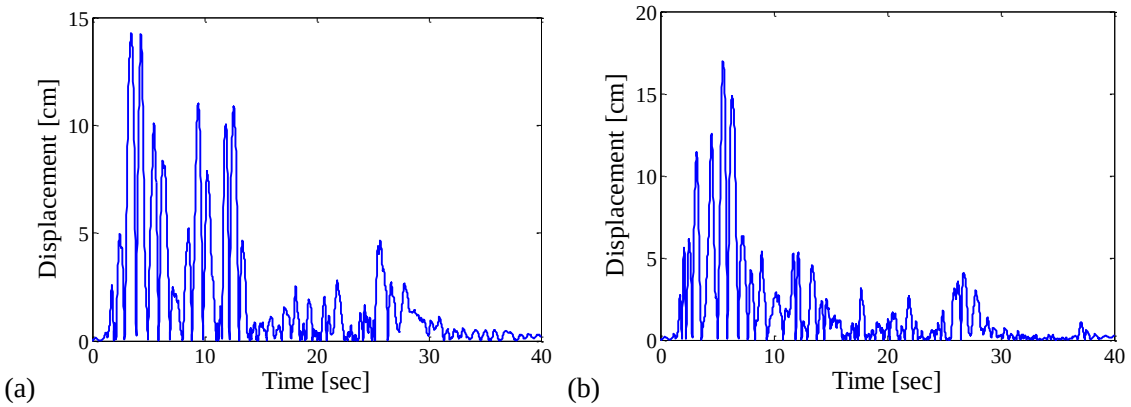

Figure 7.13 Absolute displacement plot at isolation floor a) x-direction b) y-direction due to El Centro record input for MCE

7.8.1 Force-displacement relationships

The force-displacement relationship on either direction for the lowest axially loaded STRP bearing is shown in Figs. 7.14 and 7.15. These results were obtained under El Centro records input for MCE which gives the maximum base displacement as well as maximum shear force transmitted to the superstructure. In this analysis, it can be seen that the horizontal force varies with axial compressive loads.

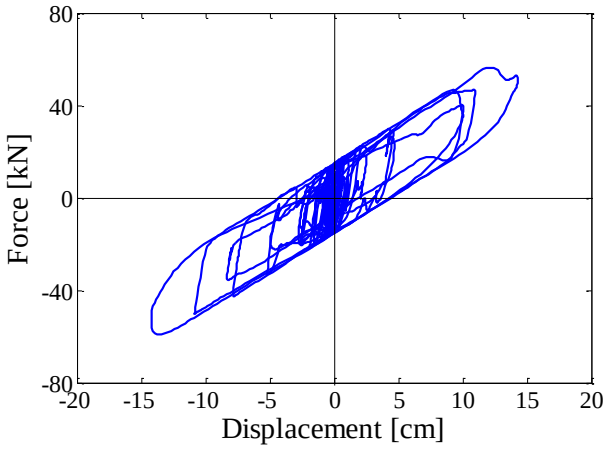

Figure 7.14 Force-displacement relationship of bearing *C12* in x-direction

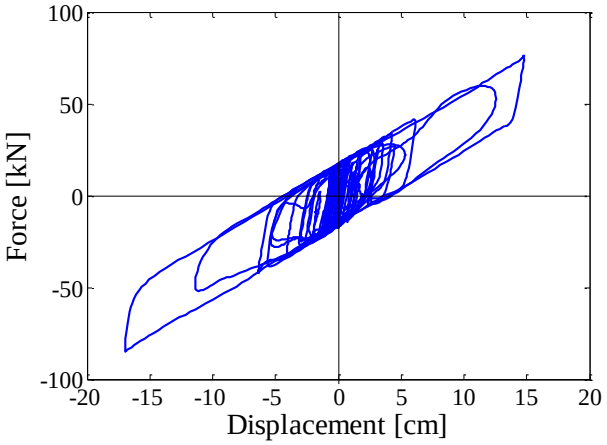

Figure 7.15 Force-displacement relationship of bearing *C12* in y-direction

Table 7.3 Maximum bearing displacement (mm)

Earthquake records	Time history analysis results						2D model
	DBE			MCE			MCE
	Longi.	Trans.	Max.	Longi.	Trans.	Max.	Longi.
Chi Chi	117	90	148	181	135	226	203
Duzce	100	62	118	141	112	180	159
El Centro	85	41	94	170	143	222	151
Imperial valley	66	30	72	174	82	192	119
Kobe	73	67	99	132	90	160	151
Loma Prieta	84	37	92	127	55	138	128
Sylmar	98	61	115	157	85	178	134
Victoria	115	51	126	167	82	186	273
Average			**108**			**184**	**164**

Longitudinal: Y, Transverse: X, Maximum: 100/100 rule

7.8.2 Variation on axial load on STRP bearings

Figure 6.1 and Table 7.4 show that the *C6* and *C12* are the highest and lowest axially loaded bearings, respectively. Due to the unbonded application of the STRP bearing with superstructure and substructure, it is extremely necessary that the bearing should always be in axial compression. This situation prevents the local uplifting effects of the structure. The variation of axial compressive loads on all the bearings was investigated during the time history analysis.

The design axial loads on each column vary between177.5kN to 620.0kN. For the MCE earthquake, the maximum axial load variation was noticed for El Centro earthquake on bearing *C12* which varies between -98.12kN to 87.6kN.

Similarly, the minimum variation of axial load is observed on bearing *C6* for all the input ground motions. The axial load variation due to El Centro earthquake records on bearing *C6* and *C12* are shown in Figs. 7.16 and 7.17, respectively. The results show that all the STRP bearings remain in compression for all level of earthquakes. This situation prevents the uplifting of the superstructure and also forces all the STRP bearings to participate in the seismic isolation system.

Table 7.4 Designed axial load on corresponding STRP bearings

Bearing Designation	LL (kN)	DL (kN)	|EL| (kN)	1.2DL+1.0LL+|EL| (kN)
C1	31.8	207.3	11.8	292.4
C2	68.5	330.3	19.1	484.0
C3	97.3	354.6	20.8	543.6
C4	74.1	280.5	16.4	427.1
C5	59.2	283.0	16.4	415.1
C6	127.3	391.2	23.3	620.0
C7	120.5	314.1	18.9	516.3
C8	85.4	307.0	18.1	471.9
C9	63.8	383.7	22.0	546.2
C10	17.5	194.1	10.9	261.3
C11	96.5	328.2	19.4	509.7
C12	41.8	107.7	6.5	177.5
C13	99.2	263.3	15.8	431.0
C14	109.8	343.2	20.4	542.1
C15	26.5	184.2	10.5	258.1

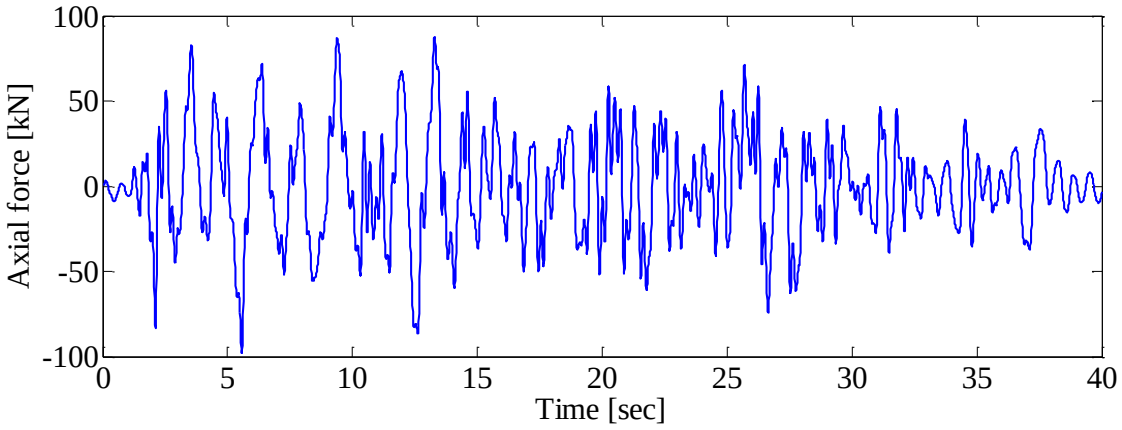

Figure 7.16 Axial load variations on bearing *C12* due to El Centro record for MCE

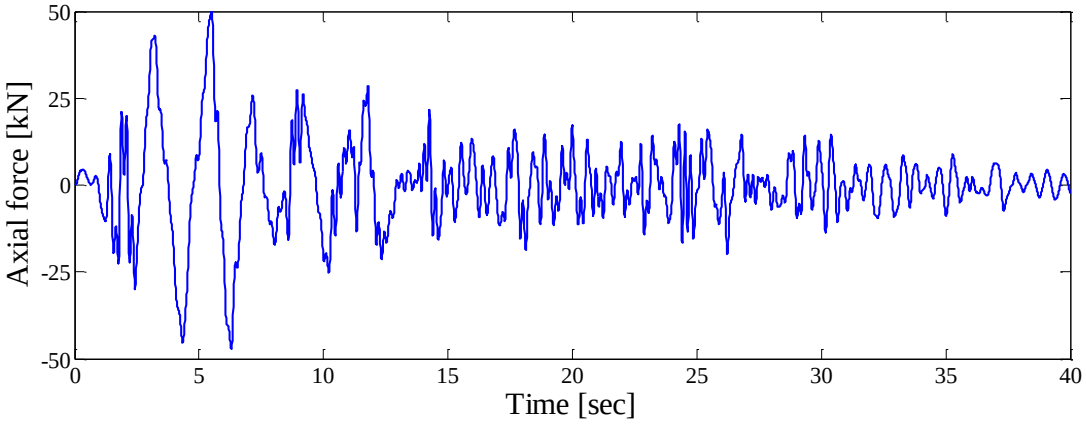

Figure 7.17 Axial load variations on bearing *C6* due to El Centro record for MCE

7.9 Conclusion

Seismic isolation system design and seismic performance evaluation of a small residential building was performed. The superstructure was designed as a fixed base building using NBC 1994. The seismic isolation provisions from UBC 1997 were adopted. The ground motion records were selected and scaled to represent the site seismicity. Nonlinear time history analyses as well as lumped mass model analysis were performed. The seismic response quantities of interest were evaluated as per the provision set forth in UBC 1997. The maximum average bearing displacement found to be smaller than the design displacement of 210mm for MCE risk level. The maximum story-drift in all the cases are very small in x-direction, while story-drifts

in case of y-direction are larger but are still within the limit of $0.02/R_I$ [2]. The floor absolute accelerations are smaller than the PGA of input earthquake records in all the cases. The average maximum top floor absolute acceleration is about 3.3m/sec^2 which is almost one third of the top floor absolute acceleration of equivalent fixed base building. The average base shear transmitted to the superstructure is about 1015kN which is equivalent to the elastic seismic coefficient of 0.24g. The variation of axial compressive load on critical STRP bearings was also evaluated in order to check the uplift condition. The maximum variation was observed in case of lowermost left corner bearing but still remains in compression. The results show that all the STRP bearings remain in compression for all level of earthquake inputs. This situation shall prevent the local uplifting of the superstructure and also forces all the STRP bearings to participate in seismic isolation system.

In this study, it can be concluded that the seismic responses are reduced for all level of earthquake risks, the building including isolation system is stable and all the STRP bearings can participate in base isolation system. These results indicate that the STRP bearings are effective in reducing the seismic response in bidirectional seismic excitations.

References

[1] Nepal National Building Code, NBC 105, 1994.

[2] Uniform Building Code, Volume 2, Structural Design Requirements, 1997, Earthquake Regulations for Seismic Isolated Structure, Whittier, CA.

[3] Trevor E. Kelly, R. Ivan Skinner, Bill (W.H.) Robinson. Seismic Isolation for Designers and Structural Engineers. National Information Centre of Earthquake Engineering (NICEE), India, 2010.

[4] C. Giarlelis, C. Kostikas, E. Lamprinou, M. Dalakiouridou. Dynamic behavior of a seismically isolated structure in Greece. 14th *World Conference on Earthquake Engineering*, 2008, China.

[5] Eurocode 8. Design of structures for earthquake resistance. 2004

[6] http://peer.berkeley.edu/smcat/search.html

[7] Wendy Taniwangsa. Seismic performance of a base isolated demonstration building. Earthquake Spectra, 2002, Vol. 18(4), pp: 777-793.

[8] SAP2000: three dimensional static and dynamic finite element analysis and design of

structures. Computers and Structures Inc., Berkeley, CA

[9] Matlab software (R2007a), The MathWorks.Inc

[10] Farzad Naeim, James M. Kelly. Design of seismic isolated structures from theory to practice. John Willey and sons, Inc. 1999.

8

Critical load and stability analysis of STRP bearings

The objective of this chapter is to briefly discuss about the types of instability that may arise in dowelled connection system under combined load of vertical compressive and lateral shear. The chapter examines the critical vertical compressive load that causes instability in the STRP bearings and corresponding shear deformation capacity. The stability study is carried out by means of FE analysis. In addition, the rollout stability of the dowelled connection system is discussed.

8.1 Introduction

When rubber bearing is subjected to large lateral displacements, this causes reduction in shear area of the bearing which may lead to significant reduction in their critical axial load. The critical load in an elastomeric bearing is the axial load for a corresponding displacement when the bearing becomes unstable. An elastomeric bearing is considered to be unstable when the horizontal stiffness is reduced to zero and the bearing is unstable to carry increased horizontal loads [1]. A reduction in the critical load accompanied by large lateral displacement may cause buckling of the rubber bearings. Figure 8.1 shows that the relationships between axial load and shear deformation capacity of the bearings. In this figure, it can be seen that the shear deformation capacity is decreased when nominal axial stress is increased.

The assessment of stability of seismic isolation bearing is essential for the single bearing as well as for the whole isolation system. Generally the stability of a single bearing is determined based on critical buckling load based on Haringx's theory. This theory consists in modifying the

classical theory of buckling by incorporating shear deflection in a column. The Euler buckling load theory is extended to determine the buckling load in elastomeric bearings. This part of study examines the analytical methods to determine the critical load that causes instability in the STRP bearings under the combined load of axial and lateral shear. The critical buckling load of elastomeric bearings is expressed by Eq. (8.1) [2].

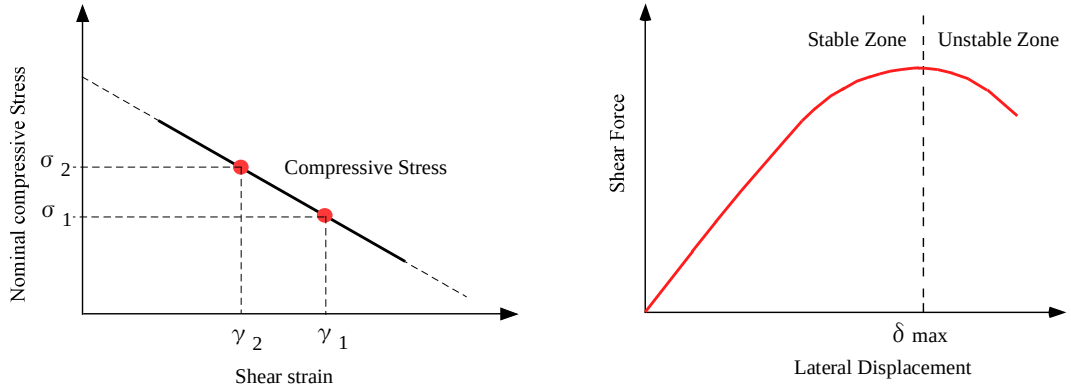

Figure 8.1 Relationship between nominal compressive stress and shear strain and stability of individual bearing

$$P_{cr,o} = \frac{2P_E}{1+\sqrt{1+4\pi^2 \dfrac{(EI)_{eff}}{(GA_s)_{eff}\, h^2}}} \tag{8.1}$$

in which, P_E is the Euler's load for a standard elastic column, h is the overall thickness of rubber bearings, $(GA_s)_{eff}$ and $(EI)_{eff}$ are the effective shear and flexural rigidity, respectively. Euler's load can be expressed as:

$$P_E = \frac{\pi^2 (EI)_{eff}}{h^2} \tag{8.2}$$

The expression for effective shear and flexural rigidity can be expressed as [3].

$$(GA_s)_{eff} = GA(h/t_r) \tag{8.3}$$

$$(EI)_{eff} = E_r I(h/t_r) \tag{8.4}$$

where t_r is the total thickness of rubber, I is the moment of inertia of the bearing about the axis of bending, A is the bonded rubber area and E_r is the elastic modulus of rubber bearing evaluated based on primary shape factor S and Young's modulus of rubber E_o (E_o = 4G) [3] as:

$$E_r = E_o(1+0.742S^2) \tag{8.5}$$

where G is the shear modulus of rubber, shape factor is the ratio between loaded area of rubber layer and force free area of rubber layer.

Some approximate formula has been devised to account for the reduced area of the bearings [4] shown in Fig. 8.2.

$$P_{cr} = P_{cr,o}\left[\frac{A_r}{A}\right] \tag{8.6}$$

where A_r is the current area at deformed state.

The horizontal stiffness is dependent on the axial load and can be approximated as [3].

$$K_H{}^* = K_H\left[1-\left(\frac{P}{P_{cr}}\right)^2\right] \tag{8.7}$$

where K_H is the horizontal stiffness of the bearing without axial load and P is the axial compressive load. In dowelled connection system, the horizontal stiffness is decreased with increase in shear displacement and to account for the reduction of footprint area, the following expression is introduced [5]:

$$K_H = \frac{GA_s}{t_r}(1-2\lambda\gamma) \tag{8.8}$$

where $\lambda = t_r/2b$ and γ is the shear strain.

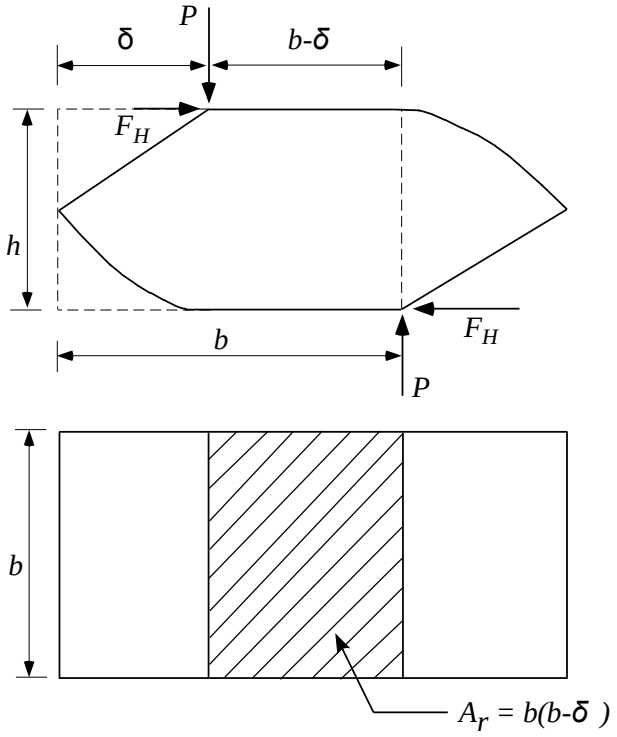

Figure 8.2 Deformed state of STRP bearing under combine loadings

The analytical study carried out on STRP-6 and STRP-4 bearings show that these type of bearings can be loaded up to 5.7MPa and 8.6MPa in order to achieve 100% and 150% shear strain in the rubber bearings, respectively.

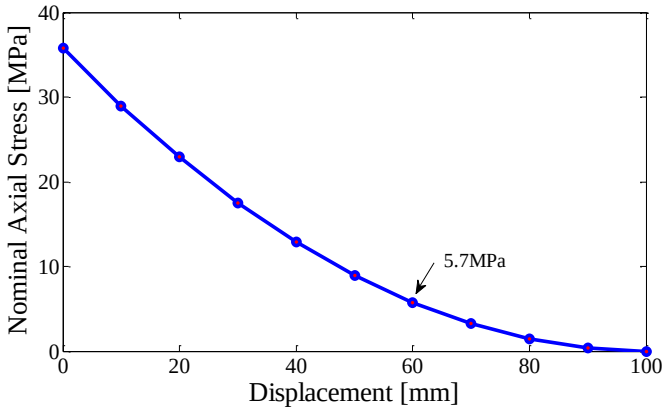

Figure 8.3 Relationship between lateral displacement and buckling load of layer-unbonded STRP-6 bearing

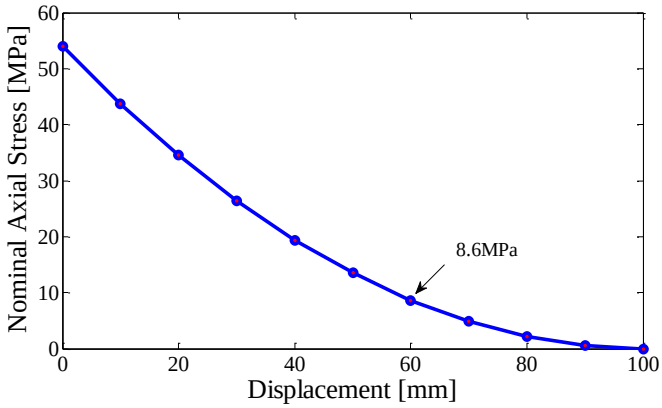

Figure 8.4 Relationship between lateral displacement and buckling load of layer-bonded STRP-4 bearing

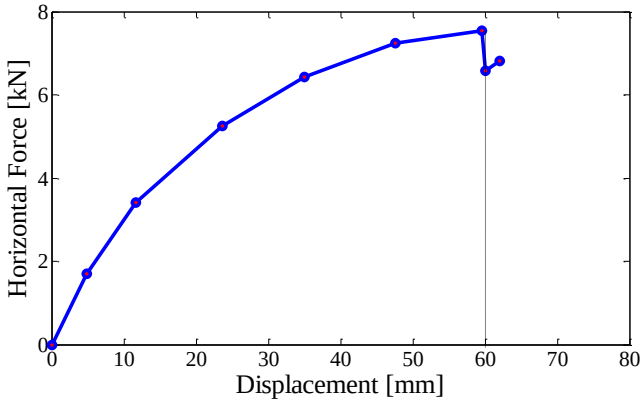

Figure 8.5 Experimentally obtained load-displacement relationship of layer-unbonded STRP-6 bearing under 5MPa nominal compressive stress

On comparing the Figs. 8.3 and 8.5, it can be seen that the nominal axial stress estimated using the buckling load analysis can be considered as reference values even though the samples were prepared without applying the adhesive. The shape factor of the tested samples was 10.4 and aspect ratio 1.4 which results in lower shear deformation capacity. Due to this reason, the layer-bonded STRP-4 specimen samples were prepared by stacking the STRP layers one on top of another with the application of adhesive in between the layers which had aspect ratio greater than two. The buckling load analysis revealed that the layer-bonded STRP-4 can sustain 8.6MPa nominal axial stress to achieve the 150% shear strain in the rubber bearings.

8.1.1 Finite element analysis

The physical properties of the STRP bearings used in FE analysis is presented in Table 5.1. FE analysis of strip layer-bonded STRP-4 bearings was conducted using general purpose finite element software [6]. The rubber part was modeled using quadrilateral elements. The reinforcing steel cords were modeled by using rebar elements. The hyperelastic material model described by the strain energy density function expressed by Eq. (5.3) with the identified constants given in Table 3.2 was utilized to model the rubber body. A series of analyses were performed using 2D FE model whereby the bearing was first loaded under designed nominal compressive stress and then sheared to a target lateral displacement by specifying a load control type of boundary conditions. The FE analysis was carried out with varying nominal axial stresses ranging from 5MPa to 15MPa. The material models, boundary conditions, analysis procedure and loading procedure were the same for each models and only the variations was nominal axial stress. The results of FE analysis were compared with experimental test results to some extent to verify the FE model. Figure 8.6 illustrates the FE analyses results.

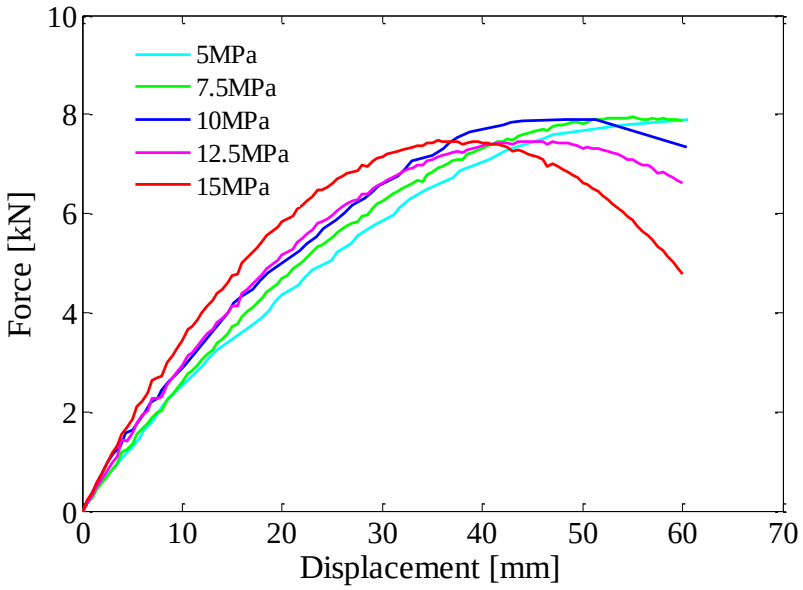

Figure 8.6 Load-displacement relationships of layer-bonded STRP-4 bearings for different nominal axial stresses

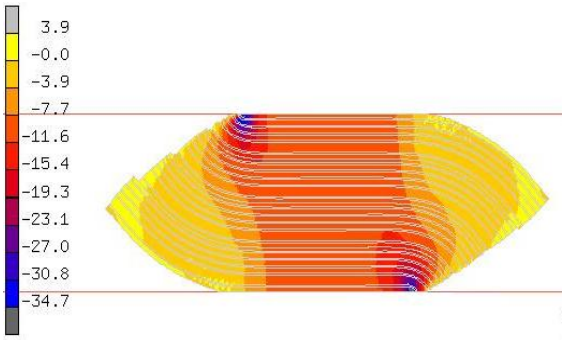

Figure 8.7 Deformed state of layer-bonded STRP-4 bearing at 150% shear strain under constant vertical load of 50kN

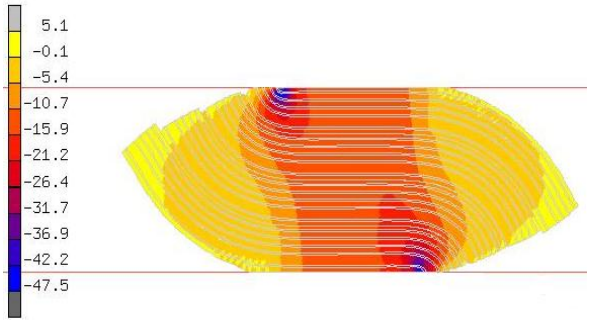

Figure 8.8 Deformed state of layer-bonded STRP-4 bearing at 150% shear strain under constant vertical load of 75kN

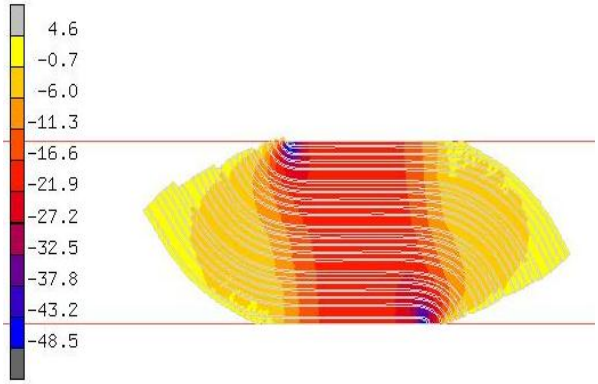

Figure 8.9 Deformed state of layer-bonded STRP-4 bearing at 150% shear strain under constant vertical load of 100kN

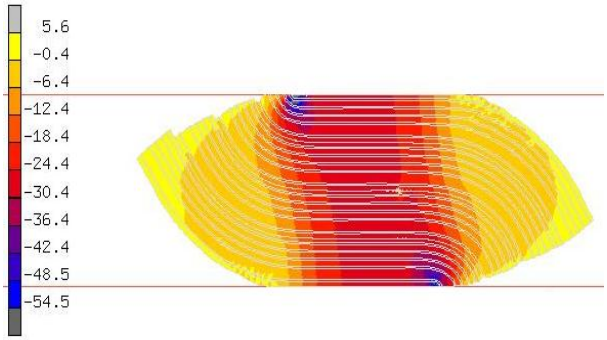

Figure 8.10 Deformed state of layer-bonded STRP-4 bearing at 150% shear strain under constant vertical load of 125kN

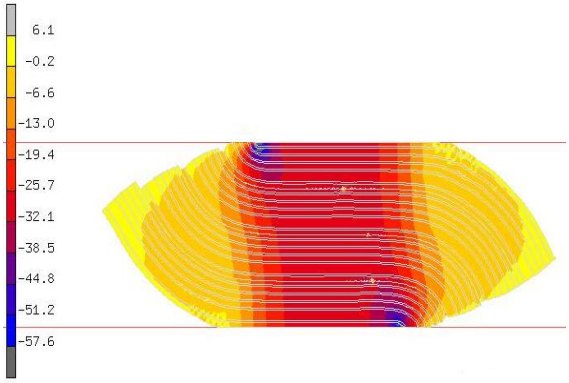

Figure 8.11 Deformed state of layer-bonded STRP-4 bearing at 150% shear strain under constant vertical load of 150kN

Figures 8.7-8.11 are the deformed state of layer-bonded STRP-4 bearing for a maximum lateral displacement of 60mm with indicated axial loads. These figures also show the component 22 of normal stress (MPa) within the rubber body. The overlapping area approach given in Eq. (8.6) for calculating the critical load of a bearing at a given displacement assumes that the critical load capacity reduces at the same rate for all bearings regardless of geometry of the bearings. In contrast, the buckling load is also varied with geometry [7], which cannot be captured by the Eq. (8.6). The shear deformation capacity of layer-unbonded STRP bearings was studied in chapter 4. This study clearly shows that the aspect ratio (second shape factor) has the key role in producing lateral displacement. In this regard, the results obtained by FE analysis are more accurate than predicted by Eq. (8.6). The FE analysis results clearly revealed that the layer-bonded STRP-4 bearings can be loaded up to 7.5MPa nominal axial stress in order to

achieve 150% shear strain in layer-bonded STRP-4 bearing.

Table 8.1 Nominal axial stress and shear deformation capacity of layer-bonded STRP-4

Nominal axial stress (MPa)	Shear deformation capacity (%)
5.0	>150
7.5	150
10.0	120
12.5	110
15.0	92

8.2 Rollout stability

Rollout instability is a failure mode that occur at large displacements, when the resultants of the vertical compressive load fall beyond the horizontal contact area of the bearing [8]. The dowelled connection system may experience another type of instability called rollout which is associated with lateral displacement and puts a limit on the maximum shear displacement that the bearing can sustain. This is because the dowelled connected bearing cannot sustain tension. When the bearing is sheared, the top and bottom of the bearings start to roll-off of the contact interfaces. This phenomenon changes the line of action of the resultant vertical load and the limit of migration of the resultant is reached when the line of action is at the edge of the bearings. The bearing is unstable in the sense that beyond this displacement the force-displacement curve has a decreasing slope [1] and [9], which is illustrated in Figs. 8.1 and 8.2.

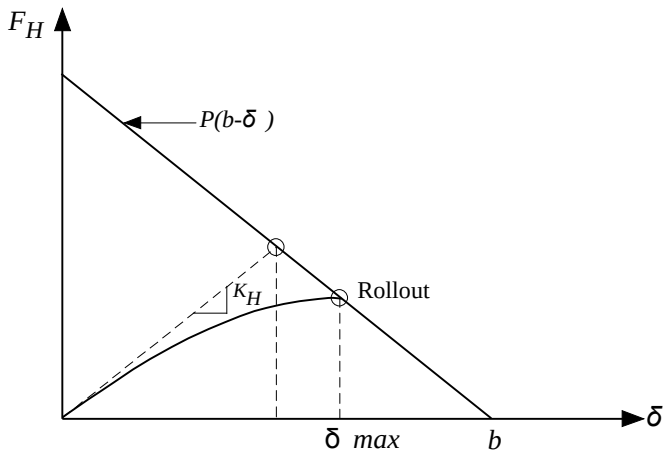

Figure 8.12 Mechanics of rollout stability in dowelled connection system

There is also the issue of buckling itself since the analysis of buckling behavior of elastomeric bearings is based on fixed boundary conditions at the top and bottom of a bearing. Exactly, how the dowelled connection system should be treated as boundary conditions for a buckling analysis is not clear.

Figure 8.2 shows the deformed state of STRP bearing at δ displacement with vertical compressive load P. The moment created by the shear force F_H shall be balanced by the applied vertical load.

$$P(b-\delta) = F_H h \tag{8.9}$$

The shear force is given by Eq. (8.10).

$$F_H = K_H \delta \tag{8.10}$$

$$K_H = \frac{GA}{t_r}(1-2\lambda\gamma) \tag{8.11}$$

where K_H is the horizontal stiffness of the bearing. Combining the Eq. (8.9), (8.10) and (8.11) and simplifying,

$$\delta^2\left(\frac{G}{t_r}\frac{h}{2b}\right) - \delta\left(p + \frac{G}{t_r}h\right) + pb = 0 \tag{8.12}$$

where $p = P/A$ (axial pressure), $\gamma = \delta/t_r$

The properties of STRP specimen bearings used in experimental test and FE analysis is presented in Table 8.2.

Table 8.2 Properties of specimen STRP bearings

Properties	STRP-6	STRP-4
G	0.89MPa	0.89MPa
h	72mm	48mm
t_r	60mm	40mm
p	5.0MPa	5.0MPa

For these combinations, on solving the Eq. (8.12), the maximum lateral displacement δ_{max} is 0.89b. Theoretically, beyond this displacement, the force-displacement curve produces descending slope. The theoretical value of shear displacement is much larger than the lateral displacement obtained in experimental tests. The monotonic shear test conducted on layer-unbonded STRP-6 bearing with properties given Table 8.2, the maximum shear displacement is 60mm beyond which the curve has descending slope which is shown in Fig. 8.5. Similar tests on layer-bonded STRP-4 bearing show that the load-displacement curve has ascending slope beyond the 60mm displacement with the equal level of vertical compressive load as discussed in chapter 5.

8.3 Conclusion

The stability of the isolation bearing is studied. The buckling load obtained by stability analysis is compared with experimental test results. A good agreement between the results of stability analysis of the STRP bearings considering accounting for large horizontal displacements and the test results is achieved. The results of FE analysis were verified by experimental test for nominal axial stress of 5MPa and 10MPa which are presented in chapter 5. In chapter 5, the tested layer-bonded STRP-4 bearing with nominal axial stress of 5MPa shows ascending slope beyond 60mm lateral displacement. Figure 8.6 shows that the force-displacement curve has ascending slope at around 60mm lateral displacement when loaded with 7.5MPa nominal axial stress. In conclusion, it can be said the layer-bonded STRP-4 bearings are viable to withstand axial pressure of 7.5MPa to achieve the target lateral displacement of 60mm, which is equivalent to 150% shear strain, even though the stability analysis shows higher value of nominal axial stress [10]. Experimental tests and FE analysis of a 4-layer bonded STRP bearing indicates that STRP bearings can show acceptable performance that can be used as a base isolation device for earthquake protection of building structures.

References

[1] ASCE-7. Minimum design loads for building and other structures, ASCE/SEI 7-05. New York, American Society of Civil Engineers, 2005.

[2] Donatello Cardone, Giuseppe Perrone. Critical load of slender elastomeric seismic

isolators: An experimental perspective. *Engineering Structures*, 2012, Vol. 40(?), pp: 198-204.

[3] Ian Buckle, Satish Nagarajaiah, Keith Ferrell. Stability of elastomeric isolation bearings: Experimental study. *Journal of structural Engineering*, 2002, Vol. 128(1), pp: 3-11

[4] Gabriela Ferraro, Giuseppe Oliveto and Nicholas D. Oliveto. On the stability of elastomeric bearings. Department of Civil and Environmental Engineering, University of Catania, Italy.

[5] Dimitrios Konstantinidis, James M. Kelly, Nicos Makris. Experimental investigation on the seismic response of bridge bearings. Department of Civil Engineering, University of California Berkley.

[6] MSC Software (2010), MSC Marc 2010 and MSC Marc Mentat 2010, Santa Ana, California

[7] Gordon P. Warn, Jared Weisman. Parametric finite element investigation of the critical load capacity of elastomeric strip bearings. *Engineering Structures*, 2011, Vol. 33(12), pp: 3509-3515.

[8] Michael G. P. de Raaf, Michael J. Tait, Hamid Toopchi-Nezhad. Stability of fiber-reinforced elastomeric bearings in and unbonded application. *Journal of Composite materials*, 2011, Vol. 45(18), pp: 1873-1884.

[9] Farzad Naeim, James M. Kelly. Design of seismic isolated structures from theory to practice. John Willey and sons, Inc. 1999.

[10] Huma Kanta Mishra, Akira Igarashi. Experimental and analytical study of scrap tire rubber pad for seismic isolation. World Academy of Science, Engineering and Technology, Issue 62, (*Proc. International Conference on Earthquake and Structural Engineering 2012*): 202-208, February 19-21, 2012, Kuala Lumpur, Malaysia.

9

Conclusion and recommendations

The primary objective of the research was to investigate the possibility of using STRPs for application to seismic isolation of structures. Further, the research intended to develop low-cost seismic isolation system applicable to structures in developing countries. The mechanical properties of the layer-unbonded and layer-bonded STRP specimen bearings in static vertical compression and shear loadings were identified. The dynamic responses of the isolation system with STRP bearings obtained by analytical modeling were validated by conducting pseudodynamic tests. Time history analyses with bidirectional seismic excitations were performed in order to identify the seismic performance of the purposed base isolation system. Stability analysis of STRP bearings was carried out to identify the axial load and corresponding shear deformation capacity. The material properties of used tire rubber were determined by conducting uniaxial tension tests. In the meantime, key ingredient of the tire rubber was identified by conducting gas chromatography analysis. Based on the study carried out, the main findings are summarized as below:

9.1 Main findings of the study

9.1.1 Layer-unbonded STRP bearings

The experimental test and analytical study on layer-unbonded STRP bearings yielded valuable information on their mechanical properties. The findings obtained in this part of the study are:

1. The vertical stiffness of the STRP bearing is sufficient to withstand structural load of low-rise structures. The vertical vibrational frequency of 11.4Hz is considered sufficient

for seismic isolation application.

2. The shear deformation capacity of layer-unbonded STRP bearings is 100%, after that layer separation occurred.

3. The damping ratio of the tested layer-unbonded STRP bearings is such that no additional damping enhancement mechanism is necessary.

4. The ratio between vertical and horizontal stiffness is more than 150, so that the SRTP bearings can be used for seismic isolation purpose.

5. The study carried out on role of aspect ratio suggests that proper aspect ratio should be maintained while designing the STRP bearings.

6. Proper bonding between the STRP layers is necessary to improve the shear deformation capacity and to improve the stability of the isolation system.

9.1.2 Layer-bonded STRP bearings

As outlined in the first part of the study, the thickness of STRP bearings was reduced by reducing the number of STRP layers to maintain the proper aspect ratio and the STRP layers were bonded to prevent the separation of layers. The key findings obtained in this part of the study are:

1. The vertical stiffness of the layer-bonded STRP bearings is improved and consequently increased the vertical vibrational frequency to 18.4Hz which is sufficient for seismic isolation purpose.

2. The layer-bonded STRP bearings provide positive incremental force resisting capacity up to shear strain level of 150% when loaded with nominal axial pressure of 5MPa.

3. The ratio between vertical and horizontal stiffness is more than 150, so that the layer-bonded SRTP bearings can be used for seismic isolation purpose.

4. The test results with different axial pressures indicate that the shear deformation capacity is sharply reduced when loaded with larger axial pressures.

5. The damping value of the tested layer-bonded STRP bearings is in agreement with the

first part of the study and is dependent on pre-loading.

9.1.3 Numerical modeling and pseudodynamic test

The seismic response of the base isolation system with layer-bonded STRP bearings was evaluated by numerical modeling and validated by conducting pseudodynamic tests. Base isolation layer was physically tested and the superstructure part was computed numerically. The main findings of the study are:

1. The comparison between pseudodynamic test and analytical results show that the maximum responses are in reasonable agreement.
2. The maximum base displacement produced by 150% El Centro record excitation is less than the designed displacement and the displacement is within the acceptable limit of the base isolation system.
3. The reduction on top floor absolute acceleration is in the range of 40-45% of the input excitations.
4. The floor inter-story drifts are reduced to permissible limit of $0.02/R_I$.
5. The response absolute acceleration on the top floor is reduced to one third of the top floor absolute acceleration of the equivalent fixed base building.
6. The reduction on base shear transmission to the superstructure is about 70% of the fixed base building.
7. These results indicate the effectiveness of the proposed base isolation system using layer-bonded STRP bearings.

9.1.4 Design displacements and seismic performance

In this part of the study, base isolation system was designed for a three-story reinforced concrete building. Three dimensional nonlinear time history analyses with bidirectional seismic excitations were performed in order to identify the seismic performance of the purposed base isolation system. The evaluated seismic response quantities are the maximum floor

displacements, inter-story drifts, absolute floor accelerations and base shear transmission to the superstructure. The key findings of the study are:

1. The average maximum bearing displacement is found to be smaller than the design displacement in all levels of seismic excitations.

2. The maximum inter-story drifts in all the cases are very small in x-direction while the inter-story drifts in y-direction are larger but still within the limit of $0.02/R_I$.

3. The response absolute accelerations are smaller than the input ground motion in all the cases. The reduction is in the range of half of the input ground motion.

4. The average base shear transmitted to the superstructure is equivalent to the seismic coefficient of 0.24g which is less than the design spectral acceleration for MCE.

5. All the STRP bearings remain in compression for all level of excitations which prevents the local uplifting of the superstructure and also forces all the bearings to participate in seismic isolation system.

6. It can be concluded that the seismic responses are reduced for all level of excitations, the building including isolation system is stable and all the STRP bearings can participate in base isolation system. These results indicate the seismic performance and effectiveness of base isolation system using layer-bonded STRP bearings under bidirectional seismic excitations.

9.1.5 Stability analysis of STRP bearings

This part of the study was focused to identify the axial load and corresponding shear deformation capacity of the STRP bearings. Some of the key findings are summarized below:

1. The assessment of stability of seismic isolation bearing is essential for the single bearing as well as for the whole isolation system.

2. It can be concluded that the axial pressure, aspect ratio and shear deformation capacity are mutually dependent parameters. In this regards, the designed axial pressure and target displacement governs the size of the STRP bearing.

3. FE analysis results conclude that the layer-bonded STRP-4 bearings can be loaded up to 7.5MPa nominal axial pressure to achieve 150% shear strain.

4. The shear deformation capacity is dependent on the nominal axial stress.

The proposed base isolation system doesn't require sophisticated manufacturing process which is a key factor in promoting the seismic isolation system. Further, the materials of the isolation bearings are also available everywhere with relatively minimum cost. The STRP bearings meet the expected criteria like vertical stiffness, horizontal stiffness and shear deformation capacity. These bearings are not available commercially but satisfy the requirements of seismic isolation of buildings and performances are in the acceptable limits. Finally, the results of experimental tests and analytical studies suggest that there is possibility of using layer-bonded STRP bearings for seismic isolation of structures.

9.2 Recommendations for further research

Some important results and findings of the proposed base isolation system have been highlighted. However, further research of the following issues is necessary in order to implement the proposed base isolation system with confidence.

1. Bidirectional cyclic shear test and properties identification of the STRP bearings.

2. Shake table tests of proposed base isolation system to observe the dynamics response of base isolated structure.

3. An analytical model based on the geometrical and material properties of STRP bearings that can predict the vertical stiffness, horizontal stiffness and force-displacement relationship.

4. Long-term durability tests of STRP bearings under sustained vertical loading and subjected to environmental condition such as extreme temperature and moisture.